Development of a haptic simulator for practicing the intraarticular needle injection under echography

Ma de Los Angeles Alamilla-Daniel

N° d'ordre NNT : 2020LYSEI017

THÈSE DE DOCTORAT DE L'UNIVERSITÉ DE LYON
opérée au sein de
l'Institut National des Sciences Appliquées de Lyon

École Doctorale N° 160
Electronique, Electrotechnique, Automatique (EEA)

Spécialité de doctorat : Automatique

Soutenue publiquement le 12/03/2020, par :
Ma. de los Angeles ALAMILLA-DANIEL

Development of a haptic simulator for practicing the intraarticular needle injection under echography

---

Devant le jury composé de :

POISSON Gérard	Professeur -PRISME Université d'Orléans	Rapporteur
BARTHOD Christine	Professeure -SYMME Université Savoie Mont Blanc	Rapportrice
VIEYRES Pierre	Professeur -PRISME Université d'Orléans	Examinateur
PROMAYON Emmanuel	Professeur -TIMC IMAG Université Grenoble Alpes	Examinateur
ZARA Florence	Maître de Conférences -LIRIS Université de Lyon	Examinatrice
REDARCE Tanneguy	Professeur - Ampère INSA Lyon	Directeur de thèse
MOREAU Richard	Maître de Conférences -Ampère INSA Lyon	Co-directeur de thèse

Département FEDORA – INSA Lyon - Ecoles Doctorales – Quinquennal 2016-2020

SIGLE	ECOLE DOCTORALE	NOM ET COORDONNEES DU RESPONSABLE
CHIMIE	**CHIMIE DE LYON** **http://www.edchimie-lyon.fr** Sec. : Renée EL MELHEM Bât. Blaise PASCAL, 3e étage **secretariat@edchimie-lyon.fr** INSA : R. GOURDON	**M. Stéphane DANIELE** Institut de recherches sur la catalyse et l'environnement de Lyon IRCELYON-UMR 5256 Équipe CDFA 2 Avenue Albert EINSTEIN 69 626 Villeurbanne CEDEX **directeur@edchimie-lyon.fr**
E.E.A.	**ÉLECTRONIQUE, ÉLECTROTECHNIQUE, AUTOMATIQUE** **http://edeea.ec-lyon.fr** Sec. : M.C. HAVGOUDOUKIAN **ecole-doctorale.eea@ec-lyon.fr**	**M. Gérard SCORLETTI** École Centrale de Lyon 36 Avenue Guy DE COLLONGUE 69 134 Écully Tél : 04.72.18.60.97 Fax 04.78.43.37.17 **gerard.scorletti@ec-lyon.fr**
E2M2	**ÉVOLUTION, ÉCOSYSTÈME, MICROBIOLOGIE, MODÉLISATION** **http://e2m2.universite-lyon.fr** Sec. : Sylvie ROBERJOT Bât. Atrium, UCB Lyon 1 Tél : 04.72.44.83.62 INSA : H. CHARLES **secretariat.e2m2@univ-lyon1.fr**	**M. Philippe NORMAND** UMR 5557 Lab. d'Ecologie Microbienne Université Claude Bernard Lyon 1 Bâtiment Mendel 43, boulevard du 11 Novembre 1918 69 622 Villeurbanne CEDEX **philippe.normand@univ-lyon1.fr**
EDISS	**INTERDISCIPLINAIRE SCIENCES-SANTÉ** **http://www.ediss-lyon.fr** Sec. : Sylvie ROBERJOT Bât. Atrium, UCB Lyon 1 Tél : 04.72.44.83.62 INSA : M. LAGARDE **secretariat.ediss@univ-lyon1.fr**	**Mme Sylvie RICARD-BLUM** Institut de Chimie et Biochimie Moléculaires et Supramoléculaires (ICBMS) - UMR 5246 CNRS - Université Lyon 1 Bâtiment Curien - 3ème étage Nord 43 Boulevard du 11 novembre 1918 69622 Villeurbanne Cedex Tel : +33(0)4 72 44 82 32 **sylvie.ricard-blum@univ-lyon1.fr**
INFOMATHS	**INFORMATIQUE ET MATHÉMATIQUES** **http://edinfomaths.universite-lyon.fr** Sec. : Renée EL MELHEM Bât. Blaise PASCAL, 3e étage Tél : 04.72.43.80.46 **infomaths@univ-lyon1.fr**	**M. Hamamache KHEDDOUCI** Bât. Nautibus 43, Boulevard du 11 novembre 1918 69 622 Villeurbanne Cedex France Tel : 04.72.44.83.69 **hamamache.kheddouci@univ-lyon1.fr**
Matériaux	**MATÉRIAUX DE LYON** **http://ed34.universite-lyon.fr** Sec. : Stéphanie CAUVIN Tél : 04.72.43.71.70 Bât. Direction **ed.materiaux@insa-lyon.fr**	**M. Jean-Yves BUFFIÈRE** INSA de Lyon MATEIS - Bât. Saint-Exupéry 7 Avenue Jean CAPELLE 69 621 Villeurbanne CEDEX Tél : 04.72.43.71.70 Fax : 04.72.43.85.28 **jean-yves.buffiere@insa-lyon.fr**
MEGA	**MÉCANIQUE, ÉNERGÉTIQUE, GÉNIE CIVIL, ACOUSTIQUE** **http://edmega.universite-lyon.fr** Sec. : Stéphanie CAUVIN Tél : 04.72.43.71.70 Bât. Direction **mega@insa-lyon.fr**	**M. Jocelyn BONJOUR** INSA de Lyon Laboratoire CETHIL Bâtiment Sadi-Carnot 9, rue de la Physique 69 621 Villeurbanne CEDEX **jocelyn.bonjour@insa-lyon.fr**
ScSo	**ScSo*** **http://ed483.univ-lyon2.fr** Sec. : Véronique GUICHARD INSA : J.Y. TOUSSAINT Tél : 04.78.69.72.76 **veronique.cervantes@univ-lyon2.fr**	**M. Christian MONTES** Université Lyon 2 86 Rue Pasteur 69 365 Lyon CEDEX 07 **christian.montes@univ-lyon2.fr**

*ScSo : Histoire, Géographie, Aménagement, Urbanisme, Archéologie, Science politique, Sociologie, Anthropologie

To my family.

Acknowledgments

Español

Este trabajo de tesis es dedicado a cada una de las personas que me han estado presente en cada etapa de mi vida para alcanzar mis sueños. Le doy gracias a Dios, que siempre ha puesto a un ángel para guiar mis pasos.

Agradezco a mi familia quienes siempre me han brindado su apoyo incondicional; A la mujer de un gran corazón que es mi madre, quien me ha ensenado a nunca vencerse. A mi linda hermana quien ha dado todo por su familia y ha demostrado que el querer es poder y que no hay fronteras para alcanzar tus sueños. A mi gemelo que siempre ha estado conmigo en las buenas y quien vence barreras por ayudarme a conseguir mis sueños. Y al final, pero no por ser menos importante, a mi lindo hermano menor, quien siempre me brinda su apoyo incondicional.

Agradezco a mi compañero de batallas, mi esposo Angel, quien por mÃ¡s de quince años hemos luchado para alcanzar esta meta de ser doctores ya que nuestro objetivo es dejar nuestra aportación al mundo científico.

English

Un especial dedicatoria a mi director y codirector de tesis, Dr Tanneguy Redarce y Dr. Richard Moreau por darme la oportunidad de trabajar con ellos, por su dedicación, paciencia y comprensión.

Agradezco también a CONACyT, quien me brindo el apoyo económico para culminar mi tesis en los últimos 18 meses de mi trabajo de tesis.

Y mi última dedicatoria especial es para el Dr. Orlando Ávila Pozos que confió en mí y me brindo su apoyo incondicional aun sin conocerme personalmente o en el ámbito científico.

English

This thesis work is dedicated to each of the people who have been there for me at every stage of my life to achieve my dreams. I thank God, who has always put an angel to guide my steps.

I thank my family who has always given me their unconditional support; To the woman

with a big heart who is my mother and has taught me to never give up. To my beautiful sister who has given everything for her family and shows me that if you want something, there are no borders to achieve your dreams. To my twin brother who has always been with me in good times and who overcomes barriers for helping me achieve my dreams. And in the end, but not less, to my younger brother, who always gives me his unconditional support.

I thank my partner in battles, my husband Angel, who for more than fifteen years has fought to achieve this goal of becoming doctors since our objective is to leave our contribution to the scientific world.

A special dedication to my thesis director and co-director, Dr. Tanneguy Redarce and Dr. Richard Moreau for allowing me to work with them, for their dedication, patience, and understanding.

I also thank CONACyT, who gave me the financial support to complete my thesis in the last 18 months of my thesis work.

And my last special dedication is to Dr. Orlando Ávila Pozos who trusted me and gave me his unconditional support even without knowing me personally or in the scientific field.

Contents

List of Figures

List of Tables

Introduction

The training of new doctors is always a crucial issue. Future doctors must study for years to accurately diagnose and provide remedies to their future patients. However, medicine is also a very technical area. Medical students must learn how to perform a lot of hand labors over patients; from the simplest ones, as apply a bandage, to the more complex as brain surgeries.

Medical students must train to learn how to perform these tasks before practicing in a real patient, as a bad movement could injure partially or permanently the patient. In recent years, the development of new technologies allows medical students to gain experience using simulators, that day over the day, are more realistics. With these simulators, students can repeat the same operations, in a wide range of environments, situations and patients' profiles.

Although simulators are becoming a standard for training medical students, due to the large number of operations that doctors must master, simulators are not sufficient nowadays.

One example of this is the practice of intraarticular needle injection to relieve the pain. Some simulators have been developed for this specific task, but their limitations prevent getting realistic training. For this reason, in this PhD thesis, we present the development of a simulator for puncture gesture under ultrasound, named SPARTE project, which is made in collaboration by five partners (four laboratories and one health facility) and aims to overcome the problems presented in the current simulators.

In chapter 1 we present the medical context that is required for the intraarticular needle injection under ultrasound guidance, the state of art of passive and active simulators, and the different technologies used by haptic devices. We also introduce how this work is developed in collaboration with other laboratories, our PhD objectives and the different phases of this work.

In chapter 2 we introduce the different methods and techniques used for rendering forces during needle insertion, as well as a new method, developed during this work, that aims to

provide a low-resourcing solution. We also provide the methods used to render the additional forces that are exerted around the needle during the insertion and help to limit the user's movements.

In chapter 3 we introduce the ultrasound probe mock. We show the model and compare three different control laws for rendering forces using a pneumatic actuator. We analyze them and determine their benefits and drawbacks.

In chapter 4 we gather the controls provide for needle force rendering in chapter 2, with our 3D environment and an environment for the ultrasound-guided, created by one of our partners. We detailed the technical problems that we face during the conjunction and how to overcome them. We test the system by inviting an expert from our health facility partner, to realize an essay of injection. The collected data and obtained results are also detailed in this section.

Finally, we gave our conclusions and proposed future works to pursue the developments of the needle simulator under ultrasound guidance.

Part I

Résumé en français

Chapter 1

Contexte générale

1.1 Contexte médicale

La ponction articulaire (genou, épaule, hanche, poignet, cheville) est une technique couramment utilisée dans divers traitements et comme procédure de routine par les rhumatologues pour soulager la douleur [Balint et al., 2002].

La ponction consiste à extraire du liquide synovial pour l'analyser et établir un diagnostic de l'arthrite inflammatoire. Une injection peut également être réalisée. Cette technique est utilisée pour introduire un stéroïde ou un anesthésique pour soulager la douleur articulaire. Cette dernière méthode est la plus couramment utilisée dans le cas d'un traitement d'ostéoarthrite [Douglas, 2014].

La ponction articulaire est utilisée depuis plusieurs décennies. Pour cela, les médecins utilisent des repères anatomiques du patient, pour l'aider à guider l'aiguille à l'intérieur de l'articulation. Dans les petites articulations (articulation interphalangienne par exemple), les médecins procèdent généralement par palpation pour guider l'aiguille dans l'articulation. La capacité de placer l'aiguille avec précision dans l'espace articulaire est essentielle pour aboutir à un traitement réussi. Cependant, la plupart des rhumatologues assurent que, sans techniques d'imagerie, il est très difficile de placer correctement l'aiguille dans une articulation. Une étude a montré que lorsque le guidage se fait uniquement par palpation, 59 % des cas débouchent sur des ponctions extra-articulaires et donc sur un échec dû à

l'impossibilité d'extraire du liquide [Peetrons and Court-Payen, 2009]. Par conséquent, les méthodes utilisant l'imagerie ont tendance à être plus précises pour réaliser correctement une ponction. En général l'imagerie utilisé est une imagerie ultrasonore en utilisant une sonde échographique.

Figure 1-1 – Photographie du genou droit pour illustrer l'approche supéro-latéral pour extraire ou introduire du liquide dans le cas d'une bursite prépatellaire [Douglas, 2014].

L'échographie est une modalité d'imagerie couramment utilisée pour aider au guidage des procédures interventionnelles dans le système musculo-squelettique. La possibilité d'observer la position exacte de la pointe de l'aiguille en "temps interactif" permet de confirmer le placement final de l'aiguille en vue d'une injection thérapeutique, d'une aspiration de liquide et dans le cas de biopsie des tissus mous [Sofka et al., 2001].

1.2 Injection intraarticulaire d'une aiguille avec un guidage échographique

1.2.1 Description de la procédure

La sonde est positionnée sur la zone ciblée qui est marquée par un "+" en pointillés (Fig. 1-2). La position de ce point d'entrée est vérifié dans les plans longitudinal et transverse (Fig. 1-3).

Lors de la réalisation de la procédure, l'aiguille est enfoncée à main levée avec une surveillance constante de son avancée à l'aide de la sonde échographique.

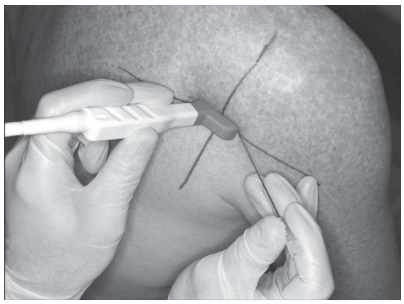

Figure 1-2 – Cas de l'articulation Gleno-humérale sous échographie. La photographie montre le positionnement de la sonde pour une coupe transverse postérieure de l'épaule droite ainsi que le positionnement de l'aiguille [Fessell et al., 2000]

.

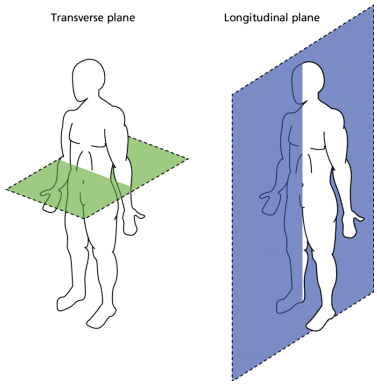

Figure 1-3 – Plans longitudinal et transverse

Si la pointe de l'aiguille n'est pas visible dans l'image échographique, un petit mouvement de la sonde est souvent recommandé avant tout mouvement de l'aiguille, afin de retrouver le bon plan de coupe. Il est généralement recommandé de maintenir l'aiguille parallèle à la surface de la sonde. Ainsi l'aiguille sera vue comme une structure hyperéchogène linéaire [1] avec un artefact de réverbération postérieure [2] [Sofka et al., 2001].

Le geste est donc assez difficile à réaliser du fait que le médecin doit utiliser ses deux mains de manière synchronisée afin de toujours visualiser l'aiguille sur l'image échographique (Fig. 1-4). Le médecin tient dans une de ses mains la sonde échographique pour explorer l'articulation et essayer de maintenir l'aiguille à l'intérieur de l'image. Pendant ce temps,

[1] Ce phénomène indique une région dans une image échographique dans laquelle la réflexion est plus forte que la normale ou que les structures environnantes.

[2] Cela se produit lorsqu'un faisceau ultrasonore rencontre deux puissants réflecteurs parallèles.

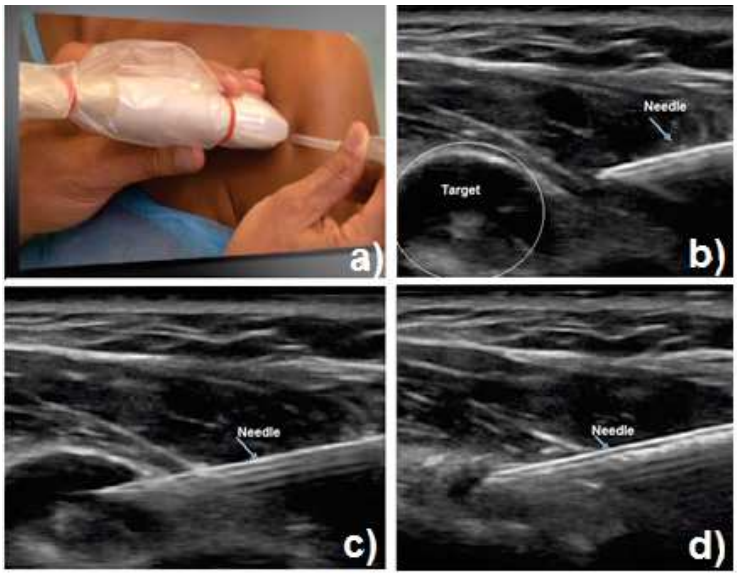

Figure 1-4 – Visualisation de l'aiguille dans une image échographique

à l'aide de sa seconde main, le médecin perce les tissus avec son aiguille jusqu'à atteindre la cible. Pendant toute la procédure, le médecin doit concentrer son attention sur l'écran où sont projetés les images échographiques plutôt que sur les mouvements de ses mains. Ainsi, une coordination visuo motrice est nécessaire pour manipuler correctement les deux outils en même temps. De plus, selon la position de l'articulation, le médecin doit savoir maîtriser ses outils des deux mains. En effet, l'aiguille peut être tenue soit par la main gauche soit par la même droite et inversement pour la sonde échographique.

1.3 Formation médicale

En général, les étudiants en médecine apprennent les aspects théoriques de chaque procédure pendant leur formation universitaire. Ensuite, concernant la partie pratique, ils regardent des vidéos de cas réels et observent dans les salles d'opération. Ils ont également une explication et font leurs premiers tests sur des mannequins avant de pratiquer sur des patients sous la supervision d'un expert.

Pour augmenter le réalisme de leur formation, ils peuvent aussi s'entraîner sur des animaux, des cadavres, des mannequins ou des simulateurs. Selon la nature de la procédure,

il n'est pas toujours approprié de s'entraîner sur des cadavres ou des animaux. Il y a aussi un problème éthique, et parfois certains pays interdissent l'utilisation d'animaux ou de cadavres. Pour ces raisons, un simulateur est un moyen adéquate pour la formation.

Concernant la ponction intra-articulaire sous échographie, l'un des problèmes majeurs lors de l'apprentissage sur simulateurs est l'impossibilité de simuler précisément différentes types de tissus (peau, graisse, muscles et ligament). La restriction du mouvement de l'aiguille est également un problème à résoudre car la plupart des simulateurs fixent les points d'insertion ce qui diminue le réalisme de la formation sur simulateur [Gonenc and Gurocak, 2012a].

1.3.1 Simulateurs

Toute opération médicale comporte des risques pour le patient, surtout si le praticien est inexpérimenté. Plusieurs autorités sanitaires, comme la H.A.S. [3] en France demandent, d'un point de vue éthique, une formation initiale sur simulateur. la H.A.S. a ainsi déclaré aux étudiants en médecine de "ne jamais pratiquer pour la première fois sur un patient" [Granry and Moll, 2012]. Pour cette raison, la popularité des simulateurs médicaux augmentent ces dernières années. Les simulateurs les plus avancés dédiés aux métiers de la santé visent à proposer un apprentissage des gestes complexes en proposant un retour haptique couplé éventuellement à de la réalité virtuelle. Dans le cadre de ce travail, nous nous intéressons en particulier sur le développement d'un simulateur permettant de s'entraîner à l'insertion d'aiguille intra-articulaire sous échographie.

Plusieurs équipes de recherche ont concentré leurs efforts sur la création de simulateurs plus réalistes et plus immersifs. Ces simulateurs peuvent être divisés en deux catégories: passifs et actifs. La dernière catégorie propose un retour d'effort. En raison de la faible quantité de simulateurs dans la littérature qui concernent notre cas d'étude, nous avons étendu notre recherche bibliographique à la procédure générale d'insertion d'aiguille pour une meilleure compréhension de l'état de l'art.

[3] Haute Autorité en Santé, autorité en charge des questions de santé en France

1.3.2 Simulateurs passifs

Les simulateurs dits passifs sont des simulateurs qui consistent généralement en des mannequins reproduisant l'anatomie mais ne proposant pas de retour haptique ni d'analyse du geste réalisé. Dans le cadre de l'insertion d'aiguille, ce sont les matériaux utilisés qui assurent le retour d'effort donc ce retour d'effort n'est pas contrôlé.

Les systèmes passifs offrent la possibilité de se former à l'insertion d'aiguille dans différentes zones du corps. L'utilisation de mannequins améliore l'immersion de la simulation en fournissant un objet solide que l'apprenant peut manipuler pendant le test. Cependant, cela limite également le simulateur à un seul type de patient. De plus, les mannequins s'usent entre chaque session, ce qui réduit sa qualité et sa durée de vie. Pour pouvoir offrir différents profils et environnements, il faudrait un système facile à reconfigurer qui ne nécessite pas de fournitures jetables. Pour cela, l'option la plus pratique consiste à utiliser des dispositifs haptiques.

1.4 Haptique

1.4.1 Définition

Le mot haptique vient du grec "haptikós". Cela concerne le contact physique et/ou l'interaction tactile [Salisbury et al., 2004]. L'interaction peut être entre une main humaine et un objectif réel, ou une main humaine et un objet simulé. L'haptique peut être divisé en deux modalités : la sensation tactile et la sensations de kinesthésie [Culbertson et al., 2018]. La sensation tactile est la capacité de recevoir des informations sur un objet comme sa texture, son élasticité ou sa forme. Quant à la kinesthésie, il s'agit de la capacité de détecter la position et les mouvements de ses membres ainsi que les forces de contact. Dans le cadre de ce travail, nous nous intéressons à cette seconde modalité.

La formation haptique peut être réalisée avec l'utilisation d'une interface haptique qui permet à l'utilisateur de s'entraîner dans des environnements virtuels.

Un dispositif d'interface haptique peut être décrit comme un système qui permet d'échanger

de l'énergie mécanique avec un utilisateur pour donner la sensation d'interagir avec des environnements virtuels. Cette interface appareil-corps peut être en contact avec n'importe quelle partie du corps, mais la plupart du temps, elle est largement utilisée comme une interface manipulée par la main.

Les dispositifs haptiques se distinguent également par leur comportement mécanique intrinsèque : l'*impédance* et l'*admittance*. Les systèmes d'impédance concernent les systèmes qui captent la position et appliquent une force. Les systèmes d'admittance concernent les systèmes qui captent la force et appliquent une position.

1.4.2 Simulateurs actifs

Par rapport aux simulateurs passifs, les simulateurs actifs permettent de contrôler le retour de force à l'aide d'actionneurs, qui peuvent donner la sensation d'une raideur différente lors de l'insertion de l'aiguille. De plus, ces systèmes permettent d'enregistrer des données pendant la réalisation du geste afin d'évaluer les performances de l'apprenant à chaque test.

De nos jours, plusieurs appareils actifs sont utilisés pour construire des simulateurs par des chercheurs ou des entreprises privées afin d'apprendre ou d'améliorer les compétences médicales. Un exemple est le simulateur commercial ARTHRO Mentor II, développé par 3D SYSTEMS (Fig. 1-5). Il prend en charge des modèles anatomiques interchangeables pour s'entraîner à l'arthroscopie avec retour haptique. Cependant, le système a un coût élevé. De plus, la conception ne permet d'effectuer qu'une seule manipulation spécifique et le simulateur ne concerne qu'une seule articulation.

Figure 1-5 – Commercial active haptic systems; 3D Systems®

Dans la littérature, des simulateurs actifs sont développés dans différents laboratoires en utilisant différentes technologies.

Ainsi dans [Gonenc and Gurocak, 2012b], les auteurs proposent un actionnement hybride avec un moteur à courant continu et des freins magnétorhéologiques pour reproduire les efforts lors de l'insertion d'une aiguille. Par contre, le système proposé fixe le point d'insertion et l'insertion ne peut être faite que verticalement ce qui limite son cas d'application.

Dans [Kurita et al., 2014], les auteurs ont utilisé un Geomagic Touch pour reproduire les efforts désirés. Cependant, leur système permet seulement de reproduire une seule couche de tissus et ne reproduit pas les contacts durs comme lorsqu'un os est touché.

Un autre simulateur est proposé par Magill et al. [Magill et al., 2010]. Ils utilisent 4 moteurs brushless et des cables pour reproduire des efforts sur l'aiguille. Ils peuvent ainsi reproduire différents tissus selon la profondeur mais le point d'insertion est fixé.

Les auteurs de [Forest et al., 2007] proposent d'utiliser deux Geomagic Touch pour simuler la ponction d'une aiguille sous échographie. Dans cette configuration, un Geomagic Touch est utilisé pour représenter les forces de l'aiguille lors de l'insertion (ponction et retrait) et l'autre pour simuler la sonde échographique. Ils ont aussi créé un environnement virtuel où une image échographique est affichée. Cependant, comme cette image provient de données obtenues à partir d'images réelles à ultrasons, un seul profil de patient peut être simulé.

En résumé, cet état de l'art permet d'identifier les principaux problèmes :

- L'absence de représentation de différentes raideurs pour caractériser les différents tissus lors de l'insertion de l'aiguille.
- L'existence d'un point d'insertion d'aiguille préétabli, qui restreint le déplacement de l'outil.
- L'absence d'un environnement virtuel pour reproduire le rendu échographique.
- Seulement une seule articulation est reproduite.

- Un seul type de patient est disponible.
- Aucune mesure des performances et des progrès des apprenants ne sont fournis.
- Aucun ajustement de difficulté n'est disponible.
- Certains des outils et/ou des surfaces sont jetables.

La prochaine section est dédiée à l'introduction du projet SPARTE dont l'objectif est de résoudre ces problèmes.

1.5 Projet SPARTE

SPARTE signifie Simulateur de Ponction ARTiculaire sous Echographie. Son principal objectif est de développer un simulateur pour l'apprentissage du geste de ponction sous échographie.

Le projet SPARTE est financé en partie par SAMSEI [4], qui est un projet IDEFI dont l'objectif est de proposer de nouvelles méthodes d'entraînement au corps médical à base de simulateurs

Le simulateur consiste en une partie numérique qui reproduit l'anatomie d'un patient et qui permet de générer en temps réel des coupes échographiques à partir d'un modèle biomécanique. Cette partie est couplée à une interface haptique pour reproduire les sensations haptiques de l'aiguille et de la sonde échographique.

Le projet SPARTE regroupe 4 laboratoires publics et un établissement de santé.

1. LBMC (Laboratoire de Biomécanique et Mécanique des Chocs - UMR_T 9406 [5]) est en charge de développer un modèle biomécanique des articulations.
2. LIRIS (Laboratoire d'InfoRmatique en Image et Systèmes d'information - *UMR* 5205 *CNRS* [6]) est en charge d'intégrer la déformation en temps réel des tis-

[4] Stratégies d'Apprentissage des Métiers de Santé en Environnement Immersion SAMSEI, URL: http://samsei.univ-lyon1.fr/

[5] http://www.lbmc.ifsttar.fr/

[6] http://liris.cnrs.fr/

sus pendant l'insertion d'une aiguille ainsi que du rendu échographique du modèle biomécanique.

3. LIBM (Laboratoire Interuniversitaire de Biologie de la Motricité - *EA* 7424 [7]) est en charge d'étudier les techniques de formation actuelle et de l'intégration d'un tel simulateur dans le cursus d'apprentissage des rhumatologues.

4. AMPERE (*UMR* 5005 *CNRS* [8]) est en charge du développement de l'interface haptique.

5. HCL (Hospices Civils de Lyon [9]) a pour charge de fournir l'expertise clinique pour valider le travail de chaque partenaire.

1.5.1 Objectifs généraux

Ce consortium vise à développer un simulateur haute fidélité pour former des médecins novices à la procédure d'injections intra-articulaires sous échographie. Cela se fera en tenant compte des exigences et des besoins du rhumatologue consultant. Le but du simulateur SPARTE est d'atteindre les critères suivants : criteria.

Criteria

1. Reproduire les forces impliquées lors de l'insertion de l'aiguille sur l'articulation.
2. Simuler le contact avec la sonde échographique et le corps.
3. Evaluer les performances des utilisateurs.
4. Mettre en œuvre un modèle 3D où une aiguille peut se déplacer et être observé.
5. Générer une image échographique virtuelle en fonction de la position de la sonde sur l'articulation (Fig. 1-6).
6. Proposer des scénarios pédagogiques.

[7] https://libm.univ-st-etienne.fr/fr/index.html
[8] http://www.ampere-lab.fr/
[9] http://www.chu-lyon.fr/)

Dans ce simulateur (Fig. 1-6), la seringue montée sur l'aiguille est représentée par un dispositif haptique (cf. section 1.4) et reproduit les forces générées lors de l'insertion de l'aiguille (zone rose). Une seconde interface haptique est attachée à une sonde échographique et exerce les forces générées lors de l'interaction avec le corps du patient (zone rose). Ces deux dispositifs haptiques permettront à l'utilisateur d'obtenir une coordination œil-main (zone grise). Un écran affiche l'environnement virtuel, qui se compose d'une image échographique générée à partir de la position de la sonde et utilisée pour montrer la position de l'aiguille à l'intérieur du corps, et d'un modèle biomécanique 3D où les tissus déformés pendant le déplacement de l'aiguille (zone verte).

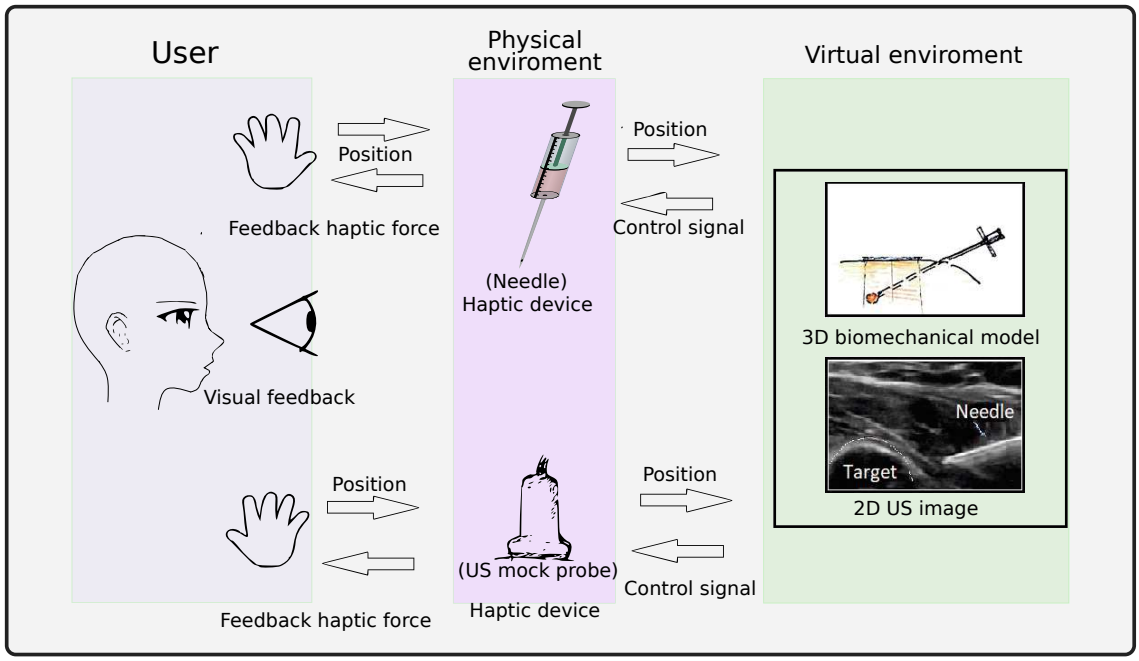

Figure 1-6 – Schéma de principe du projet SPARTE

1.6 Objectifs du doctorat

Les objectifs de ma thèse concernent deux parties du projet SPARTE : le rendu haptique des forces sur l'aiguille et celles sur la sonde échographique (zone rose de la Fig. 1-6).

Pour compléter ces objectifs, le travail a été découpé en trois phases.

1. **Phase A : rendu haptique sur l'aiguille.**
2. **Phase B : rendu haptique sur la sonde échographique.**
3. **Phase C : conception globale du simulateur et communication avec l'environnement virtuel.**

Chapter 2

Retour haptique pendant la phase d'insertion

2.1 Introduction

Ce chapitre est dédié aux méthodes développées dans le cadre de ce doctorat pour reproduire les efforts lors de l'insertion de l'aiguille.

Afin de simuler l'insertion ce l'aiguille dans une articulation à l'aide d'une interface haptique, les objectifs suivants doivent être atteints :

1. Laisser le médecin choisir le point d'insertion de l'aiguille sur l'articulation.
2. Une fois le point d'insertion choisi, l'interface haptique doit garder la même direction. Si nécessaire, la trajectoire peut être modifiée dans le corps tant que α ne dépasse pas un angle maximum préfixée (section 2.1.2).
3. Lorsque la pointe de l'aiguille pénètre dans le corps, différentes raideurs doivent être ressenties, selon les profils des patients et les pathologies.
4. Si le médecin arrête son mouvements d'insertion de l'aiguille, celle ci doit rester dans la même position.

2.1.1 Présentation des efforts

Pendant l'insertion de l'aiguille dans les tissues mous, il est possible de distinguer 3 étapes [Barbé et al., 2006]. A chaque étape des forces différentes sont générées (Fig. 2-1).

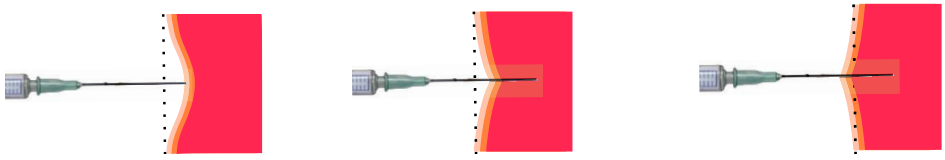

(a) Etape 1 (b) Etape 2 (c) Etape 3

Figure 2-1 – Les 3 étapes pendant l'insertion d'une aiguille dans des tissus mous.

Etape 1: pré-ponction

Fig. 2-1a illustre la force générée quand l'aiguille déforme la surface du tissu sans le percer. Cette force est notée $f_{puncture}$.

Etape 2: ponction

Fig.2-1b illustre les forces générées pendant que l'aiguille coupe le tissu. Les auteurs de [Kataoka et al., 2002] distinguent 3 forces pendant cette étape (Fig. 2-2) :

1. **La force de coupe, notée** $f_{cutting}$, qui agit sur l'extrémité de l'aiguille dans la direction axiale.

2. **La force de frottement, notée** $f_{friction}$, qui agit le long de l'aiguille dans la direction axiale.

3. **Les forces de serrage, notées** $f_{clamping}$, qui agissent sur le côté de l'aiguille dans la direction radiale.

Etape 3 : retrait

La troisième étape correspond au retrait de l'aiguille c'est à dire quand l'aiguille est retirée du tissu (Fig.2-1c). Cette force est appelée $f_{attracted}$.

Enfin, il existe un dernier type de force à reproduire. Cette force, notée $f_{HardContact}$, apparaît lorsque l'aiguille touche une surface dure comme un os par exemple.

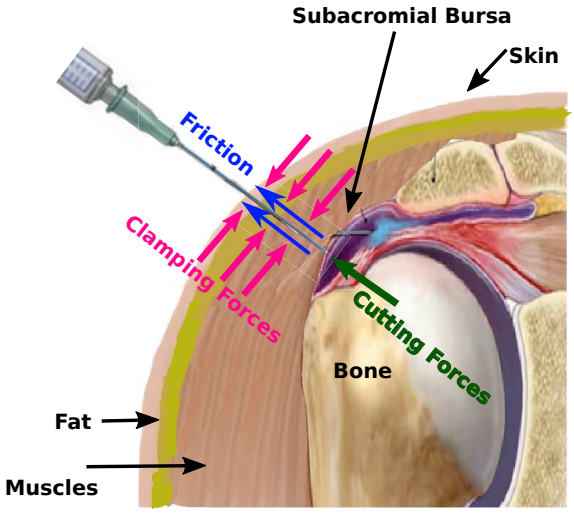

Figure 2-2 – Les forces existantes pendant l'insertion de l'aiguille.

L'ensemble des forces pouvant agir sur l'aiguille est représenté par (2.1)

$$f_{total} = \begin{cases} f_{pre-puncture} + f_{cutting} + f_{friction} + f_{clamping} + f_{attracted} & \text{soft} \\ f_{HardContact} & \text{hard} \end{cases} \tag{2.1}$$

Où la condition $soft$ indique lorsque l'aiguille est en contact avec du tissu mou et la condition *hard* lorsque l'aiguille rentre en collision avec os.

2.1.2 Angle d'insertion

α est un paramètre qui permet de gérer le changement de direction de l'aiguille pendant son insertion pour éviter de toucher un os, un nerf ou une veine. Cet angle dépend de la profondeur de l'aiguille. Au début de l'insertion, l'angle maximum autorisée est de 45° par rapport à l'axe principal de l'aiguille (Fig. 2-3). Cependant, plus l'aiguille avance, plus le corps de l'aiguille est restreint par les tissus environnants ce qui tend à réduire la valeur de l'angle α. Lors du retrait de l'aiguille, c'est l'inverse.

L'équation (2.2) permet de déterminer l'angle "α" en fonction de la longueur de l'aiguille.

$$\alpha = tan^{-1}(\frac{n_L + d_t}{n_L - d_t}) \tag{2.2}$$

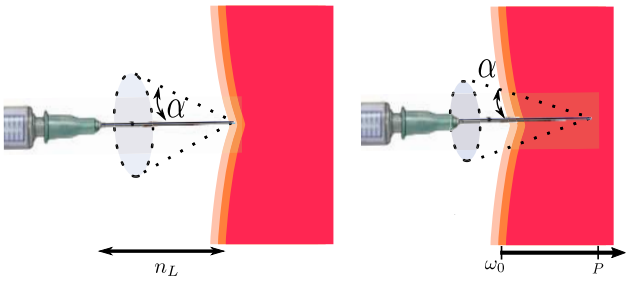

Figure 2-3 – Comportement de l'angle α pendant l'insertion de l'aiguille. ω_0 et P sont le point d'insertion et le point actuel. n_L représente la longueur de l'aiguille.

où $d_t = \left\| \overrightarrow{P\omega_0} \right\|$ est la profondeur actuelle de l'aiguille et n_L est la longueur de l'aiguille (généralement $n_L = 3.5$ cm ou $n_L = 2.5$ cm)

2.2 Méthodologie

Cette section est dédiée aux différentes méthodes employées pour reproduire les efforts décrits ci dessus.

2.2.1 Decaying Sinusoid: $f_{HardContact}$

Pour reproduire le contact avec un objet rigide, il est nécessaire d'envoyer un signal significatif à la main de l'utilisateur. En raison de la force limitée du dispositif haptique, il est impossible de reproduire la rigidité de l'os. Pour cela, la méthode *Decaying Sinusoid* [Kuchenbecker et al., 2006] peut être implémentée car elle décrit la dynamique du contact avec des objets rigides comme deux forces superposées, l'une avec une fréquence élevée et l'autre avec une réponse étendue plus lente (Eq. (2.3)). La réponse de la force est calculée en fonction de la durée et de la vitesse entrante de l'outil. L'avantage de cette méthode est que le système reste passif du fait que la force n'est calculée que pendant un court laps de temps.

$$f_{HardContact} = A\,|v_{in}|\,e^{ln(0.01)t/d} sin(2\pi f t)\,\text{for}\,0 < t < d \tag{2.3}$$

où A est l'amplitude nominal ($A = 19.9$ Ns/m), d est la durée ($d = 0.055$ s), f est la fréquence ($f = 55$ Hz).

2.2.2 Modèle de LuGre : $f_{friction}$

Plusieurs approches existent pour expliquer et prédire le comportement du frottement. Bien qu'il s'agisse d'un phénomène très complexe, il existe toujours deux paramètres principaux que l'on retrouve dans la majorité des modèles : les coefficients de frottement de Coulomb et visqueux. Le coefficient de frottement de Coulomb représente le frottement sec qui existe entre deux surfaces lors d'un contact normal. Le frottement visqueux représente le frottement entre deux surfaces préalablement lubrifiées. Bien que leur présence soit constante à travers tous les modèles proposés, parfois ces approches simples ne suffisent pas pour des tâches plus sophistiquées comme l'insertion d'aiguille. À cet effet, d'autres modèles comme le modèle LuGre sont utilisés [Asadian et al., 2011].

Le modèle de LuGre est un modèle dynamique représentants les contacts microscopiques de surfaces irrégulières avec des balais élastiques qui se plient à cause de l'insertion de l'aiguille ce qui créent le frottement (Fig. 2-4)

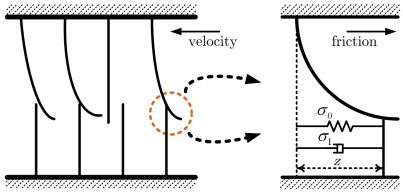

Figure 2-4 – Déformation des balais microscopiques [Asadian et al., 2011]

2.2.3 Virtual fixture : $f_{clamping}$

Les virtual fixtures sont utilisés comme guides pour effectuer des tâches en évitant que l'outil entre dans une région interdite ou quitte une trajectoire établie. Dans notre cas, la mise en place d'un virtual fixture nous aide à représenter les forces de serrage.

2.3 Méthode Tracking wall : $f_{cutting}$ and $f_{attracted}$

Une des contributions de ce doctorat réside dans l'implémentation de la méthode tracking wall. Celle ci résout les problèmes de chattering lors de la reproduction des raideurs élevés

pour représenter les différents tissus du corps. Elle repose sur l'utilisation d'un ressort mobile qui ne dépend que de la position de l'aiguille.

L'intérêt de ce ressort mobile est de maintenir la position quand un arrêt de l'insertion a lieu et éviter d'éjecter l'aiguille [Alamilla D et al., 2019].

2.3.1 Force de coupe lors de l'insertion de l'aiguille

Pour la mise en œuvre du tracking wall, deux paramètres pour décrire la position du mur sont nécessaires : ω_0 et ω_n. La position ω_0 établit le bord du mur ou dans notre cas, la surface de l'articulation. Cette valeur est fixe et ne peut pas être mise à jour car il s'agit du point de consigne de l'environnement virtuel, par exemple, lorsque l'aiguille est en contact avec la peau. A l'initialisation, ω_0 et ω_n sont égaux. ω_n est la position du mur mobile, qui suit le déplacement de l'aiguille à une certaine distance. Cette position est mise à jour en fonction du déplacement de l'outil dans l'articulation. Pour mettre à jour ω_n, l'équation (2.4) est utilisé. Ce processus est appelé *"Update with movement"*.

$$\omega_n = \begin{cases} \Delta_{new} - x_t & \text{if } x_t > \omega_0 \\ \omega_0 & \text{if } x_t \leq \omega_0 \end{cases} \quad \text{Update with movement} \tag{2.4}$$

x_t est la position actuelle de l'extrémité de l'aiguille. Δ_{new} est une variable appelée *"safety position"*. Elle permet de calculer la distance maximale pour reproduire la force désirée.

$$\Delta_{new} = \frac{f_R}{K_t} \tag{2.5}$$

Où f_R est la force désirée pour reproduire la force de coupe et K_t est un paramètre de réglage qui permet d'établir la valeur de la *"safety position"*. K_t décrit la nature du tissu mou traversé par l'aiguille.

2.3.2 Force de rappel lors d'un arrêt

Quand l'aiguille s'arrête dans le corps, ω_n est calculé selon l'Eq. (2.6). Où m est calculée par l'Eq. (2.7) qui représente le coefficient directeur de la droite définie par le point d'arrêt et ω_n.

$$\omega_n = \begin{cases} m * i + \omega_{n-1} & \text{if } i \leq n \\ \omega_{n-1} & \text{if } i > n \end{cases} \quad \text{Update with stop} \tag{2.6}$$

$$m = \frac{x_t - \omega_n}{n} \tag{2.7}$$

Une fois m défini, sa valeur reste constante jusqu'à la fin du processus. n est le nombre total d'itérations pour mettre à jour ω_n et i est le nombre d'itérations nécessaire pour que ω_n pour atteigne la position où l'arrêt a eu lieu. Ce principe est appelé *"Update with stop"* dans le diagramme présentant l'algorithme.

2.3.3 Algorithme du Tracking wall

La figure 2-5 présente le diagramme de l'algorithme du tracking wall pour calculer les forces $f_{cutting}$ et $f_{attracted}$ selon le sens de progression de l'aiguille.

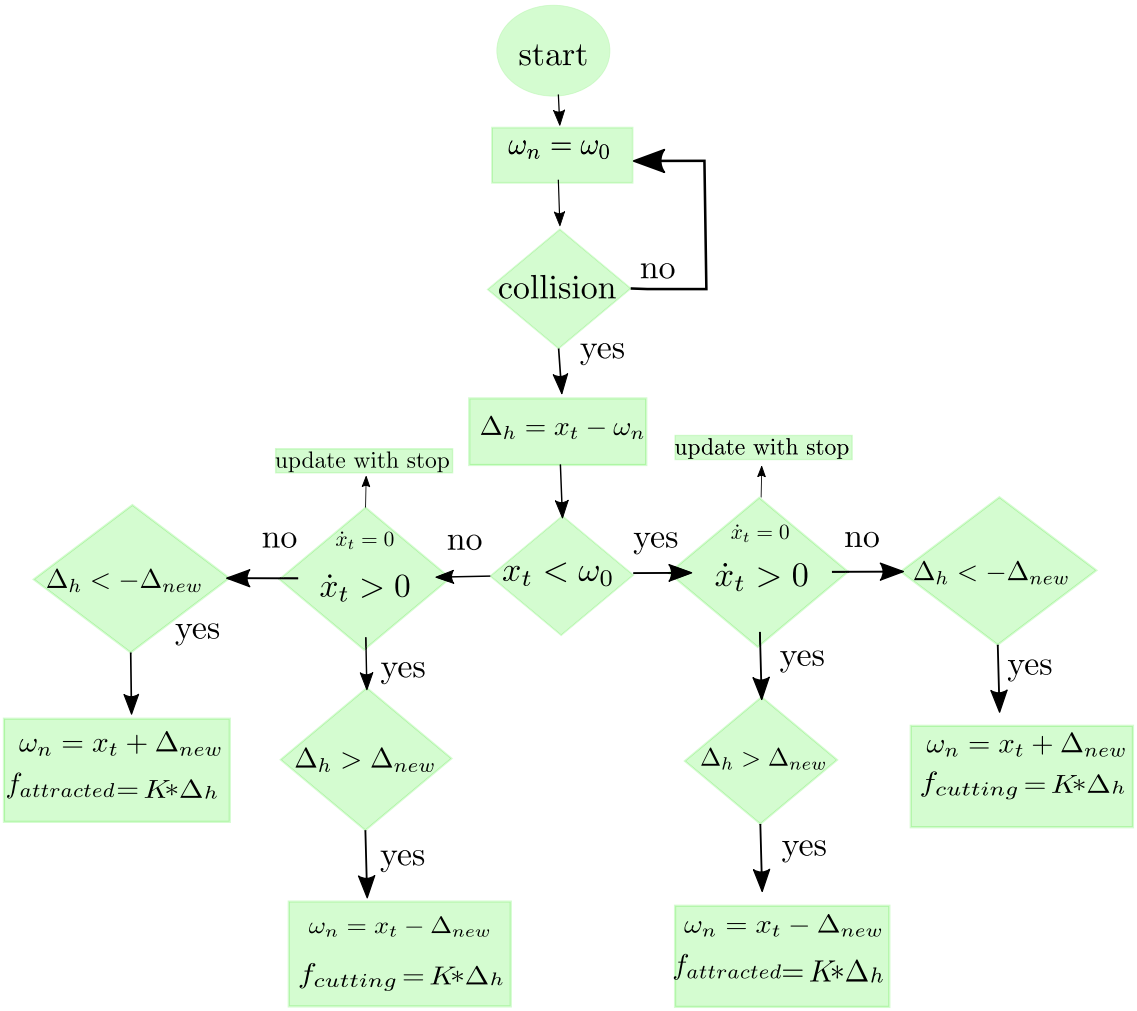

Figure 2-5 – Algorithme pour calculer les forces $f_{cutting}$ et $f_{attracted}$.

Chapter 3

Retour haptique pour la sonde échographique

3.1 Introduction

Cette section est dédiée aux forces générées sur la sonde échographique lorsqu'elle est en contact avec l'articulation du patient. La sonde factice est un point crucial pour aider les médecins à développer leurs compétences au cours de la procédure. Les deux outils (sonde échographiques et aiguille) permettent aux utilisateurs de développer la coordination visuo-motrice souhaitée. Pour garder la pointe de l'aiguille visible sur l'image échographique, la sonde peut être déplacée autour du point d'insertion. Au cours de ce mouvement, différents tissus sont en contact avec la tête de la sonde, qui peuvent être rendus sous forme de surfaces molles ou dures. De plus, il est nécessaire que les utilisateurs puissent manipuler la sonde factice avec la même liberté que lors de la situation réelle.

Les objectifs pour atteindre ces critères sont:

1. Manipulation de la sonde factice avec retour haptique.
2. Rendu du contact mou et dur pendant l'interaction sur l'articulation.
3. Transmission de la position et de l'orientation en fonction de l'articulation et de l'aiguille.

3.2 Contraintes

Lorsque la sonde est en contact avec la peau, une force normale, appelée $f_{surface}$, apparaît (Fig. 3-1). Comme on peut le voir sur la Fig. 3-1a lorsque la sonde explore une zone molle (une zone qui a un comportement élastique), le tissu sous la peau génère une résistance lorsque l'utilisateur presse la sonde contre le patient. Cette résistance provient de la rigidité du tissu. Quand l'utilisateur continue d'explorer l'articulation, $f_{surface}$ change en fonction de la pression exercée par l'utilisateur sur la sonde qui s'enfonce plus sur le tissu. Lorsque l'outil interagit avec une zone dure (un os par exemple), la sonde ne pourra se déplacer que d'une petite distance. Comme il n'y a pas de déplacement significatif, une force importante est créée par le contact entre l'outil et la zone dure que l'utilisateur interprète comme un contact dur (Fig. 3-1b).

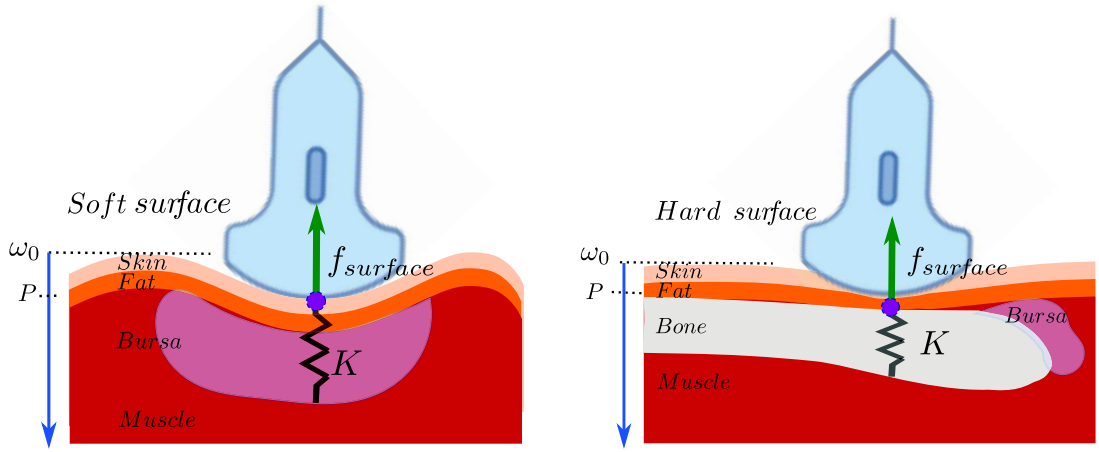

(a) Soft contact (b) Hard contact

Figure 3-1 – Collision force diagram between two virtual objects

Pour concevoir une sonde factice, un actionneur électrique peut être utilisé. Cependant, leur rapport volume / puissance est faible et en raison de la dimension de la sonde, ce type d'actionneurs ne rentre pas à l'intérieur de celle-ci. Ils sont également très limités dans la force maximale qu'ils peuvent exercer, ce qui réduit le réalisme du retour haptique.

Pour cette raison, une solution optimale consiste à utiliser un actionneur pneumatique. L'une des principales raisons de choisir un actionneur pneumatique pour générer les forces de la sonde est la possibilité d'obtenir une sonde factice proche de l'outil réel en terme

Figure 3-2 – Photographie d'une sonde échographique couramment utilisée en rhumatologie

de taille (Fig. 3-2). Les dimensions de la vraie sonde sont plus adaptées à un actionneur pneumatique (Fig. 3-3) et augmentent donc le réalisme du simulateur. L'avantage que ces actionneurs offrent est un rapport de volume / puissance plus élevé sans limiter les performances et grâce à la compressibilité de l'air dans leur chambre, les actionneurs offrent une compliance naturelle. Il est ainsi possible de reproduire les différentes raideurs des tissus en modifiant les pressions dans les deux chambres.

Figure 3-3 – Actioneur pneumatique

3.3 Lois de commande pour systèmes pneumatiques

Pour commander la sonde factice, plusieurs lois de commande ont été implémentées et comparées. La loi de commande doit permettre de reproduire différentes raideurs afin de donner la sensation d'exercer un effort sur le patient pendant la phase d'exploration de l'articulation avec la sonde.

Les lois de commande implémentées et testées ici sont celles trouvées dans la littérature

commme un simple PID et une loi de commande non linéaire de type Backstepping (BS). Ces lois de commande ont été comparées à la loi de commande proposée dans le cadre de ce doctorat : IPC (Intrinsically Passive Control).

3.3.1 Intrinsically passive control

La commande IPC, proposée initiallement par [Stramigioli, 1996], utilise le concept de passivité pour prouver la stabilité. Le principal concept est que tant que le système reste passif il reste stable. Le modèle IPC est un modèle masse ressort amortisseur comme illustrer sur la figure 3-4

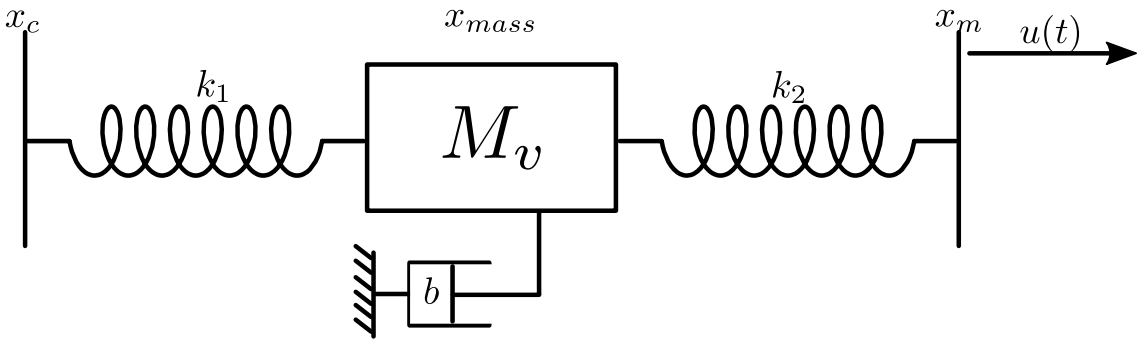

Figure 3-4 – Commande IPC

Le modèle IPC correspond à :

$$\begin{aligned} \ddot{x}_{mass} M_v &= -k_1(x_{mass} - x_c) - k_2(x_{mass} - x_m) - b\dot{x}_{mass} \\ u(t) &= -k_2(x_m - x_{mass}) \end{aligned} \tag{3.1}$$

où k_1 et k_2 sont les paramètres de raideur, b est le paramètre d'amortissement, M_v est la masse virtuelle de l'IPC, $u(t)$ est la commande. x_c est la position désirée de l'utilisateur, x_m est la position de l'interface, $\ddot{x}_{mass}$ et $\dot{x}_{mass}$ sont l'accélération et la vitesse de la masse respectivement.

Dans la commande IPC, le système nécessite la seule connaissance de la position désirée et de la position de l'interface. Grâce à l'approche passive, la commande IPC assure la stabilité du système quelque soit l'interface ou les actions de l'utilisateur.

La commande IPC peut être utilisée en admittance avec une raideur désirée comme le montre la figure 3-5.

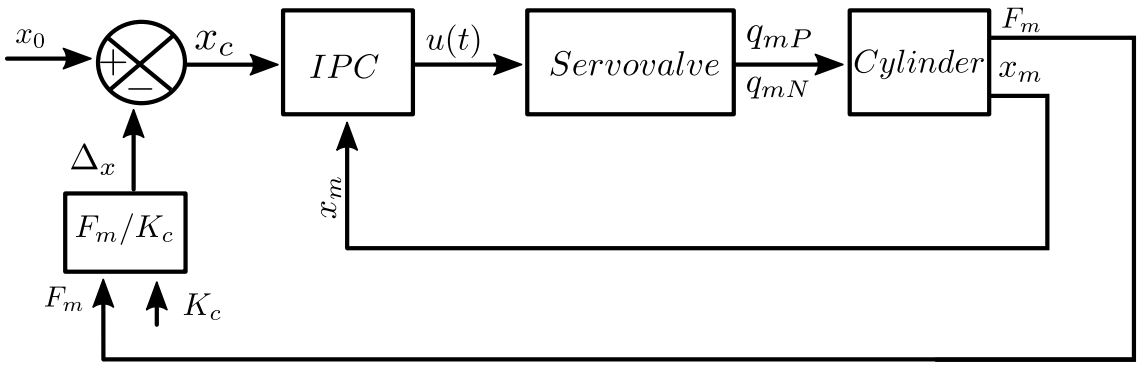

Figure 3-5 – IPC en admittance

Où les seules valeurs d'entrée requises sont la position de la tige, la position souhaitée calculée par la rigidité souhaitée et la force mesurée du capteur.

3.3.2 Comparaison des lois de commande

Deux tests ont été réalisés pour comparer les 3 lois de commande implémentées (PID, IPC, BS). Ces tests consiste en deux profils de raideurs différents : Increasing Stiffness Profile (ISP) et Step Stiffness Profile (SSP).

Increasing Stiffness Profile (ISP)

Le profil ISP utilisé pour le PID et l'IPC est disponible sur la figure 3-6a. Dans le cas du BS, le profil est montré sur la figure 3-6b.

Step stiffness profile (SSP)

Les profils SSP ont été établis pour simuler le cas où la raideur change subitement. Ce test sert à prouver la robustesse de la commande dans le cas d'un changement abrupt de raideur. En réalité, un utilisateur ne rencontrera quasiment jamais ce cas car il déplace lentement la sonde échographique pendant l'examen. Pour le PID et l'IPC, le SSP utilisé est montré sur la figure 3-7a. Dans le cas du backstepping, le profil est montré sur la figure 3-7b.

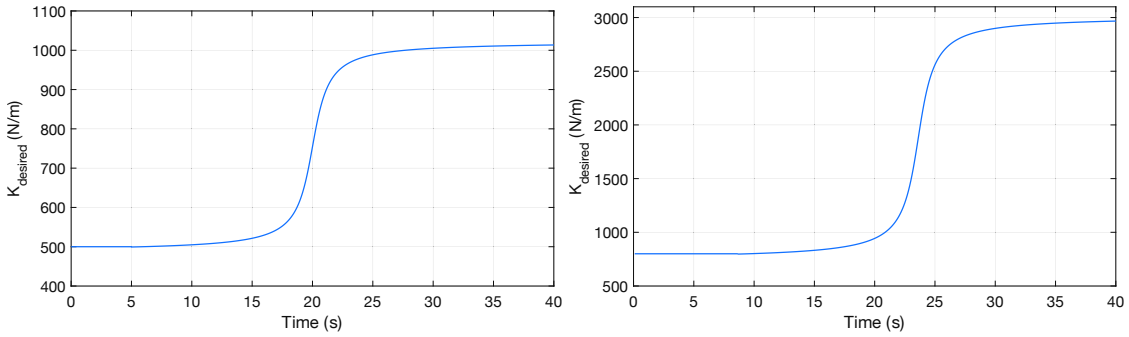

(a) Increasing Stiffness Profile (b) BS-ISP: profile stiffness

Figure 3-6 – Profils en raideur des tests

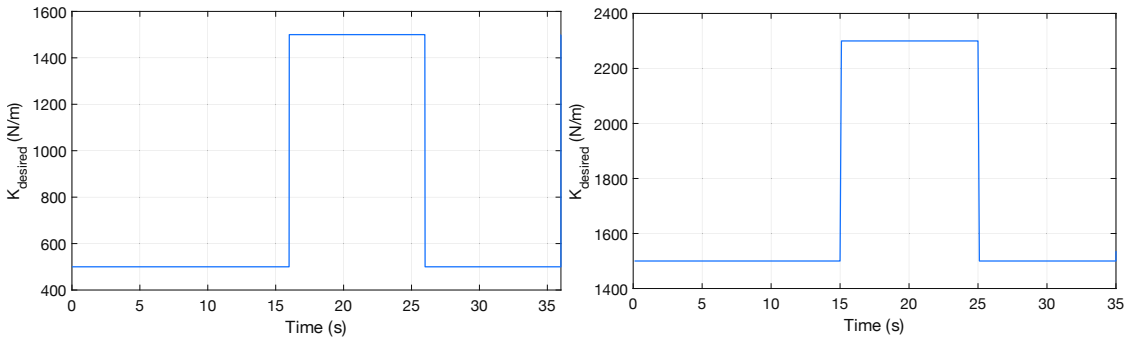

(a) PID and IPC: Step Stiffness Profile (b) Backstepping: Step Stiffness Profile

Figure 3-7 – SSP profiles

3.4 Discussion

Pour mettre en œuvre la commande sur la sonde factice, nous avons opté pour l'utilisation d'un vérin pneumatique. Nous avons comparé trois lois de contrôle différentes (PID, Backstepping et IPC) pour trouver celle qui correspond le mieux à nos besoins.

Deux profils de rigidité ont été proposés, ISP et SSP, pour tester les lois de commande et trouver les avantages et inconvénients de chacune. Ainsi, le PID et l'IPC se comportent de manière similaire pour l'ISP et le SSP, avec quelques différences mineures entre l'erreur d'état stationnaire et la tension de commande. Dans le cas du backstepping, ce contrôle présente, dans les deux tests, une erreur d'état stationnaire plus importante, mais sans chattering dans le test SSP (contrairement au PID et IPC). Cela indique que le contrôle est plus robuste aux changements brusques de rigidité. En effet, le backstepping est une loi de commande non linéaire qui correspond mieux au comportement non linéaire du vérin et de la servovalve. De plus, il n'est pas nécessaire de mettre en œuvre un capteur de force pour mesurer la force sur la sonde, car la commande par backstepping est adaptée pour le rejet de perturbation (ici la force appliquée par l'utilisateur est considérée comme une perturbation). Ceci est considéré comme un avantage pour le contrôle de backstepping par rapport au PID et à l'IPC.

D'un point de vue quantitatif, le PID et l'IPC sont probablement les meilleures options, en raison de leur précision. Cependant, comme notre objectif final est de fournir un rendu réaliste de la force agissante sur la sonde, la robustesse du backstepping présente donc de plus grands avantages par rapport aux deux autres, car les profils de rigidité peuvent varier d'un patient à l'autre. Pour déterminer le contrôle le plus optimal, une campagne de test avec des praticiens experts doit être effectuée afin que leur ressenti qualitatif aide à déterminer le meilleur contrôle.

Chapter 4

Conception du simulateur et communication avec l'environnement virtuel

4.1 Introduction

L'objectif du projet SPARTE est de créer un simulateur de ponction d'articulations sous échographie. Pour y parvenir, il est nécessaire de choisir un dispositif haptique qui reproduit la sensation haptique d'insertion d'une aiguille mais également celle de l'utilisation d'une sonde échographique lorsqu'elle est en interaction avec l'articulation.

Différentes conceptions mécaniques sont proposées pour représenter la seringue / aiguille avec le dispositif haptique ainsi que la sonde échographique. Pour toutes les conceptions et implémentations mécaniques, l'articulation choisie est celle de l'épaule. Cependant, l'articulation peut être modifiée dans les tests et implémentations futurs, car il n'y a pas de limite au nombre possible de scénarios dans lesquels le simulateur peut être utilisé.

L'assemblage du simulateur est présenté dans ce chapitre. Nous avons collaboré avec le laboratoire LIRIS pour coupler son modèle numérique avec notre environnement virtuel et notre conception mécanique. Dans ce chapitre, nous présentons également les résultats d'un test effectué par notre partenaire médical des HCL.

4.2 Conception mécanique

4.2.1 Interface haptique pour l'aiguille

Premièrement il est important que l'outil tenu par le praticien soit le plus proche de la réalité. Pour cela, une aiguille montée sur une seringue a été reproduite en fabrication additive. La figure 4-1 montre une photographie de l'outil réel et de celui fabriqué pendant ce doctorat.

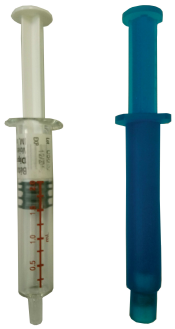

Figure 4-1 – Aiguille montée sur une seringue : outil réel et outil factice

La figure 4-2 présente le prototype final obtenu dans le cadre de ce doctorat. Il est composé d'une interface haptique Virtuose 6D Desktop de chez Haption qui permet de reproduire les efforts lors de l'insertion de l'aiguille. Sur cette interface est montée l'aiguille factice présentée ci dessus. Un support existe entre les deux afin de permettre au praticien de poser sa sonde échographique mais aussi sa main afin de stabiliser son mouvement.

4.2.2 Interface haptique pour la sonde échographique

Comme indiqué dans le chapitre précédent, la sonde factice a été réalisée à partir d'un vérin penumatique. Pour récupérer sa position et son orientation, la première idée est d'utiliser un capteur de position (par exemple un capteur magnétique tel que trakSTAR) par Ascension Technology Corporation pour localiser la sonde dans le l'espace de travail qui simule l'articulation. Cependant, ce capteur ne peut pas encore être implémenté dans le logiciel partenaire. Pour cette raison, dans un premier temps, la sonde échographique est simulée en mettant en œuvre un dispositif électrique haptique (Geomagic Touch), sans retour d'effort

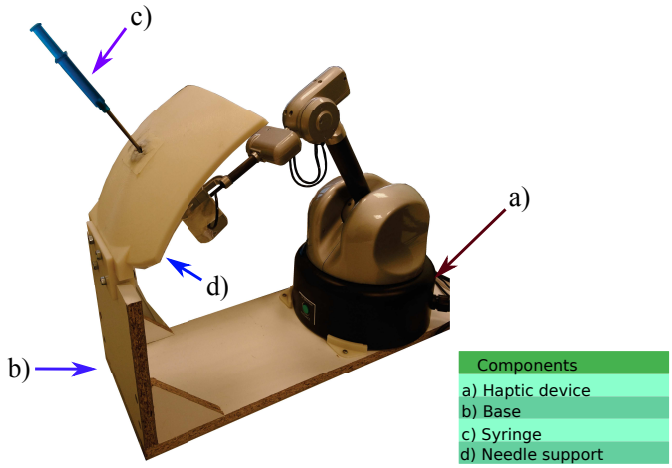

Figure 4-2 – Photographie de l'interface haptique pour l'aiguille

(Fig. 4-3b). Les seuls paramètres utilisés sont la position et les quaternions pour localiser la position de la sonde dans l'espace travail du logiciel développé par le LIRIS.

(a) Sonde échographique factice avec un vérin pneumatique (b) Sonde échographique avec un Geomagic Touch

Figure 4-3 – Sonde échographique

4.3 Communication entre les 2 environnements

4.3.1 CHAI3D framework

L'algorithme du tracking wall, le virtual fixture et le contrôle d'orientation ont été réécrits en C++ et une interface plus conviviale a été implémentée en utilisant le framework CHAI3D

[Conti et al., 2003]. L'environnement virtuel consiste en une articulation virtuelle pour permettre à l'utilisateur d'avoir une expérience plus immersive en se rapprochant de la réalité (Fig. 4-4).

Pour assurer la connexion avec l'interface haptique, une bibliothèque a été créée qui communique avec le framework CHAI 3D et l'API du Virtuose. L'environnement virtuel a été compilé dans Visual Studio 2017 pour la création de binaires Windows et dans QT creator pour UNIX.

La création de cet environnement virtuel nous permet d'établir différents profils de force lors de l'insertion de l'aiguille. Il permet également à l'utilisateur de pivoter librement l'articulation virtuelle et de choisir librement le point d'insertion. La Fig. 4-4 montre l'environnement virtuel créé dans CHAI3D.

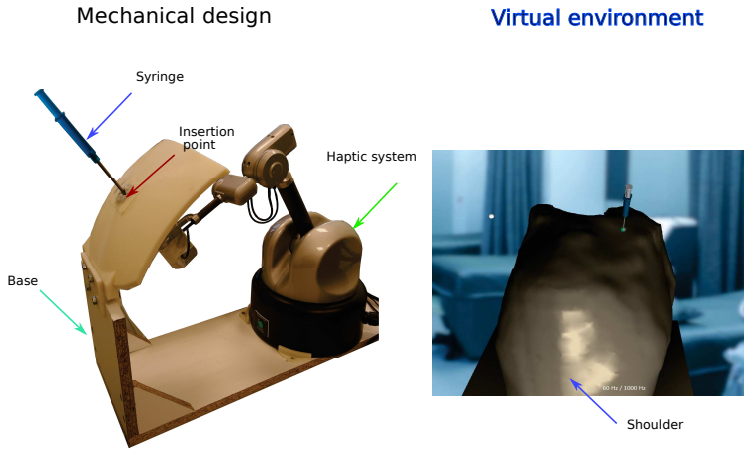

Figure 4-4 – Banc d'essai

4.3.2 Partage de mémoire

Il est à noter que les algorithmes ont été testés avec des valeurs de forces arbitraires. Des valeurs plus réalistes peuvent facilement les remplacer. Ces valeurs seront issues des travaux du LBMC et du LIRIS, nos partenaires dans le projet SPARTE. En effet, le LIRIS a créé un environnement [Barnouin et al., 2018] qui génère l'image échographique et peut nous envoyer la nature du tissu ou directement les forces. Cependant, comme chaque partenaire utilise un environnement et des frameworks différents, il n'existe pas de support officiel pour

communiquer entre eux. Pour cette raison, la solution choisie est de mettre en œuvre une méthode de partage de mémoire, appelé Memory Sharing, pour exécuter les deux logiciels en parallèle. Ainsi il est possible d'envoyer à l'autre les informations sur la position et sur l'orientation de l'interface haptique et recevoir en retour les forces. Ce partage de mémoire se fait grâce aux bibliothèques Boost [1].

La figure 4-5 présente un schéma de fonctionnement de ce partage de mémoire entre CHAI3D et l'environnement développé par le LIRIS.

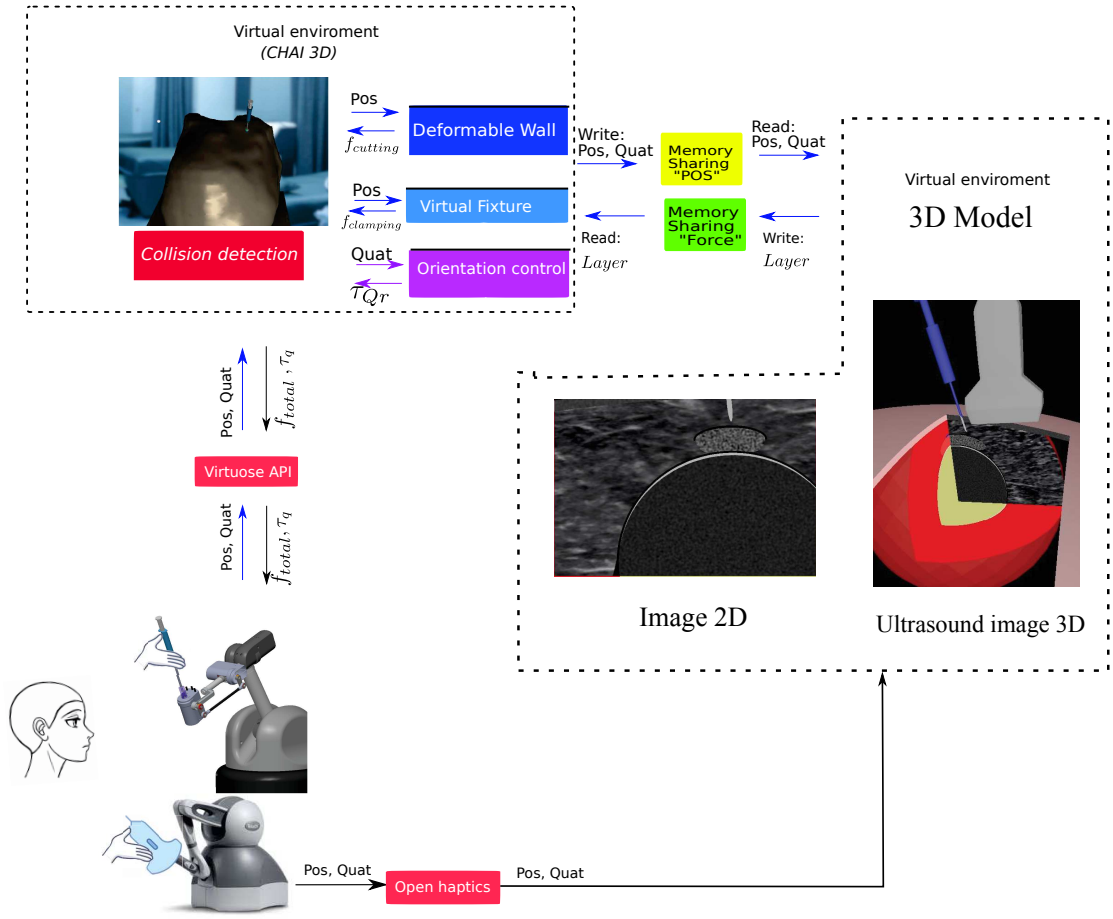

Figure 4-5 – Schéma de principe du partage de données

[1] The BOOST libraries-https://theboostcpplibraries.com/

4.4 Résultats expérimentaux

4.4.1 Mise en place de l'expérience

Une expérience a a été réalisée par un médecin expérimenté (notre partenaire médical de HCL), qui consistait à tester les forces exercées par le dispositif haptique lors de l'insertion de l'aiguille, ainsi qu'à tester la visualisation de l'image échographique lors de la performance.

Dans cette première expérience, au lieu d'utiliser le modèle complet de l'épaule qui est pour l'instant incomplet, un modèle de l'articulation plus simple a été utilisé. Ce modèle contient les couches élémentaires ; la peau, les muscles, la bourse, le tendon, le cartilage et l'os (Fig. 4-6).

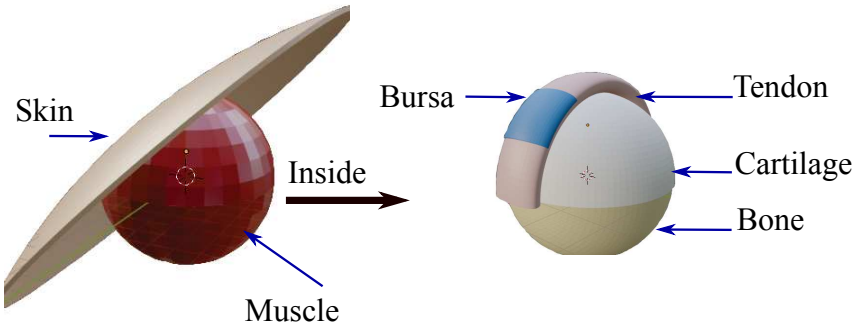

Figure 4-6 – Modèle simple de l'articulation [Barnouin et al., 2020]

Pendant la simulation, ce modèle est chargé à la fois dans l'environnement développé par le LIRIS pour gérer le modèle 3D (fig. 4-7a) et le rendu échographique (Fig. 4-7b) et à la fois dans l'environnement CHAI3D pour calculer les efforts sur la sonde et sur l'aiguille (Fig. 4-7c).

4.4.2 Résultats

Dans cette expérience, trois injections ont été effectuées, notées injection 1, 2 et 3 sur la figure 4-8. La première et la deuxième injection ont atteint la bourse et l'aiguille est toujours resté visible. Le médecin a modifié la trajectoire de l'aiguille, en retirant l'aiguille de

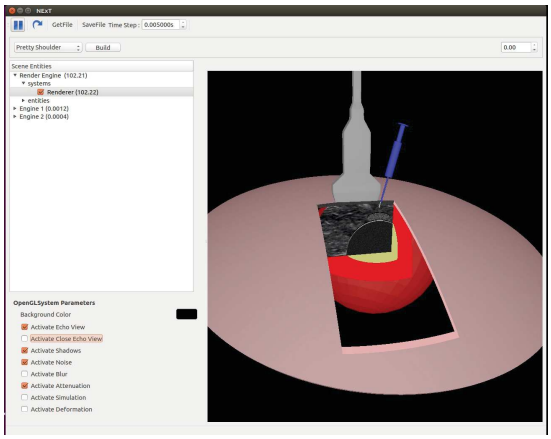

(a) Logiciel pour générer l'image échographique en temps réel

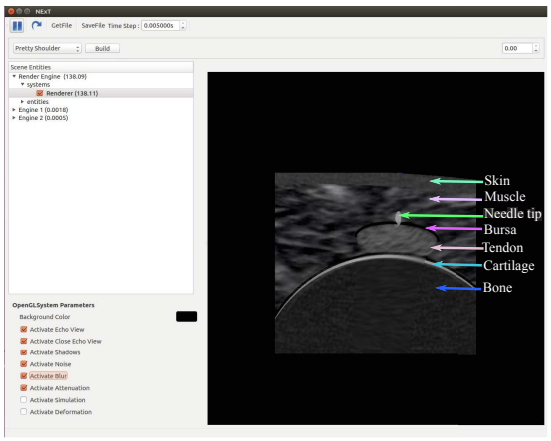

(b) Image échographique générée.

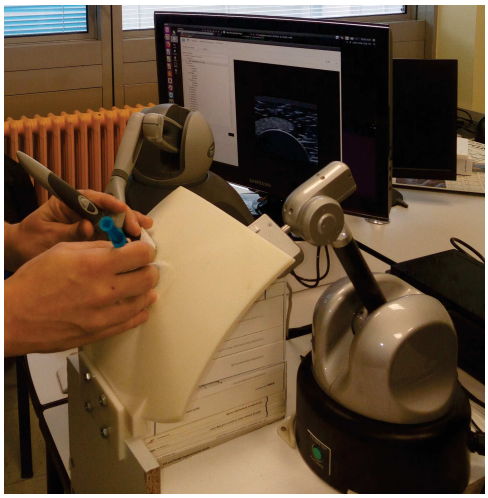

(c) Interfaces haptiques de la sonde et de l'aiguille

Figure 4-7 – Simulateur complet du projet SPARTE

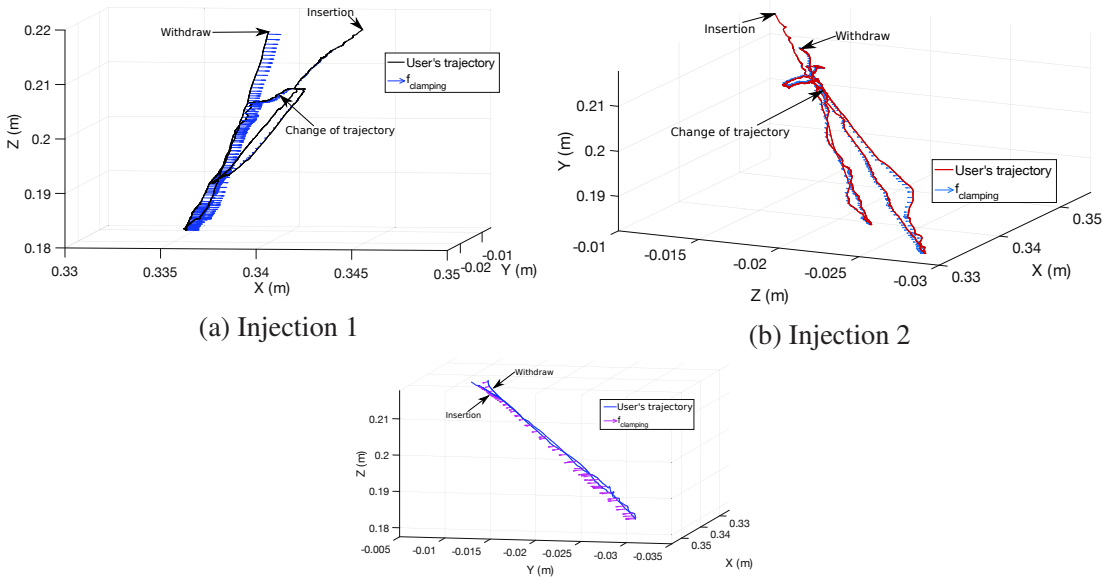

(a) Injection 1

(b) Injection 2

(c) Injection 3

Figure 4-8 – Trajectoires de l'aiguille lors de 3 injections

quelques centimètres, puis en changeant son orientation. Enfin, la dernière injection a consisté à perforer et à récupérer l'aiguille sans changer de trajectoire, mais dans un mouvement rapide pour voir le comportement de la force lors d'un contact dur.

La figure 4-9 présente les déplacements de l'aiguille selon les axes x, y et z dans le repère global de l'interface haptique. Chaque zone bleue indique lorsque l'aiguille est à l'intérieur du corps (phase d'insertion). Quant aux zones blanches, elles indiquent quand l'aiguille est en dehors du corps. Pour ces trois insertions, les forces de serrages (clamping forces) et les forces de coupes (cutting forces) sont représentées sur les figures 4-11 et 4-10 respectivement .

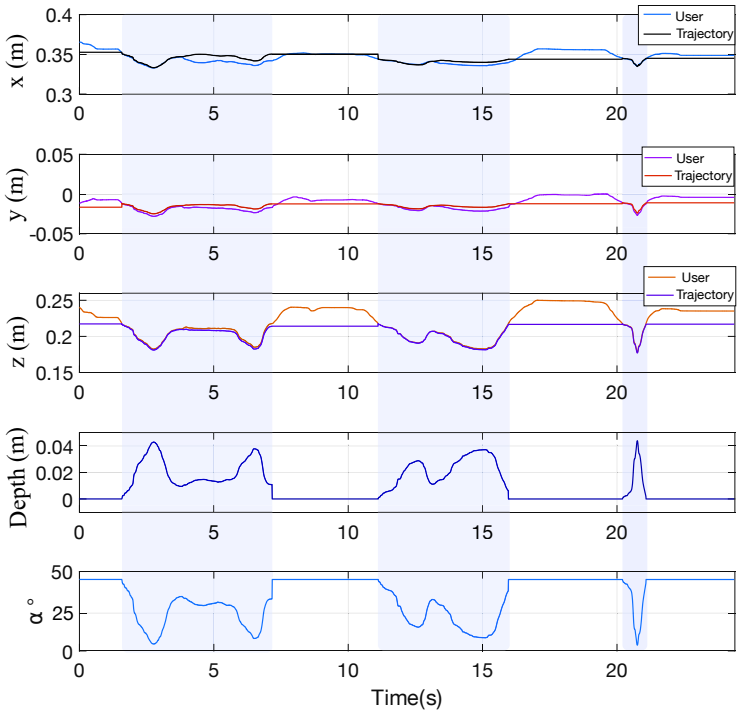

Figure 4-9 – Trajectoires de l'aiguille et trajectoires idéales

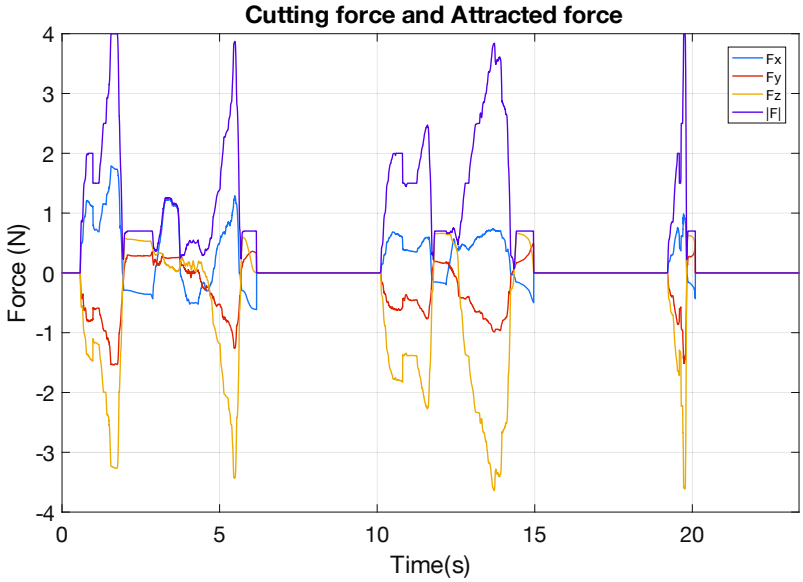

Figure 4-10 – Forces lors de l'insertion et du retrait de l'aiguille

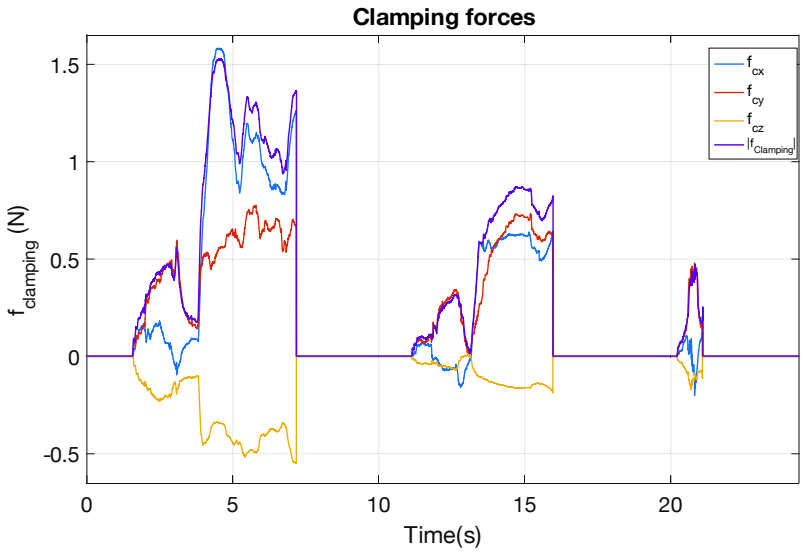

Figure 4-11 – Forces de serrage

4.5 Discussion

Dans ce chapitre, le prototype permettant la manipulation de l'aiguille et de la sonde a été présenté. L'utilisateur a la possiblité de choisir son point d'insertion sur le modèle virtuel. Ce prototype inclut également une surface permettant de reproduire la surface de l'articulation et qui permet au médecin de poser ses mains pour stabiliser son geste et ainsi améliorer le réalisme du simulateur.

L'utilisation des bibliothèques Boost a permis de partager des informations entre la partie haptique et la partie numérique développée par le laboratoire LIRIS. Ainsi, il est possible non seulement de générer en temps réel une image échographique en fonction de la position de la sonde mais aussi de calculer les efforts s'exerçant sur l'aiguille en fonction de sa position dans l'articulation

Afin d'améliorer le réalisme de ce simulateur, il sera nécessaire d'améliorer la partie mécanique en permettant la rotation de la pièce représentant la surface de l'articulation et en utilisant un modèle anatomique plus précis de l'articulation souhaitée.

Conclusion et perspectives

L'utilisation de simulateurs pour la formation des étudiants en médecine commence à devenir la nouvelle norme dans les écoles de médecine et les centres de formation. Ces simulateurs commencent à offrir une expérience plus réaliste et immersive, qui aide les étudiants à assimiler plus facilement les compétences requises avant de pratiquer sur des patients.

Dans ce doctorat, nous avons proposé un prototype de simulateur d'injection intra-articulaire. Afin de reproduire les efforts lors de l'insertion de l'aiguille, nous avons proposé une nouvelle approche de méthode, appelée "tracking wall", qui calcule les forces lors de l'insertion et le retrait de l'aiguille et permet d'obtenir un rendu haptique sans chattering. Les avantages de cette méthode sont sa simplicité en terme de temps de calculs tout en gardant une capacité de restituer différents tissus du corps et de gérer la force de rejection. Les inconvénients proviennent de l'absence de modèle biomécanique qui peut réduire le réalisme, de l'impossibilité de l'appliquer dans un système haptique d'impédance et le nombre d'itérations pour une simulation appropriée doit être déterminé en fonction des interfaces ou des langages choisis.

Concernant la méthode mise en œuvre pour calculer les forces de serrage, nous avons proposé l'utilisation de virtual fixture pour simuler les forces normales. L'inconvénient de la méthode proposée est qu'elle ne peut être utilisée dans le cas de trajectoires courbes.

Pour mettre en œuvre la sonde échographique factice, nous avons opté pour l'utilisation d'actionneur pneumatique. Nous comparons trois lois de commande différentes pour trouver celle qui correspond le mieux à nos besoins. Par exemple, le PID et l'IPC se comportent de manière similaire pour les profils ISP et SSP, avec quelques différences mineures entre eux. Dans le cas d'une loi de commande de type backstepping, l'erreur stationnaire est un plus

importante, mais le chattering est plus limité.

D'un point de vue quantitatif, le PID et l'IPC sont probablement les meilleures options, mais d'un point de vue qualitatif, il est nécessaire de mener une campagne de test avec des praticiens experts pour déterminer la commande proposant le meilleur rendu haptique lors de l'utilisation pratique. De plus, il est à noter que le PID et l'IPC ont besoin d'un capteur de force entre la sonde et la surface alors qu'un contrôle de backstepping n'en a pas besoin.

Pour communiquer avec l'environnement développé par notre partenaire, nous avons utilisé les bibliothèques Boost pour créer un espace de partage de mémoire. Ce choix nous aide à échanger la position du dispositif haptique avec l'interface utilisateur. Avec cette méthode, nous avons pu déterminer la couche dont l'aiguille interagissait et calculer les forces souhaitées pendant le test.

Le système proposé est le premier prototype partiellement fonctionnel du simulateur d'injection dans le cadre du projet SPARTE. Ce simulateur peut être mis en œuvre pour des études et des tests avec des praticiens experts, afin d'obtenir un retour qualitatif pour améliorer le réalisme et l'immersion du système.

Part II

Thesis's Development in English

Chapter 1

General context

1.1 Medical Context

The aspiration of joint effusion, soft tissue fluid collection, and injection inside the articulation (knee, shoulder, hip, wrist, ankle) are common techniques utilized in various treatments and as routine procedures used by rheumatologists to relieve pain [Balint et al., 2002].

Aspiration techniques are used to extract the synovial fluid, in order to analyze it and to establish the diagnostic of inflammatory/septic arthritis. The injection is used to dose local steroid and anesthetic for pain relief. The last method is used as a treatment of osteoarthritis that is the most common reason for articulation injection [Douglas, 2014]

The aspiration or injection process has been used during decades. The use of anatomical landmarks in the body helps to guide the needle inside the articulation. The palpation-guided proximal interphalangeal is a traditional method used by doctors to guide the needle into the articulation as well as to aspirate synovial fluid. The ability to place a needle accurately within the joint space is quite essential to obtain a successful treatment. However, most rheumatologists ensure that without the help of imaging guidance, the location of the needle is quite challenging in small articulations or even in large ones such as the knee. Some studies reveal that under palpation guides, 59% of the cases were extra-articular, without the possibility to extract any fluid due to this [Peetrons and Court-Payen, 2009]. Therefore, methods based on ultrasound images tend to be more accurate during the puncture.

Figure 1-1 – Photograph of right knee demonstrating the superolateral approach to aspiration or injection of the knee via the suprapatellar bursa [Douglas, 2014].

Ultrasonography is an available imaging modality used for guiding interventional procedures in the musculoskeletal system. The possibility to observe the exact needle tip placement in real-time confirms the accurate needle placement in the therapeutic injection, fluids aspiration, and soft tissue biopsies [Sofka et al., 2001]. This method also has several advantages over the traditional ones: it is no invasive (in comparison to fluoroscopy imaging or computed tomography) and it does not have limitations like the fluoroscopy when the disease is confined to the soft tissue (muscle and tendons). The use of echography also helps to examine the joint and can reveal the presence of fluid collection such as bursitis; even before performing an unnecessary aspiration attempt on a joint that does not need it. This can prevent contamination of an aseptic joint that can occur by a blind procedure or a fluoroscopic aspiration, through an overlying soft-tissue infection (abscess, septic bursitis, or septic tenosynovitis) [Douglas, 2014].

1.2 Intraarticular needle injection under Ultrasound-Guided

1.2.1 General technique

Once the joint problem is detected, the needle's size is selected by measuring the depth from the skin entry point to the deepest portion of the fluid. Then with the transducer positioned over the effusion, a doted " + " is formed using ink on the skin to mark the entry point

(Fig. 1-2). This entry point of the needle is checked for accuracy in both longitudinal and transverse planes (Fig. 1-3).

The mark must be carefully placed, as its bad positioning is a major cause of an unsuccessful injection or aspiration process. After that, the surface is correctly cleaned with Betadine or sterile drapes, and the transducer covered with a sterile probe cap. During the process, a freehand aspiration or injection technique is commonly used, with constant monitoring of the needle advanced using the ultrasound probe (US).

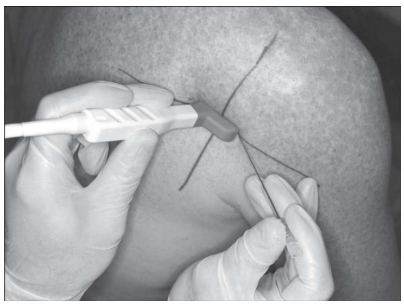

Figure 1-2 – Glenohumeral joint aspiration using sonographic guidance. Photograph shows transducer positioning for transverse sonography of posterior right shoulder and needle positioning for aspiration [Fessell et al., 2000]

.

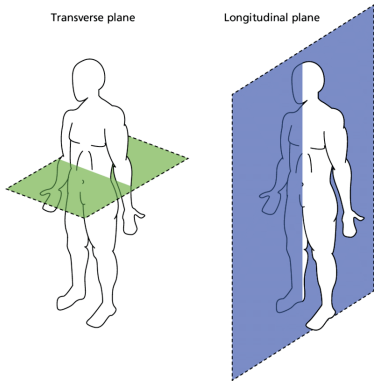

Figure 1-3 – Longitudinal and transversal plane

If the needle tip is not visualized in the 2D image during the performance a small movement of the transducer is widely recommended before any progression of the needle, in order to find the correct cutting plane, also to enhance the needle's localization, a Doppler evaluation can be helpful to detect it within the soft tissue [Peetrons and Court-Payen, 2009].

As well, it is suggested that the more parallel the needle is to the surface of the transducer, the better the needle will be visualized as a linear hyperechoic[1] structure with posterior reverberation artifact[2] [Sofka et al., 2001].

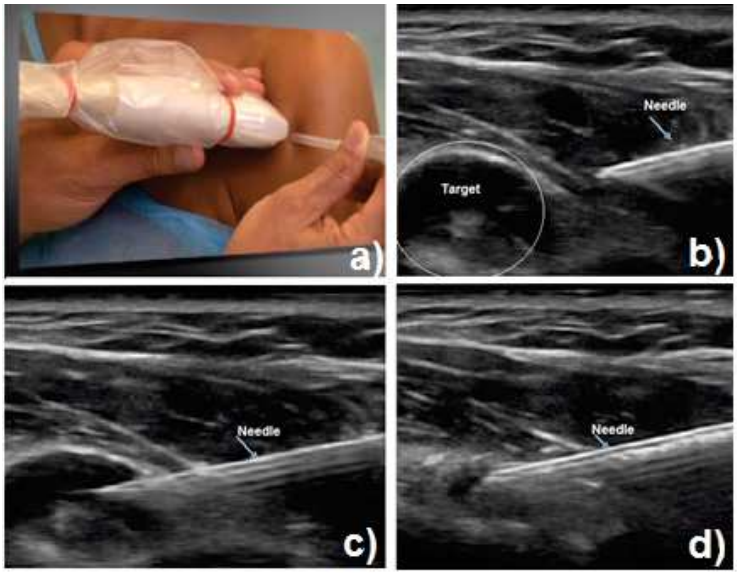

Figure 1-4 – Needle advance monitoring using ultrasound-guided

Thus, the technique is quite challenging due to the fact the user requires to use both hands at the same time and synchronize their motion in order to make the needle visible in the 2D image (Fig. 1-4). With one hand, the ultrasound probe is held to explore the articulation and try to keep the needle inside the image. Meanwhile, using the other hand, the needle is manipulated to pierce the articulation to retrieve or inject but doing a wiggling movements to avoid touching a vein or cartilage. During the process, doctors must focus his attention on observing the monitor instead of his hands' movements. So, doctors need to develop a motor visual-coordination dexterity that is acquirable with practice and allows them to coordinate both tools at the same time, with both hands. Moreover, according to the position of the joint and the doctor, he will need to exchange hands. It means instead of holding the syringe with the right hand it will be held by the left hand and the same case for the ultrasound probe.

[1] Denoting a region in an ultrasound image in which the echoes are stronger than normal or than surrounding structures.

[2] It occurs when an ultrasound beam encounters two strong parallel reflectors.

Doctors must train to master this technique as a bad injection could lead to several problems like:

- Infection during infiltration: septic arthritis estimated at 1 in 78,000.
- Joint inflammatory reaction: 15% but generally mild.
- Hot flush: 12% but mild.
- Tendon rupture.
- Chondrolysis.
- Depigmentations and skin atrophy.
- Cytosteatonecrosis.

1.2.2 Anatomy

For our case of study and similitude with the rest of the articulations (hip, ankle, knee), we are going to focus on the shoulder articulation. This section concerns the different tissues that interact with the needle during the injection or aspiration. The shoulder girdle consists of the scapula and clavicle, which articulates with the chest wall, and the proximal humerus, which articulates with the scapula (the glenoid). The humeral head and the glenoid vault of the scapula form the osseous components of the glenohumeral joint of the shoulder (Fig. 1-5).

Soft tissue components

The most common location on shoulder injection is the subacrominal space of the shoulder. The subacromial space exists as a bursal cavity lying between the rotator cuff and the acromion. Also, the most lateral component of this cavity becomes contiguous with the subdeltoid bursa/space (Fig. 1-6)

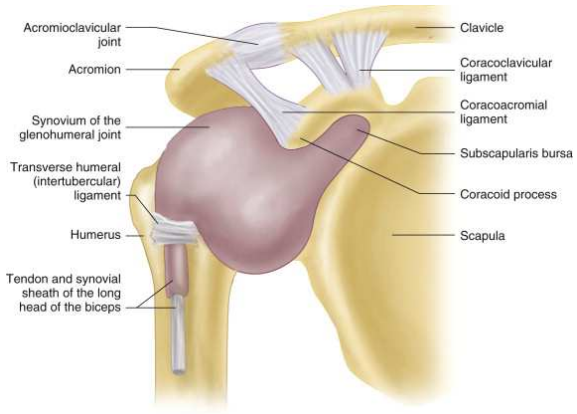

Figure 1-5 – Shoulder girdle [V. Lawry et al., 2010]

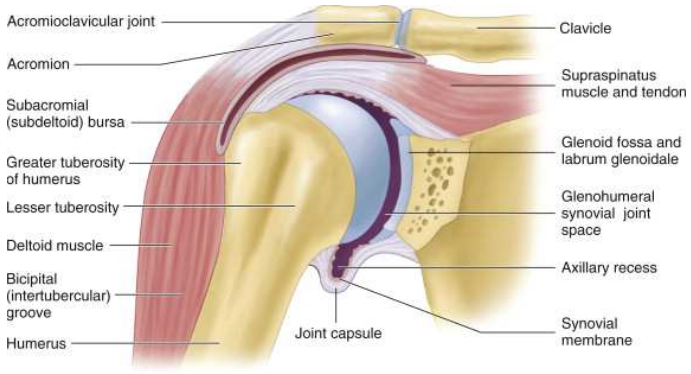

Figure 1-6 – Subacrominal space [V. Lawry et al., 2010]

1.3 Medical Formation

In general, medical students learn the theoretical aspects of any procedure during the lectures. Then they proceed to observation using videos of real procedures and watching real procedures in operation rooms. They also have an explanation and make their first tests on manikins before acting in real under the supervision of an expert.

For a more realistic test, several possibilities are available for medical students. They can practice on animals, corpse, manikins, or simulators, to help them improve their skills before practicing on real patients, but this can lead to a problem. According to the nature of the procedure, it is not always suitable to train on cadavers or animals (for instance, in obstetrics). There is also an ethical problem, and sometimes it could be forbidden in certain countries (Muslim countries). For this reason, a simulator can be a suitable way of training.

Concerning the intraarticular needle injection under ultrasound probe, one of the problems that occurs while learning on simulators is the impossibility to simulate different stiffness that are inherent in the body (skin, fat, muscles, and ligament). The restrictive movement of the needle is another issue to solve, as these simulators fix the insertion points, losing realism during the process [Gonenc and Gurocak, 2012a].

1.3.1 Simulators

Any medical process entails risks for the patient, especially if the practitioner is inexperienced. Several health authorities demand, from an ethical point of view, a way to practice without risk for the patients. One example is the French H.A.S. [3] who stated to medical students to "never make it the first time on a patient" [Granry and Moll, 2012]. Because of this, medical simulators increase their popularity in recent years.

The most advanced simulators dedicated to the health professions aim to offer the learning of complex, precise, or delicate gestures with the contribution of haptics and virtual reality. There are several types of simulators for medical procedures, among which we can mention those for gynecology, surgery, or anesthesia. For needle training, common processes include obtaining blood or biopsy samples. Also, they can be used in procedures to suture wounds from surgical procedures, or even in complex tasks where the performance must be accurate as in lumber puncture [Coles and John, 2010]. For our particular study case, we are focusing on the development of an intraarticular needle insertion under echography, as it is explained in section 1.5.

In [Coles et al., 2011], the authors presented an augmented reality simulator for femoral palpation and needle insertion. For the palpation part, they used two Nolvint falcons that support the touching zone a recreates the behavior of the patient's skin. For rendering the insertion, they used a modified Phantom Omni, whose end effector resembles a real needle. The force feedback is taken from a set of recorded data of multiple patients and evaluated by its partners. Although the presented results are satisfactory for the palpation part, the needle injection simulations lack realism, as it is required 6 DoF (3 cartesian and 3 articular) of

[3] Haute Autorité en Santé, the authority in charge of healthcare issues in France

force feedback and the phantom Omni can only provide on the cartesian space.

In [Podder et al., 2006], authors proposed to use a statistical model based on acquired data from a measurement campaign. The model includes parameters for several pathology and patient profiles. However, the model does not include data for intraarticular needle injection of the desired joint (knee, shoulder, wrist), which limits its use to our purpose.

The use of FEM is widely spread due to its accuracy in calculating the behavior of the tissue during puncture or deformation. One example is the method presented by [Yang et al., 2014] where authors used a tetrahedral mesh to successfully compute the reaction forces in the needle while injecting. However, FEM is very well known for its highly demanding resources, which impedes by the moment, being applied in online estimations for haptic simulators.

Several researchers around the world have focused their efforts on the creation of a more realistic and immersive simulator. These simulators are divided into two categories: passive and active, depending on their nature and how they generate force feedback. Because of the low quantity of simulators found in the literature that focus on our study case, we expanded our bibliography research to general needle insertion procedure for a better understanding of the state of art.

1.3.2 Passive simulators

Nowadays, it exists some passive simulators that try to reply to the needle insertion sensation. The force feedback is given by the materials that compose the simulator and such stiffness resemble the skin, muscle, and fat of a patient, hence this force feedback is not generated by any actuators and thus it can not be controlled.

The EIT 100 developed by Pharmabotics Ltd, is a device focused on training epidural and spinal anesthesia procedures. This simulator has a fake skin made of rub where the student can palpate and found the insertion point of the needle. During the injection, it is permitted to adjust the needle in all degrees of freedom, which improves the realism. The device also provides the simulation of fluid in the syringe due to the dural mater puncture and the simulation of epidural catheter insertion (Fig. 1-7a).

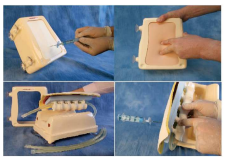
(a) EIT100 Lumbar puncture


(b) Simulator Life/form ®


(c) M43B Epidural simulator

Figure 1-7 – Commercial passive haptic systems.

Developed by eNasco, the simulator Life is used to train spinal injection techniques and epidural analgesia. It provides a realistic palpation simulation and offers resistance during the injection, and the change of needle positioning/orientation. As it is dedicated for epidural injection, it also allows collecting fluid during dural mater puncture (Fig. 1-7b). Although this simulator allows a free needle movement insertion in the back, and it closely resembles the human lower back, it is only able to reproduce one patient profile, without the possibility of providing different force patterns.

Other simulators to train doctors in needle puncture are the M43B, MW18, and US-9, all developed by Kyoto Kagaku [4]. The M43Bm is used to simulate the needle insertion in the back. This manikin can simulate different patient anatomy profiles, with the possibility of having a real needle attached to the syringe. It provides force feedback in the resistance and pressure during needle insertion. It also allows palpating the surface of the needle's insertion (Fig. 1-7c).

The MW18 (Ultrasound-guided of the peripherally inserted central catheter) helps to practice positioning of the catheter in central venous network with the help of the needle; the ultrasound is used to supervise the needle entrance in the vein. The simulator provides different levels of challenges to insert the catheter.

Finally, the US-9 is a simulator of ultrasound-guided breast biopsy. The phantom is used to practice fine-needle aspiration biopsy, core needle biopsy, and Mammotome biopsy that can be performed under ultrasound guidance. The simulator provides tissue of the breast phantoms, which helps to represent the softness and the resistance of the mammary gland.

[4] www.kyotokagaku.com

It also provides a different level of training as well as it is designed to improve the skills in hand-eye coordination in ultrasound biopsy.

One no commercial simulator has been developed to train the use of ultrasound during the needle insertion for different procedures (tissue biopsy abscess, drain). The system developed by [Magee et al., 2007] includes physical elements like a full-scale mannequin made of plastic latex and foam, a mock ultrasound and a needle, both attached with a magnetic 3D position/orientation sensor. The used Software generates a virtual ultrasound localized on the measured position of the mock probe and the needle, creating an anatomy model with the collected data. The virtual anatomic images were generated based on anatomic data derived from a full-body scan of a live human. Visual feedback is provided when the needle is inserted in the body. However, the main limitation lies in the fact that it is not easy to change the mannequin texture.

A more rustic simulator can be implemented by using simple methods. In the investigation performed by the authors [Pedersen et al., 2017], it is demonstrated that the Greengrocer's Model, which simply consists of a banana, can be implemented to teach needle insertion to the medical students affordably. The objective of this study was to prove that simulators are not efficient enough and need improvements; as they deliver the same haptic sensation that a banana, which obviously is a cheaper system. It is stated by the authors, that the Greengrocer's Model method presents some disadvantages against simulators. One of them is the hard zones, like bones, as the banana's consistency is not able to exert the required stiffness for simulated them. The second main disadvantage is realism during the insertion. For the Greengrocer's Model, this procedure feels unreal while in simulators the sensation is more immersive. From this context, authors encourage the use of simulators, instead of the Greengrocer's Model, followed by training on real patients.

In conclusion, the presented passive systems offer the possibility of train needle insertion in several areas of the body. The use of mannequins improves the immersion by providing a solid object that the student can identify during and examine during the test. However, this also limits the simulator to one profile, impeding the student to train with several environments or profiles. Also, the mannequins wear down between each season, which, in turn,

reduces its quality and life-time. To be able to offer different profiles and environments, will need an easy-to-reconfigure system that does not depend on physical supplies. The most convenient option is to use haptic devices.

The next subsection introduces the definition of haptic, the technologies used to render the force feedback and a study of active simulators.

1.4 Haptic

1.4.1 Definition

Haptic comes from the greek "haptikós". This broadly refers to physical contact or touch interaction [Salisbury et al., 2004]. The interaction can be between a human hand and a real objective, or human hand and a simulated object. Haptic can be divided into two modalities: tactile sensation and kinesthesia sensations [Culbertson et al., 2018]. Tactile sensation is the ability of the human to receive information about an object like its texture, elasticity or shape. In this work, we are more interesting in the second modality.

On the other hand, kinesthesia is the ability of the human to sense the position and movements of his/her limbs. Kinesthesia made use of the proprioceptive cues that arise from the receptors that are ubicated in joints and muscles. Humans also can get a kinesthesia memory, which helps them to remember the position of their limbs that have been exposed during long times. Thanks to kinesthesia memory, humans can remember patterns, positions, and forces through a haptic training [Feygin et al., 2002].

Haptic training can be achieved with the repetition of the task of interest and can be achieved with the use of a haptic interface that allows the user to train in virtual environments.

A haptic interface device can be described as a system that allows exchanging mechanical energy with a user to give the sensation of interacting with virtual environments. This device-body interface can be in contact with any part of the body, but most of the time are widely used as hand interfaces.

Haptic devices also can be distinguished by their intrinsic mechanical behavior: *impedance*

and *admittance*. Impedance systems concern the systems which read the position and apply a force. Admittance systems concern the systems which read the force and apply a position.

1.4.2 General technologies

For practical issues, the implementation of electrical haptic systems are mainly used because of their advantages such as the low cost, clean, easy to use, no auditory noise, and no complicated installation requires (Fig. 1-8) in comparison with pneumatic and hydraulic systems.

(a) Geomagic Touch (b) Novint Falcon 3D Touch

Figure 1-8 – Electrical haptic interfaces

An advantage of pneumatic actuators which their output is a force in the function of the compressed air used to transform the energy from the power source. Considering that the air is clean, cheap and inflammable (and the air does not need to return to the compressor, unlike hydraulic systems) is an excellent choice when a high volume/power ratio is needed compared to electric actuators.

There are different haptic systems that exist with classic and novel actuators. Both have advantages and disadvantages depending on the application these can be chosen.

New actuators using novel technology, like piezoelectric actuators, have certain beneficial characteristics such as feedback of tactile information by applying high voltage to change the crystal shape and obtain a translation. However, the translation is given in μm, which can be a disadvantage when large translations are needed.

On the other hand, it exists the Shape memory alloys, which are a group of metals that

return to its previously defined shaped when they are subjected to the appropriate temperature. These can generate large forces if they encounter resistance during its transformation. The disadvantage is the time required to respond, as they vary from ranges of seconds to minutes, leaving out for the use of haptic feedback tasks.

Although it exists Electro-rheological fluids. These materials change their viscosity behavior instantaneous. By applying an electric field and returning to its liquid state by deactivating the electrical field. However, that overcome the problems like the time of response, and for generating the electrical field, a high voltage is necessary (around 2- 4kV per millimeter gap between the electrodes) which make it risky and unsafe to work with it [Le, 2011]

1.4.3 Active simulators

Compared to passive simulators, active simulators allow to control the force feedback that is generated using actuators, that can give the sensation of different stiffness during the needle insertion. Also, these systems allow recording all the data information during the process, which can be studied and compared to evaluate the student 's performance on each test.

Nowadays, several active devices are used to built simulators by researchers or private companies to learn or improve the medical's skills. One example is the commercial simulator ARTHRO Mentor II, developed by 3D SYSTEMS® (Fig. 1-9) supports interchangeable anatomical models to train arthroscopy with haptic feedback. However, the system has a high cost, which could impede its acquirement. Also, the restricted design only allows performing one specific manipulation, and the simulator concerns only one joint.

The use of a DC servomotor and magnetorheological brakes are also present in the creation of a virtual needle insertion simulator. In [Gonenc and Gurocak, 2012b] authors proposed a hybrid actuator design, which is formed by coupling a miniature DC servomotor with a powerful brake through a winding path design technique which can demand forces up to 10N in the presence of stiff tissues such as bone. The simulator allows reproducing the forces generated during the needle puncture, insertion, and withdrawal. However, they demonstrated with experimental validation that to have a more realistic force rendering, the

Figure 1-9 – Commercial active haptic systems; 3D Systems®

process should be done with both motor and a brake coupled. However, some drawbacks exist like the fact that needle insertion can be performed only in the vertical direction, the point of insertion is fixed, and it is not possible to change the trajectory during the simulation.

Different ideas have been developed to improve the rendering haptic of needle insertion. For example, [Kurita et al., 2014] instrumented a Geomagic Touch in a virtual environment, they set a virtual needle that can interact on a rubber sheet to obtain several forces needle responses like the pushing force from the needle and the reaction force of the rubber sheet. And thus, as the forces are reproduced when the virtual needle tears on the rubber sheet, and the force when the needle passing through the rubber sheet as well. Despite introducing the rubber to improve the rendering forces, it does not allow to work with different layers at the same time, different tissues and hard surfaces like the bone.

A simulator developed by [Magill et al., 2010] uses four brushless motors and a cable arrangement to apply motor-generated forces to the needle. The system can reproduce different stiffness of the skin in varying depths through a linear elastic model. The main problem is that it does not allow to choose the needle's insertion point.

In [Heng et al., 2006], authors developed a Chinese acupuncture simulator by modifying a Geomagic Touch, and using a Fuzzy controller. The original stylus of the haptic device was unclipped, and they attached a needle on it to give more immersion. The simulation is visualized in a transparent mirror display that offers a stereo vision. Due to the nature of the process for which it was created, the simulator works over predefined pressure points. It also lacks the main property of changing the angle during the process due to the Geomagic

Touch being actuated only around 3 degrees of freedom (DoF).

By using two Geomagic Touch, authors of [Forest et al., 2007] achieve a simulator for ultrasound-guided needle puncture. In this configuration, one Omni is used to represent the needle forces during the insertion (puncture and removal) and the other to simulate the ultrasound probe. They created a virtual environment where a 2D image ultrasound is displayed during the performance; this image was based on data obtained from real ultrasound images. Hence the ultrasound image only displays one real patient profile. However, the simulator does not offer surface support where the user can lie his hand to avoid trembling during the needle insertion.

Another ultrasound-guided needle simulator is the one presented in [Magee, 2005]. The authors use a mannequin to represent the patient. The ultrasound probe and the needle have 3D position sensors. On a screen, the software recreates the ultrasound image, and for the force feedback, the needle has a slide mechanism that contracts itself when collisions occur with the plastic mannequin. This simulator allows to puncture any part of the patient's body but does not constrain the position of the needle, avoiding the reproduction of clamping forces.

Several authors propose the use of haptic devices to simulate the ultrasound probe. An example is [Sclaverano et al., 2009], where authors presented an ultrasound simulator that uses a Geomagic Touch 3D. The haptic device allows free movement in the workspace, and the ultrasound probe is rendered in a virtual environment with a virtual patient. When the simulated ultrasound probe collides with the virtual patient, the image is rendered on the screen. The echography is obtained by interpolating, from a database, the images of real ultrasound tests. The system compares the position of the haptic device with the exerted force and the patient profile to deliberate a result.

Some ultrasound probe have been simulated using two haptic devices at the same time. Authors of [Goksel et al., 2011] proposed a simulator for prostate brachytherapy. The operation consists of the insertion of the ultrasound probe through the rectus and the needle that carries the treatment in the lower part of the pelvis using a template as a guide. During the process, the doctors see the trajectory of the needle to ensure the correct collocation of

the radioactive seeds. The proposed simulator (Fig. 1-10) used a Geomagic Touch attached to a mechanical structure that replicates the template used for the needle insertion. For the ultrasound probe, two Novint falcon are used. The system uses FEM (Finite Element Method) to simulate the deformation of the tissue and the image of the probe by determining the coordinates of the needle. Despite this simulator accomplishes some of the desired haptic interaction needed in our case (needle insertion and the use of an ultrasound probe) impossibilities the user to choose a free insertion point.

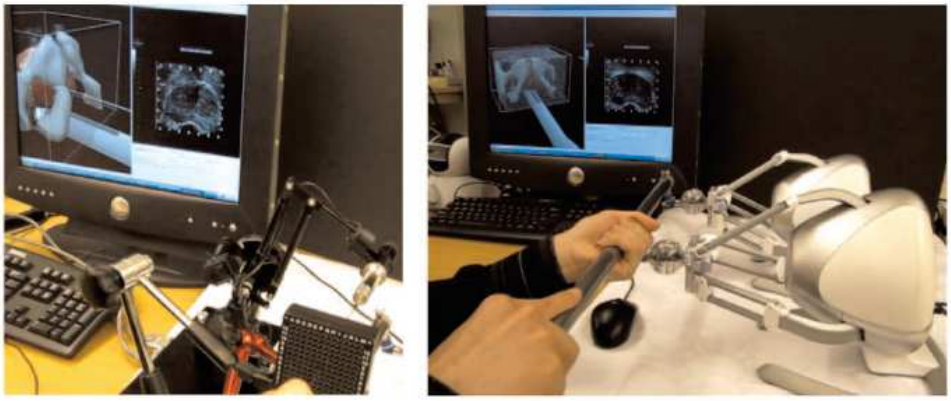

Figure 1-10 – (a) Needle insertion through template using a brachyther- apy needle instrumented with a Sensable Phantom device, and (b) manipulation of a mock probe instrumented with two Novint Falcon devices [Goksel et al., 2011].

The use of pneumatic actuators can help in the simulation of the ultrasound probe as well. Authors of [Raitor et al., 2017], create a wearable pneumatic haptic guidance device. This device uses plastic sheeting that is inflated to provide a normal force on the user's receptor sensors. This wristband was design to teach pattern tracking, but the authors also made tests simulating an ultrasound probe and a camera to localize the device during the task. Although the device gives more movement freedom that previous proposed haptic systems, the exerted force is not enough to get a realistic sensation of the probe touching the skin.

The authors of [Zhu et al., 2007] developed a simulator that helps to introduce the needle into a patient body under ultrasound guidance. This work is focused on including surfaces

and volumetric registration, solid texture modeling, spatial calibration, real-time synthesis, and rendering of ultrasound images to reproduce the gesture as closely as possible to reality. The use of a motion sensor attached to the ultrasound probe allows capturing the position and the orientation of it, although it is necessary to use a calibration process to locate the probe and needle using a square fitting algorithm. Soft tissue deformation appeared according to the needle movements, and the needle model is also considered during the process. Many imaging-graphic techniques were implemented to simulate ultrasound-specifics artifacts to generate a better image. Although the systems have a good improvement, it is still needed to introduce a virtual self-deformation model of the human body that simulates the motions of the internal anatomies, as well as an external dummy to offer the medical practitioners the ability to improve its spatial representation and hand-eye coordination skills.

In [Grottke et al., 2009] a virtual reality simulator for anesthesia training is presented. This simulator uses acquired data to determine the patient's tissue behavior during the injection, and a Phantom Omni with VR glasses to provide immersion to the student. Although this system allows the student to choose any entry point, it does not provide any wrist restriction, so the force feedback is only axial, and not limits the orientation of the needle.

For a better comprehension of the different characteristics of each simulator, Table 1.1 summarizes their different properties. For those simulators that do not have a proper name, we cite the author's name.

Table 1.1 – Needle injection Simulator comparaison table

Name or Authors	Classifcation	Syringe's haptic feedback	Ultrasound mock	Simulator
EIT 100	Passive	Fake skin Can adjust the needle in all DOF	No	Epidural training Only 1 profile
Life (eNasco)	Passive	Fake skin Can adjust the needle in all DOF	No	Epidural training Only 1 profile
MW18	Passive	Fake skin Can adjust the needle in all DOF	Haptic feedback with the fake skin	Epidural training Different levels of training
US-9	Passive	Fake skin Can adjust the needle in all DOF	Haptic feedback with the fake skin	Breast Biopsy Different levels changing the fake breast

Table 1.1 continued from previous page

Name or Authors	Classifcation	Syringe's haptic feedback	Ultrasound mock	Simulator
[Magee et al., 2007]	Passive	Full scale mannequinn made of latex Can adjust the needle in all DOF	Haptic feedback with the fake skin	Tissue biopsy Only 1 profile
Greengrocer's Model	Passive	Haptic feedback through a banana	No	Injection only Cheap Haptic feedback variable
[Gonenc and Gurocak, 2012b]	Active	DC servomotor Only vertical insertion No tilt restriction	No	Injection training Different profiles

Table 1.1 continued from previous page

Name or Authors	Classifcation	Syringe's haptic feedback	Ultrasound mock	Simulator
[Kurita et al., 2014]	Active	Geomahic Touch Rubber skin No tilt restriction	No	Injection only Only one layer Only 1 profile
[Magill et al., 2010]	Active	Brushless motors and cable arrangement Can adjust the needle in all DOF	No	Injection only Entry point fixed
[Heng et al., 2006]	Active	Geomagic Touch Can adjust the needle in all DOF Do not constraint the needle No tilt restriction	No	Acupuncture Only 1 profile

Table 1.1 continued from previous page

Name or Authors	Classifcation	Syringe's haptic feedback	Ultrasound mock	Simulator
[Forest et al., 2007]	Active	Geomagic Touch No hand support No tilt restriction	Geomagic Omni Set of images predefined	Ultrasound-guided needle puncture
[Magee, 2005]	Active	Slide mechanism Can adjust the needle in all DOF Do not constraint the needle	Ultrasound mock probe	Ultrasound-guided needle puncture
[Sclaverano et al., 2009]	Active	Geomagic Touch Can adjust the needle in all DOF Do not constraint the needle	Geomagic Touch Echography obtained by interpolating	Ultrasound-guided needle puncture

Summarizing, the main problems that found in the previously proposed simulators are:

- The lack of representing the different tissue stiffness during the needle insertion.
- The existence of a pre-established needle's insertion point, which restrains the tool's free movement.
- The lack of a virtual environment, which made them unrealistic.
- Only one specific body part is concerned that restrings study cases.
- Only one patient profile is available.
- No metrics or evaluation of student performances and progress are provided.
- No difficulty adjustment are available.
- Some of the tools/surfaces are disposables.

The next section, is dedicated to the introduction of the SPARTE project, who aims are to overcome these problems.

1.5 SPARTE Project

SPARTE stands for Simulator of Puncture for ARTiculations under Echography. Its main objective is to produce a simulator for learning puncture gestures on large joints under ultrasound. It aims to fulfill the requirements of the perfect simulator and overcome the main problems that the current needle simulators face.

The SPARTE project is partly funded under the impulsion of SAMSEI [5], which is an IDEFI project, whose aims to offer new training methods for medical students. Is mainly focused on developing simulators that help novices to gain experience before acting on patients, as HAS requires it.

[5]Stratégies d'Apprentissage des Métiers de Santé en Environnement Immersion SAMSEI, URL: http://samsei.univ-lyon1.fr/

The simulator consists of a digital part that reproduces the patient's anatomy and it can create US images from a biomechanical model of the joint in real-time ultrasound images. This part is coupled with a physical element that reproduces the haptic sensations the needle and the ultrasound probe.

SPARTE project brings together 4 laboratories and one health facility.

1. LBMC (Laboratoire de Biomécanique et Mécanique des Chocs - UMR_T 9406 [6]) is in charge of developing biomechanical models of the articulation.

2. LIRIS (Laboratoire d'InfoRmatique en Image et Systèmes d'information - *UMR* 5205 *CNRS* [7]) is in charge of computing real-time deformation of the soft tissues during needle insertion and the visual rendering based on the biomechanical models developed by LBMC.

3. LIBM (Laboratoire Interuniversitaire de Biologie de la Motricité - *EA* 7424 [8]) is in charge of studying current medical teaching/learning/training techniques concerning the intraarticular puncture and how to integrate it into the courses.

4. AMPERE (*UMR* 5005 *CNRS* [9]) our laboratory, which is in charge of developing the haptic devices that will be manipulated by operators.

5. HCL (Hospices Civils de Lyon [10]) is in charge of providing the medical expertise to check the relevance of each partner.

1.5.1 The "perfect" simulator

Based on the work by LIMB and discussion with practitioner the "perfect simulator" to train doctors in needle insertion under echography should have the following characteristic to allow a complete and immersive training experience:

[6] http://www.lbmc.ifsttar.fr/
[7] http://liris.cnrs.fr/
[8] https://libm.univ-st-etienne.fr/fr/index.html
[9] http://www.ampere-lab.fr/
[10] http://www.chu-lyon.fr/)

- To implement the use of a mock syringe with a real needle and a mock ultrasound probe to visualize it inside the body. Both must be as close as possible to their real-life counterparts.
- To offer haptic feedback of the forces rendering during the needle injection and the ultrasound probe interacting with the body.
- To be a customizable product, that helps to reproduce different patient/pathology profiles and also works with different joints/anatomy.
- To work under a pedagogic scenario where the needle's insertion point is not limited at just one point.
- To manage different levels of training: from finding the correct plane with the ultrasound probe (easy), to avoid touching critical points (nerves, veins, cartilage) with the needle during the insertion while watching the ultrasound images (expert).
- To get metrics of the student's gesture and progress during each session, to adjust the training process and evaluation of the acquired knowledge.
- To allow repetition of several study cases without the need of tools or disposables essay banks.

1.5.2 General objectives

This consortium aims to develop high fidelity simulators to train novice doctors in the procedure of intraarticular injections under echography. This will be done by considering the requirements and needs of the consultant rheumatologist. The purpose of the SPARTE simulator is to achieve the following criteria.

Criteria

1. To reproduce the forces involved during the needle insertion on the articulation.
2. To simulate the US Probe contact and the slip on the body.
3. To evaluate medical performance.
4. To implement a 3D model where the needle displacement inside the body can be observed.
5. To implement a visual 2D image that gives realism at the simulation when the US mock probe is rendering over soft and hard surfaces on the body. (Fig. 1-11)
6. To implement different pedagogic scenario

In this simulator (Fig. 1-11), the syringe/needle is represented by a haptic device (see section 1.4) and provides the forces generated during the needle insertion (pink zone). Another haptic device represents the ultrasound probe and exerts the forces generated during the interaction with the body (pink zone). These two haptic devices will allow the user to gain hand-eye-coordination (gray zone). A screen displays the virtual environment, which consists of a 2D ultrasound image supposedly generated by the ultrasound probe and used to show the needle's position inside the body, and a 3D biomechanical model where the deformed tissues are appreciated during the needle displacement (green zone).

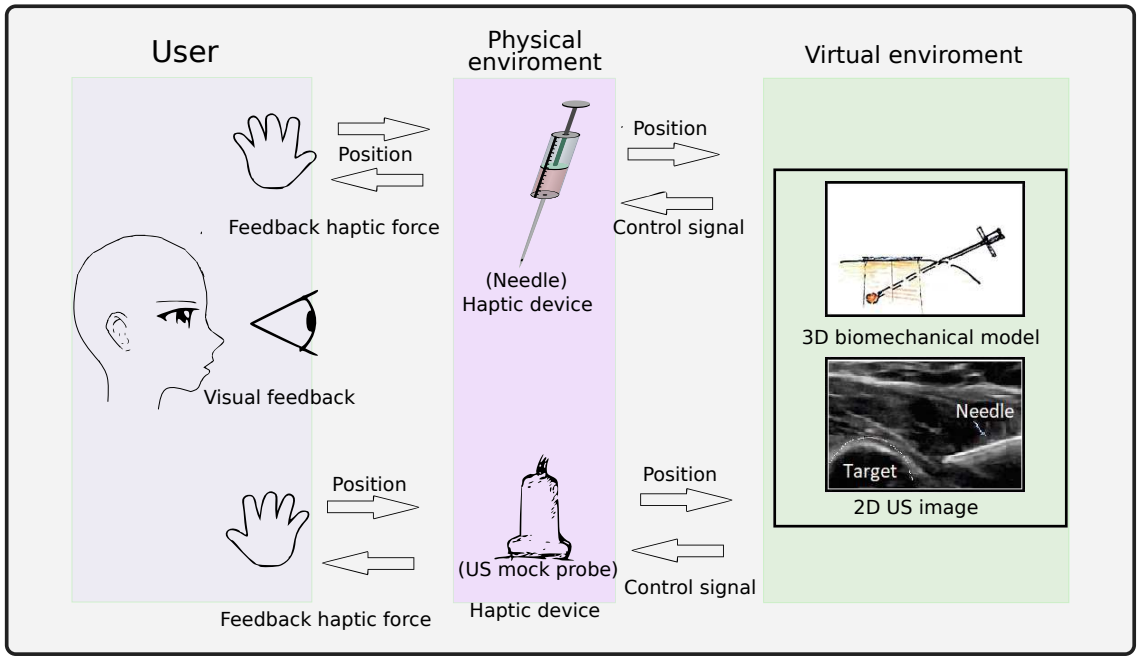

Figure 1-11 – SPARTE project, user-haptic interface scheme.

1.6 Objectives of my PhD thesis

As was mentioned previously, SPARTE project is a collaborative work between several instances. The objective of this PhD thesis is focused on the first two general criteria of the SPARTE project: haptic rendering of the forces produced by tools that will be used by the students (needle and US probe as shown in the pink zone of Fig. 1-11).

To accomplish these objectives, we divided the PhD work into three phases.

1. **Phase A: Needle implementation.**
2. **Phase B: Ultrasound probe implementation.**
3. **Phase C: Global design and communication with virtual environment.**

1.6.1 Phase A: Needle implementation

To simulate the needle insertion onto the articulation, using the haptic device, the following objectives must be achieved:

1. To allow the doctor to choose a needle insertion point in any place on the articulation.
2. Once the insertion point is selected, the haptic interface must keep the same direction, and if it is necessary, the trajectory can be modified within the body as long as "α", a prefixed maximum angle, is not exceeded (section 1.6.1).
3. When the needle tip is penetrating the body, different body stiffness must be rendered, according to patient's profiles and pathologists.
4. If the doctor stops his movement within the body, the needle must remain in the same position.

During the needle piercing in soft tissue, there are three primary stages, according to [Barbé et al., 2006], and each stage generates a set of forces (Fig. 1-12).

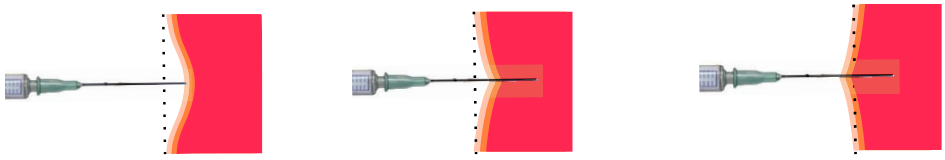

(a) Stage 1. (b) Stage 2. (c) Stage 3.

Figure 1-12 – Transition stages during the needle insertion in soft tissue.

Stage 1: Pre-puncture

Fig. 1-12a describes the forces $f_{puncture}$ that is generated when the needle is pushing the surface of the tissue which become deformed without being piercing. This behavior is described as a viscoelastic interaction [Y.C. Fung, 1993].

Stage 2: Puncture

Fig.1-12b describes the interaction forces generated after the needle pierce the skin. they correspond to the necessary forces to cut soft tissues. The authors [Kataoka et al., 2002] describe three forces that act during the puncture (Fig. 1-13). Considering that the needle shaft rubs against the tissue while it cuts the skin, three forces are considered, which are:

1. **The cutting force** $f_{cutting}$, this force acts on the needle tip in the axial direction. Its intensity differs according to the various tissue layers as well as the shape of the needle tip.

2. **The friction force** $f_{friction}$ acts along the side of the needle shaft in the axial direction.

3. **The clamping forces** $f_{clamping}$ are the forces that act on the side of the needle shaft in the normal direction by the tissue that surrounds it and help to constrain the needle's movements.

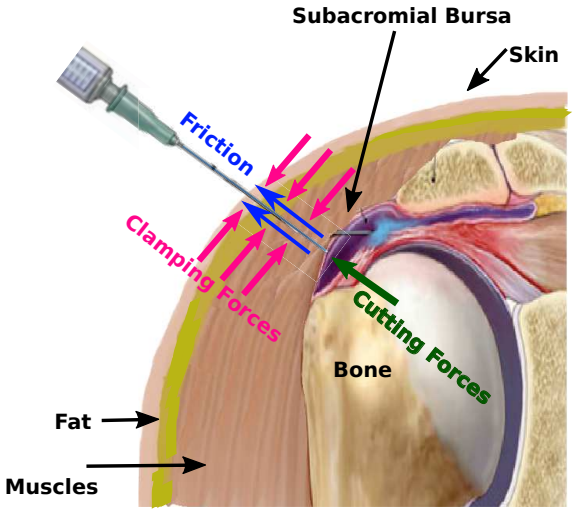

Figure 1-13 – Interaction forces during needle insertion.

Stage 3: Withdrawal

The third stage describes the force when the needle is extracted from the tissue, and it is attracted in the needle motion direction. This force will be considered as the **Attracted Force** $f_{attracted}$.

Another force that is considered in our work is the $f_{HardContact}$ which is generated when the needle tip collides with the bone during the insertion. Also considering this force helps us to warn the user to stop his movement to withdraw the tool from the tissue to avoid moving forward.

Thus, the total forces that act on the needle are represented by Eq.(1.1)

$$f_{total} = \begin{cases} f_{pre-puncture} + f_{cutting} + f_{friction} + f_{clamping} + f_{attracted} & \text{soft} \\ f_{HardContact} & \text{hard} \end{cases} \tag{1.1}$$

Where the condition $soft$ is computed during needle tip is in contact with tissue and *hard* when the needle tip collides with bone.

Insertion angle

α is a parameter that allows changing the needle's direction during the insertion to avoid touching a bone, nerve, or vein. This angle is in the function of the needle's depth, limiting the angle during the injection when the needle is in phase two and cut for the first time the tissue. At this moment, the maximum angle allowed to change the trajectory is 45° respecting the main axis of the needle, forming a cone in the space (Fig. 1-14). However, as the needle is moving forward, the needle's body is restrained more and more, and therefore, the angle starts to reduce as much the depth increases. Moreover, when the needle is extracted from the tissue, the needle's body is released, and the angle α increases its value

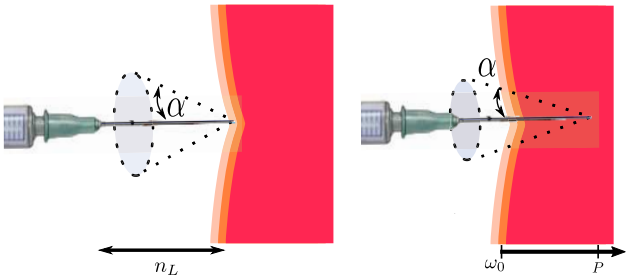

Figure 1-14 – α behaviour during needle insertion. Where ω_0 and P are the insertion point and the current point respectively and n_L represents the needle length.

The Eq. (1.2) is proposed to determinate the angle "α" depending the needle depth.

$$\alpha = tan^{-1}(\frac{n_L + d_t}{n_L - d_t}) \tag{1.2}$$

where $d_t = \left\|\overrightarrow{P\omega_0}\right\|$, which is the current needle depth and it is calculated when the tool pierces the tissue, and n_L is the needle length used to infiltrate the articulation (generally $n_L = 3.5$ cm or $n_L = 2.5$ cm)

1.6.2 Phase B: Ultrasound probe implementation

This phase is focused on introducing the forces that the ultrasound probe generates when it is in contact with the patient's articulation. The representation of the ultrasound probe mock is a crucial point to help the doctors to develop their skills during the procedure. Having the two physical tools (ultrasound probe and needle) will help the students to develop the desired motor coordination. It is important to remember that the ultrasound image helps to guide the needle movement inside of the tissue using the ultrasound probe. To keep the needle tip visible in the 2D image, the ultrasound probe can be displaced around the point of insertion. During this movement, different tissues are in contact with the head's probe, which can be rendered as soft or hard surfaces. As well it is required that the users can manipulate the mock with the same freedom they have on a real-life procedure.

The objectives to accomplish these criteria are:

1. Manipulation of US mock probe with haptic feedback.
2. Rendering of soft and hard contact during the interaction with the articulation.
3. Position/ orientation according to the joint/needle.

Constraints

When the ultrasound probe is in contact with the skin, a normal force named $f_{surface}$, is generated (Fig. 1-15). As can be appreciated in Fig. 1-15a when the ultrasound probe is exploring a soft zone (a zone that has elastic behavior), the tissue that is under the skin generates resistance when the user is pressing the ultrasound probe against the patient. This resistance is given by the tissue's stiffness. As the user continues exploring the limb, $f_{surface}$ changes depending on the depth of the probe on the tissue. When the tool interacts with a hard zone (a bone for example), the probe will be only able to displace a small distance between the skin and the hard zone. As there is no significant displacement, a large force is caused by the contact between the tool and the hard zone, which the user interprets as a hard contact (Fig.1-15b).

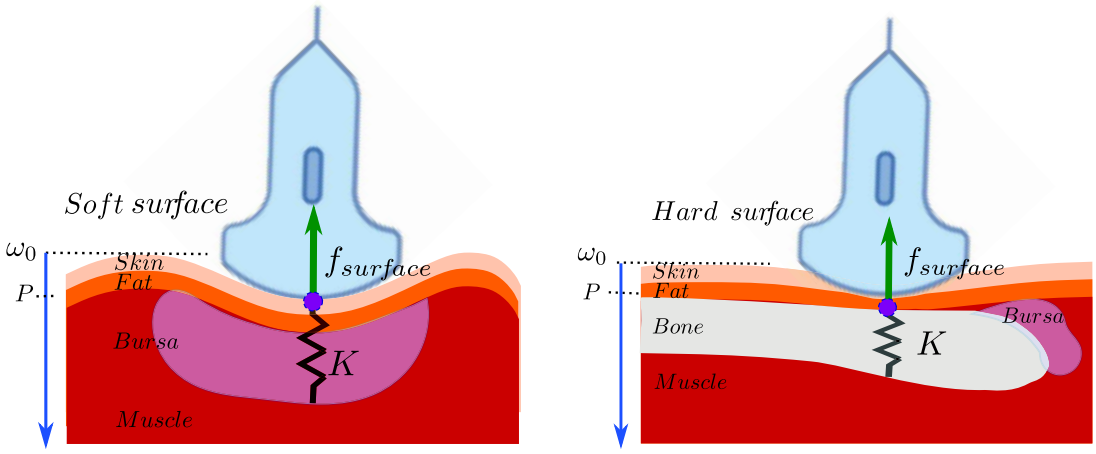

(a) Soft contact (b) Hard contact

Figure 1-15 – Collision force diagram between two virtual objects

1.6.3 Phase C: Global design and communication with virtual environment

This part corresponds to assemble a functional prototype of the simulator.

For instance, we need to physically represent the syringe and the ultrasound probe with our haptic devices. For this, we require to develop a mechanical design that increases the immersion of the created virtual environment and meet the comfort requirements of the medical staff. To achieve this, the medical partner must evaluate the prototypes that will be developed. From each iteration, we would improve the design until it fulfills the practitioner' needs.

Once this is provided, we must assemble our haptic device, mechanical base, force feedback algorithm, and virtual environment to work with our partners. As well as establishing the communication between the our partners' algorithms and ours, to exchange data.

1.6.4 Scientific approach

Based on the requirements given in section 1.5.2, a bibliography review of existing injection/ultrasound probe simulators involved forces during needle injection and methods used for rendering forces was effectuated. From this review, we determinate the advantages

and disadvantages of the previously proposed simulators and approaches used for rendering forces. In this part, we select the haptic devices to be used for the needle injection and the ultrasound probe, based on their mechanical characteristics and limitations. We also decide which force rendering methods to use, improve or even propose a new one that fulfills our expectations. At the beginning of the research, we do not have a realistic environment developed by LIRIS, we create a proper one by using an open-source multi-platform framework that helps to ubicate the tool in the virtual world during the tests. Finally, with the system prototype and the environment provided by the LIRIS, we experimented with a medical expert from our partner HCL to receive qualitative feedback about the realism and immersion of the system, in order to continue its improvements.

Chapter 2

Haptic feedback during needle insertion

In this chapter, we are going to introduce the different models and method approaches to render the forces of each stage during the needle insertion. For testing these models and the development of the simulator, we used a Haptic Virtuose 6D desktop, which is a haptic device with 6 motorized degrees of freedom and can offer a peak force of 10 N. More details of this device are given in chapter 4.

Remembering Eq. (1.1), two original methods are proposed for rendering $f_{cutting}$ and $f_{clamping}$.

$$f_{total} = \begin{cases} f_{pre-puncture} + f_{cutting} + f_{friction} + f_{clamping} + f_{attracted} & \text{soft} \\ f_{HardContact} & \text{hard} \end{cases}$$

The first method is named "Tracking wall", developed to reproduce the forces that are generated when the needle moves forward and cuts the tissue ($f_{cutting}$), and the forces when the needle is withdrawn ($f_{attracted}$). Due to the simplicity of this method, it is easy to compute and the most important we can achieve two objectives of the needle insertion:

- To compute the different body stiffness according to the patient's profiles and pathology.
- To ensure that the needle remains in the same position if the needle stops within the body without using any dissipative element.

The second method named, "Orthogonal projection", helps to compute the normal forces that constrain the needle's movement during the insertion ($f_{clamping}$), in order to guide the needle and follow the desired trajectory.

2.1 Model and method approach to render the forces during needle insertion

While developing injection simulators, the main issue to face is to give realistic haptic force feedback of the tissue pierced. Recompiling the methods and techniques that researchers use, two approaches can be highlighted: model approach and method approach [Corrêa et al., 2019].

The model approach, as their names suggest, is based on the use of biomechanical mathematical models. These models consider the plasticity, viscosity, and elasticity of the tissues during needle penetration and, due to their mathematical complexity, require many resources and time to process the information, which limit the possibility to obtain results for real-time application such as control of haptic feedback device.

For method approach, researchers use algorithms that aim to imitate the feeling of needle insertion. The use of low demanding resources of these methods allows them to be used in mid-range computational equipment in real-time simulations, however, they are considered as semi-realistic.

2.1.1 Model approaches

The use of finite element approaches (FEM) is widely spread in the use of medical simulators. As FEM are also known for their high computing requirement, [Zhang et al., 2014] proposed a method for deformable objects. Their method is based on a layered rhombus-chain-connected, which can be interpreted as a pyramid of spring interconnected. Their results prove that their method is a good replacement for FEM at a lower cost.

Based also on this approach, [Li et al., 2014], proposed a modification of the FEM

method named Co-rotational Linear FEM. The technique allows them to simulate the dissection of a body part. The authors enlighten that the main disadvantage of this method is that it is only possible to make a cut per element, so the size of the element determinates the number of cuts that are possible in the virtual object.

The use of advanced software and hardware implementations is commonly found in the bibliography. These methods can be applied to compute cutting and friction force, due to both forces are axial. One example of this is the method explained by [Courtecuisse et al., 2010], where the authors used a finite element approach to mesh a 3D model of a virtual liver for a laparoscopic procedure. The method is heavily hardware dependent as it uses GPU units to process the algorithm in parallel. The results show that the haptic training can be performed with a realistic behaviour of the laparoscopic procedure. It is also possible to cut the model in real-time as the algorithm introduces new elements into the mesh when this occurs. All the process is rendered at 70 Fps (Frames per second) for the animation. However, as the authors have established it, the optimization is a difficult process and the high requirements of hardware limit the method implementation for other medical procedures.

Pre-puncture: $f_{pre-puncture}$

Another model approach also has been obtained from the characterization of tissues during needle insertion. Several authors have parameterized the tissue behaviour when it is in the *stage 1*(section 1.6.1), obtaining models that response close to the real one. One model is obtained by authors [Simone and Okamura, 2002] where they obtained the forces during the pre-puncture $f_{pre-puncture}$ in a bovine liver. As the pre-puncture behaviour is non linear, this can not be modeled as a linear elastic material. The authors describe the forces using a second-order polynomial (Eq.(2.1)) where the puncture forces increase steadily, and a sharp

drop in the amount of force indicates the puncture event [Abolhassani et al., 2007].

$$f_{pre-puncture} = \begin{cases} 0, & P_{tip} < d_1 \\ a_1 P_{tip} + a_2 P_{tip}^2, & d_1 < P_{tip} \leq d_2 \\ 0, & P_{tip} > d_2 \end{cases} \tag{2.1}$$

where P_{tip} is the needle's tip position and d_1, the starting position of the layer and d_2 is the end position of the layer. $a_1 = 0.0480$ N/mm and $a_2 = 0.0052\ N/mm^2$, which were obtained by authors to fit a real puncture.

Another model that describes $f_{puncture}$, but in *vivo*, was performed by the author [Barbé et al., 2006] on the abdomen of an adult living human. The model takes into account the penetration depth between two bodies.

$$f_{puncture} = \begin{cases} -(\mu P_{tip}^n + \lambda P_{tip} v) & \text{when } P_{tip} \text{ is in contact with the tissue} \\ 0 & \text{when } P_{tip} \text{ is out of the tissue} \end{cases} \tag{2.2}$$

where $\lambda = 1.5$, $\mu = 240$ are constant parameters that depend on the material properties, and $n = 1.3$ describes the viscoelastic behaviour of soft materials. P_{tip} and v are the needle tip position and the speed, respectively.

Decaying Sinusoid: $f_{HardContact}$

Another approach that helps to identify when the tool is in contact with a rigid object is the one proposed by the authors [Kuchenbecker et al., 2006]. As in our case, we need to prevent the user goes beyond the bone. It is necessary to send a significant signal at the user's hand. Due to the limited force of the haptic device, it is impossible to reproduce the bone's stiffness. For that, the method *Decaying Sinusoid* can be implemented since this describes the dynamics of contact with rigid objects as two superimposed forces, one with a high-frequency and another one with a slower extended response (Eq. (2.3)). The force response is computing depending on the lapse of duration and the incoming velocity of the tool. The benefit of this method is that the system remains passive due to the fact that the

force is only computed during a short lapse of time.

$$f_{HardContact} = A\,|v_{in}|\,e^{ln(0.01)t/d} sin(2\pi ft)\,\text{for}\,0 < t < d \tag{2.3}$$

where A is the nominal amplitude ($A = 19.9$ Ns/m), d the fixed duration ($d = 0.055$ s), f is the frequency ($f = 55$ Hz). The authors obtained these values from tapping contact between the tool and wood.

LuGre model: $f_{friction}$

Friction is one of the most studied subjects in mechanics. Several approaches have been proposed to explain and predict its behaviour. Despite being a very complex phenomenon, there are always two principal parameters that can be found in the majority of the models: the Coulomb and viscous friction coefficients. The Coulomb friction coefficient represents the dry friction that exists between two surfaces during normal contact. The viscous friction represents the friction between two surfaces that had been previously lubricated. Although their presence are constant through all the proposed models, sometimes these simple approaches are not enough for more sophisticated tasks like needle insertion. For this purpose, other models like the LuGre model are used [Asadian et al., 2011].

The LuGre model is a dynamic model based on the microscopic representation of irregular contact surfaces and elastic bristles. When the bristles bend (because of needle insertion) the friction force is generated (Fig. 2-1)

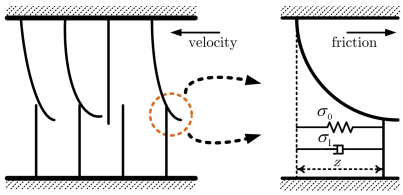

Figure 2-1 – Microscopic bristles bending process ([Asadian et al., 2011])

The LuGre model uses an internal state z that represents the bending of the bristles. It is

gave by

$$\dot{z} = v - \frac{\sigma_0 |v|}{g(v)} z \tag{2.4}$$

Where v is the velocity of the insertion, σ_0 is the coefficient of stiffness for the microscopic deformations during pre-sliding displacement, and $g(v)$ describes the Stribeck effect given by

$$g(v) = \mu_c + (\mu_s - \mu_c) e^{-\alpha |v|} \tag{2.5}$$

Where μ_c and μ_s are the coulomb and stiction coefficients, and α is a constant determined by parametrization. So, the friction exerted by the LuGre model is determined as

$$f_{friction} = F_n(\sigma_0 z + \sigma_1 \dot{z} + \sigma_2 v) \tag{2.6}$$

Where σ_1 is the damping coefficient associated with $\dot{z}$ and σ_2 is the viscous damping and F_n is the injection cutting force.

The parameters of the LuGre model must be obtained experimentally. Authors in [Asadian et al., 2014] proposed a method based on a periodic penetration in a Gellan Gum with a needle attached to a 5-DoF manipulator. Based on the frequency of the puncture and the length of the needle, the following parameters have been proposed (Table 2.1).

	$d = 20mm$		$d = 40mm$	
Parameters	$f_{in} = 0.025hz$	$f_{in} = 0.05hz$	$f_{in} = 0.025hz$	$f_{in} = 0.05hz$
σ_0	1.326	1.419	2.469	2.592
σ_1	1.423	1.312	0.845	0.879
σ_2	$1.04x10^{-4}$	0.001	$2.76x10^{-4}$	$2.40x10^{-3}$
μ_c	0.628	0.913	1.386	1.763
μ_s	0.045	0.033	0.084	0.052
α	0.256	0.152	0.079	0.075

Table 2.1 – Parameters for LuGre model [Asadian et al., 2011] where d represents the needle's length

In our case, the values that better fit our implementation corresponds to the parameters obtained for the needle's length of 40mm because the maximum length of our needle is

35mm. For the time of insertion, we can opt for both frequencies, but it is necessary to develop a study with medical experts and students to determine the average time that is required for a training sessions. Meanwhile, we consider that students will take the longest time to reach the objective with the needle as they are novices, so the frequency of 0.025hz is chosen, which corresponds to an insertion of 40s.

2.1.2 Method approaches

Collision detection: Proxy *God-Object*

The fundamental principle of haptic devices is to identify the position (in case of impedance systems) of the virtual element driven by the user, then link it up with the localization of virtual objects that are intended to work, by comparing the coordinates and calculate the possible collisions with virtual objects.

One method to render forces in the virtual environment is using the *God-Object* algorithm (Fig. 2-2), also known as a surface contact point, proxy point, or IHIP (Ideal Haptic Interface Point) [Basdogan and Srinivasan, 2002], which is implemented in several haptic simulators [Zilles and Salisbury, 1995]. This algorithm begins with the assumption that it is not possible to avoid that the user overpasses the virtual location of a surface in the real world. This is due to the in-exactitude of the human body to sensor small forces from the haptic device. To avoid unreal behaviour, the algorithm uses a virtual point called the God-Object, which is located at the edge of the virtual object. The forces are rendered using impedance control techniques based on the relative position of the god object against the real tool. This method is useful and straightforward for solid and soft contact, avoiding ambiguities when the tool makes interaction with complex surfaces, it avoids also tracking and updating the location of the god object too fast [Vidal et al., 2008], [Basdogan and Srinivasan, 2002].

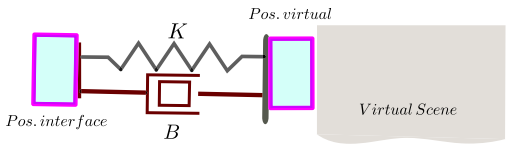

Figure 2-2 – God-Object representation

Rendering of soft tissues: $f_{cutting}$

With haptic devices, it is possible to create different virtual environments like objects/wall collision scenarios. This can be done by controlling the desired force applied by the device on the hand of the user, which is the simplest method called *direct method*. The forces and torques are generated to give the sensation of interaction by computing the distance between the tool and the surface [Ryden and Chizeck, 2013]. In theory, this solution can be the most suitable, but in practice, chattering problems can occur on the tip of the tool due to the sudden change of applied force perturbing the haptic rendering.

A virtual surface also can be modeled as an elastic element [Basdogan and Srinivasan, 2002], which can be rendered using a virtual spring being a possible solution to render different body stiffness [Kuchenbecker et al., 2006]. The force acting on the user is computed by (Eq. 2.7).

$$f_{cutting} = K(\omega_0 - P) = K\Delta x \tag{2.7}$$

Where $f_{cutting}$ represents the cutting force exerted on the virtual needle, ω_0 represents the ideal haptic interaction point, P the current tool position, and K is the stiffness coefficient that is different in each layer of the body. However, setting a high K value would cause undesirable chattering. Another problem is that the user stops his movement inside of the tissue; the tool will be no longer able to remain at the position when user stops its motion due to all the force generated during the displacement.

Another way to render the cutting forces is to implement Voigt model [Brett et al., 1997].

This method uses a virtual spring and a damper in parallel described by the Eq. (2.8) .

$$f_{cutting} = \begin{cases} K(\omega_0 - P) - B\dot{P} & \text{if } P \geq \omega_0 \\ 0 & \text{if } P(t) < \omega_0 \end{cases} \tag{2.8}$$

Where B is the viscosity coefficient of the damper, $\dot{P}$ is the velocity of the haptic interface. It is well known that adding the damping term helps to improve the coefficient of restitution between the user and the virtual surface, giving a good perception of collision response on the user when interacting with hard surfaces [Salisbury et al., 1995].

However, to implement this last method, it is necessary to estimate the speed of the tool. One way is Levant's differentiator. This technique not only determines the velocity but also improves the impedance-width [Chawda et al., 2011]. However, the calculation of the gain is a quite tricky process, and also it is necessary to implement a filter to reduce the chattering. Another simple method is the one proposed in [Constantinescu et al., 2005], where it is easy to estimate the velocity by just reading the position in a period of time. However, if the sampling rate increases, the noise also is amplified. Taylor series expansion is another method where the time is fixed, and the number of encoder lines detected are counted during a fixed period [Chawda et al., 2011]. Nevertheless, higher-order algorithms tend to magnify measurement errors, and lower order is not enough to estimate velocity [Brown et al., 1992].

Another problem to face is the sampling rate, which is an essential element to consider in haptic systems when rendering forces because this can improve or affect the dynamic range of impedance [Colgate et al., 1993]. Two cases should be considered with this. The first one happens when the tool collides with the wall, but the sampling has not updated the tool's position. At this moment, the tool moves into the wall, and for hence the requested force by the haptic system will be low because the sampling T had not updated the position at the precise moment when the collision occurred (Fig. 2-3a). This produces lost of energy, and the sensation of touching a wall is not respected. The second case occurs when the tool is leaving the wall, and the sampling rate has not updated the position. In this case, the tool is

supposed to be inside the wall, but in reality, the tool has already exited it, so the requested force remains high until the sampling T updates the position (Fig. 2-3b).

(a) Penetration force diagram of the tool inside the wall

(b) [Penetration force diagram of the tool out of the wall

Figure 2-3 – Collision force diagram between two virtual objects

Impulse-Based simulation: $f_{HardContact}$

The render of hard contact presents technical problems for haptic devices. As it is marked in [Kuchenbecker et al., 2006], for giving the sensation of touching a hard surface, a high stiffness is required which can rise up to $1x10^6$N/m, which is not reachable with actual haptic systems.

One approach to overcome this problem is to use the Impulse-Base simulation. This approach gives the user a pulse of force whenever hi/she touches the hard surface. This pulse alerts the user of a contact with a hard surface, which in the case of needle injection indicates the collision with a forbidden zone, like a bone.

To calculate the pulse force, this approach consider that a collision between two objects has been made. An impulse is applied to the haptic tool (needle in our case) with an opposite magnitude (Eq. (2.9)).

$$\vec{v_1} = -e \times \vec{v_0} \tag{2.9}$$

Where e is a coefficient of restitution that takes values between one or zero. Where one represents an elastic collision, and zero a plastic collision. For our case, the coefficient e is set in one as the bone is not deformed by the collision with the needle. $\vec{v_0}$ is the previous velocity normal to the wall, and $\vec{v_1}$ is the velocity normal to the wall. To calculate the force

applied by the wall, Eq. (2.10) is used.

$$\vec{f}_{HardContact} = \frac{-(e+1)M\vec{v}_0}{T} \tag{2.10}$$

Where M, $\vec{v}_0$ and T, represent the Inertia matrix, speed and the period time, respectively [Alès Roux et al., 2016].

2.1.3 Virtual fixture: $f_{clamping}$

Virtual fixtures are used as guides to perform tasks, avoiding that the tool enters into a forbidden region or quit an established trajectory. In our case, the implementation of a virtual fixture helps us to represent the clamping forces. They are forces that surround the needle when it is inserted in the tissue. In [Kikuuwe et al., 2007] authors describe two types of virtual fixtures, bilateral and unilateral. The bilateral fixture is used to avoid that the tool departs from a curve or a surface. Thus if the tool departs from the reference trajectory, a large force is exerted to force the tool to stay along the desired path. In the case of unilateral, this one helps to limit an area where the user can move without restriction, but if the tool enters in a forbidden zone, a large force is computed to keep the tool out from the forbidden zone.

In our case, the type of virtual fixture that we need to implement is a bilateral one that restrains the needle to follow only a desired trajectory.

Impedance-type friction (plasticity) model is implemented, where the position (p) of the tool (haptic interface) is measured. The reaction force (f) from the virtual world is calculated and applied to the actuators.

The impedance establishes the transformation between the position and the speed of the effector's end, and the force applied, as it is shown in Eq. (2.13).

Where the measured position $p(i)$ of the stylus of the device was converted into the input position $p*(i)$ by Eq. (2.11), and the proxy position $q(i)$ is determined through the Eq. (2.12). K and B are the stiffness and the viscosity coefficient respectively and $k = M/T^2$,

where T the timestep and M the mass. [Kikuuwe et al., 2007].

$$p*(i) = p(i) + \frac{B\,(q(i-1) - p(i-1))}{KT + B} \tag{2.11}$$

$$q(i) = gsat\left(p*(i) - \frac{F}{k}, q(i-1), p*(i) + \frac{F}{k}\right) \tag{2.12}$$

where $gsat(a,x,b) = max(a, min(x,b))$

$$f(i) = k\,(q(i) - p*(i)) \tag{2.13}$$

The virtual fixture $f(i)$ helps to guide the direction of the tool within the body to avoid entering forbidden regions and track a specific path.

2.1.4 Discussion

In this section, we presented some method and model approaches that help to compute the forces during the needle insertion. The main problem using them is the reproduction of sensation when the needle is in stage 2 (inside of tissue). The first problem is the chattering caused when different high stiffnesses are set, and a poor speed estimation is done; which perturb the haptic perception when the cutting forces are computed. The second problem is when the doctor stops his movement within the body and the tool does not remain in the same position due to the reaction force of the spring.

Due to this reason, a new method is presented in the next section. This method helps to compute the cutting and attracted forces that accomplish the desired objectives of the stage 2, avoiding chattering problems and also allowing us to remain the tool in the same position where the user performs a stop.

In the case of hard contact ($f_{HardContact}$), from the two studied methods, Decaying Sinusoid and Impulse-Based simulation, we opt to chose the first one for the following reason: The reaction force from Decaying Sinuoid when the collision occurs is attenuated during a pre-established period of time, which gives the impression of touching a hard object for

a short lapse of time. While the Impulse-Based simulation reaction force is felt as an instantaneous change of force, which the user interprets more like a hit rather than touching a wall. This last one perturbates the haptic sensation and breaks the immersion of the student. However this assumption has only be tested internally, a more detailed study with several test subjects is required to evaluate the more appropriate approach.

Concerning the virtual fixture, the previously shown method helps to follow a desired path. However, this method can be used only to follow a curve or a surface. But in our case, as the trajectory must be a line that, on specific occasions, can change its direction depending on the user's needs. In the next section a new method to compute the clamping forces is also introduced.

2.2 Tracking wall method: $f_{cutting}$ and $f_{attracted}$

The implementation of the tracking wall method overcomes the problem of chattering caused by setting high values of stiffness to represent the different tissues of the body. This method does not require any speed estimation, since the energy dissipation when the tool enters the wall and stops inside of the virtual environment, is made by a mobile spring, which depends only on the needle's position. The concept of adding a mobile spring ensures that the tool preserves its position when the stop occurs and will not be rejected by the stored force during the displacement [Alamilla D et al., 2019]. For a better understanding of the problems that we are going to overcome proposing the tracking wall method, we make a comparison with two classic methods for computing the cutting force. The first method is called direct method, and the second one is using a virtual spring.

A test is performed to have a better comprehension of the problem when the tool collides with the virtual environment and when the tool stops inside the joint articulation. The virtual environment is set around 12 cm and a desired cutting force of 1 N; this force was taken from the parametrization obtained by [Gordon et al., 2015]. As can be seen in Fig.2-4a when the tool collides with the virtual joint at $t = 7.5$, chattering problem occurs due to the suddenly change of force, damaging the haptic rendering. On the other hand, when the virtual spring

is implemented, the force increase gradually (Fig.2-4b $t = 3.8$ sec) increasing the force smoothly. However, if a high stiffness value is set, chattering problems occur too. Other problem that we faced in both methods, is that the tool does not remain in the position when a stop occurs (Fig.2-4a $t = 7.5$ sec and Fig.2-4b $t = 13$ sec), as can be appreciated the tool is rejected when the user releases it.

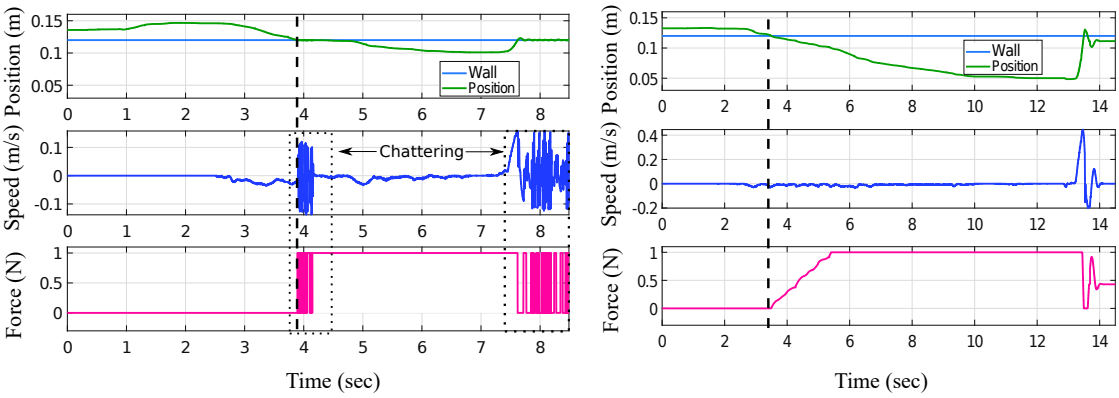

(a) Direct method (b) Virtual spring

Figure 2-4

2.2.1 Force computation during motion

For the implementation of the tracking wall, two parameters to describe the wall's position are necessary: ω_0 and ω_n. The position ω_0 establishes the edge of the wall or in our case, the surface of the joint. This value is fixed, and it cannot be updated as this is the set point of the virtual environment. So, when the needle is in contact with the skin (or the surface of the joint) for the first time, ω_0 and ω_n are equals. ω_n is the position of the mobile wall, which follows the needle's displacement with a certain distance. This position is updated depending on the tool displacement through the joint (or articulation). To update ω_n Eq. (2.14) is used, and this process is declared as *"Update with movement"* in the flow diagram presented in Fig. 2-7.

$$\omega_n = \begin{cases} \Delta_{new} - x_t & \text{if } x_t > \omega_0 \\ \omega_0 & \text{if } x_t \leq \omega_0 \end{cases} \quad \text{update with movement} \tag{2.14}$$

x_t is the current position of the needle's tip. Δ_{new} is a variable called *"safety position"*. It computes the maximum distance required to reproduce the desired force, and the separation between the current point and ω_n while the tool is moving.

$$\Delta_{new} = \frac{f_R}{K_t} \tag{2.15}$$

Where f_R is the desired force to reproduce the cutting force, and K_t is a tuning parameter that allows establishing the value of the *"safety position"*. K_t depends on the nature of the soft tissue (or layer) in which the needle is located. So, this should be calculated for each layer according to the desired force.

The force profile used to test the tracking wall were obtained from the experiments made by [Kataoka et al., 2002]. In this paper, the authors developed an instrumented needle to measure the involved forces during the insertion of a needle in canine prostate, we use the force profile results and adjust our parameters to obtain a value of the first layer, where the cutting forces is 1 N and the tissue layer width is 12 mm. With these parameters it is possible to tune K_t to calculate Δ_{new}.

The chosen value for the stiffness is $K_t = 500$ N/m and the desired cutting force is 1 N. According to Eq. (2.15), the value of Δ_{new} corresponding to these values is 2 mm. The wall (virtual set point) is initially in $\omega_n = 0$ mm.

Fig. 2-5 shows the results obtained along 1-DoF using the values aforementioned. In this test, the needle is in free motion until 0.65 s. Therefore the value of ω_n and ω_0 remain null.

Once the needle gets into the pink zone (virtual environment), the force is computed, raising its value softly as long as the needle is moving. Once the maximum force is reached (1 N at $t = 1.2$ s), the force stops increasing and remains at this value. This test helps to illustrate how the algorithm updates the position of ω_n.

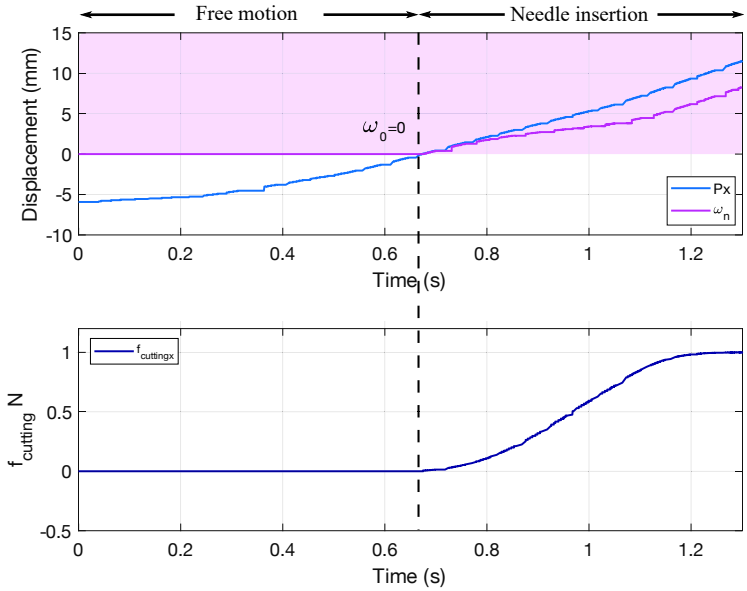

Figure 2-5 – ω_n "Update with movement"

2.2.2 Repeal force during a stop

When the tool stops inside the body, ω_n is computed now by Eq. (2.16). Where m is calculated by Eq. (2.17) which represents the director coefficient of the line defined by the stop point and ω_n. n is a constant which will be defined in the next paragraph.

$$\omega_n = \begin{cases} m * i + \omega_{n-1} & \text{if } i \leq n \\ \omega_{n-1} & \text{if } i > n \end{cases} \quad \text{Update with stop} \tag{2.16}$$

$$m = \frac{x_t - \omega_n}{n} \tag{2.17}$$

Once m is defined, its value remains unchanged during the rest of the process. n is the total number of iterations to update ω_n, and i is the number of iteration necessary for ω_n to reach the position where the stop occurs.

This process that involves the computation of m and the update of ω_n is called in the flow diagram *"Update with stop"*. In the case of n, this value must be tuned as it depends on the controller performances.

This experiment (Fig. 2-6) concerns the wall's response and behavior of the force when

a stop occurs inside the virtual articulation. During the test, the parameter K_t, Δ_{new}, and the desired force have the same value than the previous test. Concerning ω_0 its value is fixed at 15 cm. When the needle reaches the blue zone, the force begins to increase until the desired value, which is reached $t = 2.8$s. After approximately 1 second, the user starts to slow its motion before completely stopping it at $t = 4.5$ s. The speed and the force thus decrease until zero. Then at $t = 5.1$ s, the user started its movement again, and the force begins to increase gradually as well as the speed.

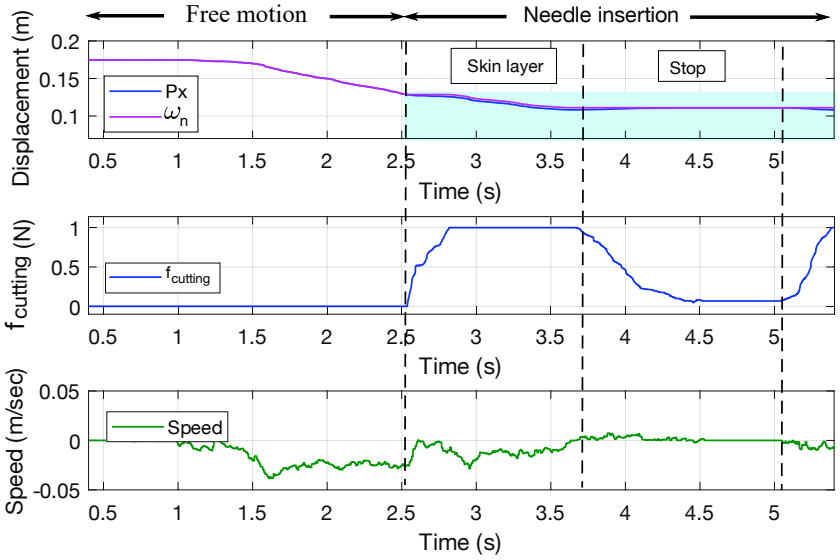

Figure 2-6 – ω_n "Update with stop"

2.2.3 Tracking wall algorithm

The purpose of this algorithm is to move the wall in front of the needle, so the next time the user moves the needle, he will face a wall as he found it when the virtual limb was penetrated the first time. The force exerted by the system ($f_{cutting}$) is calculated using (2.18)

$$f_{cutting} = \begin{cases} K_t(\omega_n - x_t) & \text{if } x_t \geq \omega_0 \\ 0 & \text{if } x_t < \omega_0 \\ 0 & \text{if } x_t < x_{t0} \end{cases} \tag{2.18}$$

where x_{t0} is the position corresponding to the tool when the user stops his motion inside the body.

With these parameters, it is now possible to detail the operation of the tracking wall algorithm. Fig. 2-7 shows the flow diagram of the algorithm. The steps are as follows:

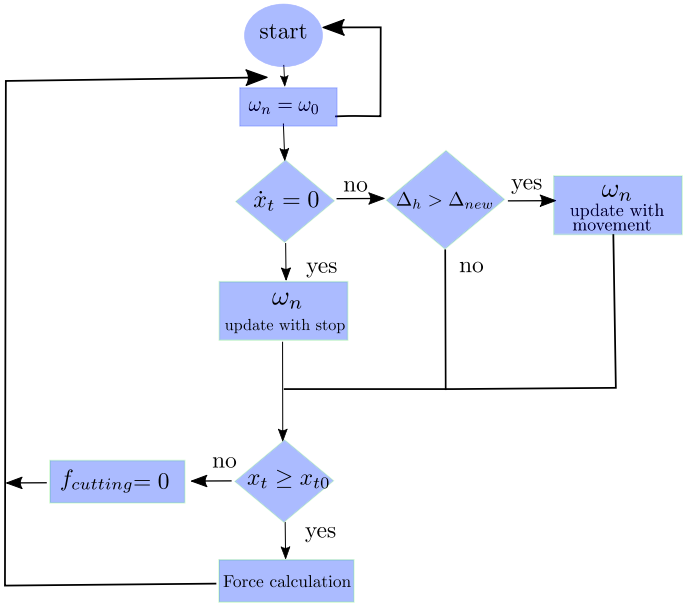

Figure 2-7 – Flow diagram of tracking Wall algorithm.

1. Initial conditions: $\omega_n = \omega_0$.

2. When the tool overpassed ω_0, the force exerted is calculated using (2.18) and is updated in each iteration of the algorithm.

3. The tool continues its trajectory through the virtual body. The algorithm compares Δ_h to Δ_{new}.

4. If $\Delta_h > \Delta_{new}$, it means that the tool overpassed the "safety position". The system exerts the desired force for this layer.

5. The tool continues its trajectory, and now the value ω_n is updated using (2.14).

6. When the system detects that the tool velocity $|\dot{x}_t| < \varepsilon$, which means that the user stopped his motion, we are in the situation "Update with stop". The current position is saved as x_{t0}, and the algorithm computes ω_n to update the wall using (2.16), while the speed remains null.

7. When the user moves the tool again, the algorithm compares the actual position x_t with the value x_{t0} saved when the stop occurred. The value x_{t0} helps to memorize the position of the needle.

8. if $x_t < x_{t0}$, the force exerted is null, that means that the tool is removed and then moved forward but not enough to start to cut new part of tissues, but if $x_t > x_{t0}$ the force is calculated and the process restart from step 2.

Fig. 2-8 shows a graphical representation of the algorithm steps, where each number of the figure corresponds to each number of the step described aforementioned.

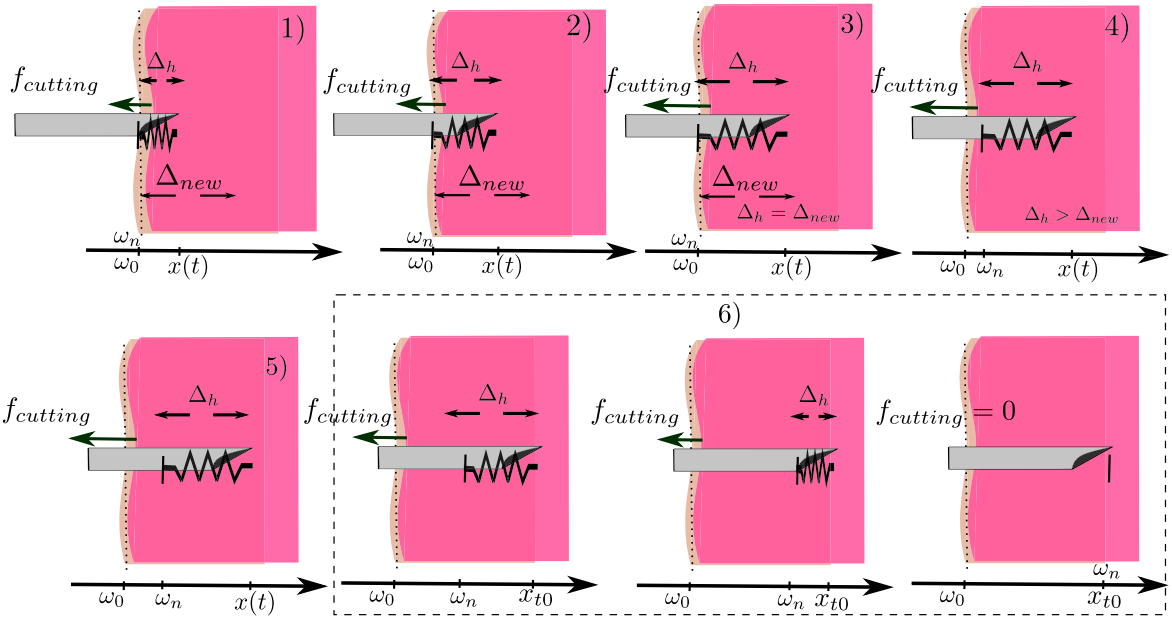

Figure 2-8 – Evolution of a needle insertion, step by step, with the state of the virtual spring.

However, this method does not allow to give bidirectional force feedback, which limits the user case. To improve this, the method was modified to work from left to right (vice-versa) and from top to bottom (vice-versa), giving the possibility to set the virtual limb in any part of our workspace. For this, Eq. (2.19) is used.

$$\omega_n = \begin{cases} x_t - \Delta_{new} & \text{if } x_t > \omega_0 \\ x_t + \Delta_{new} & \text{if } x_t < \omega_0 \end{cases} \tag{2.19}$$

As shown on the next flow diagram (2-9), the condition established to compute force $f_{cutting}$ and $f_{attracted}$ depends on the tool's sense. $f_{cutting}$ represents the force exerted by the needle tip when it is progressing inside the tissue, which is considered as cutting force, and $f_{attracted}$ represents the attracted force when the needle is withdrawn from the body.

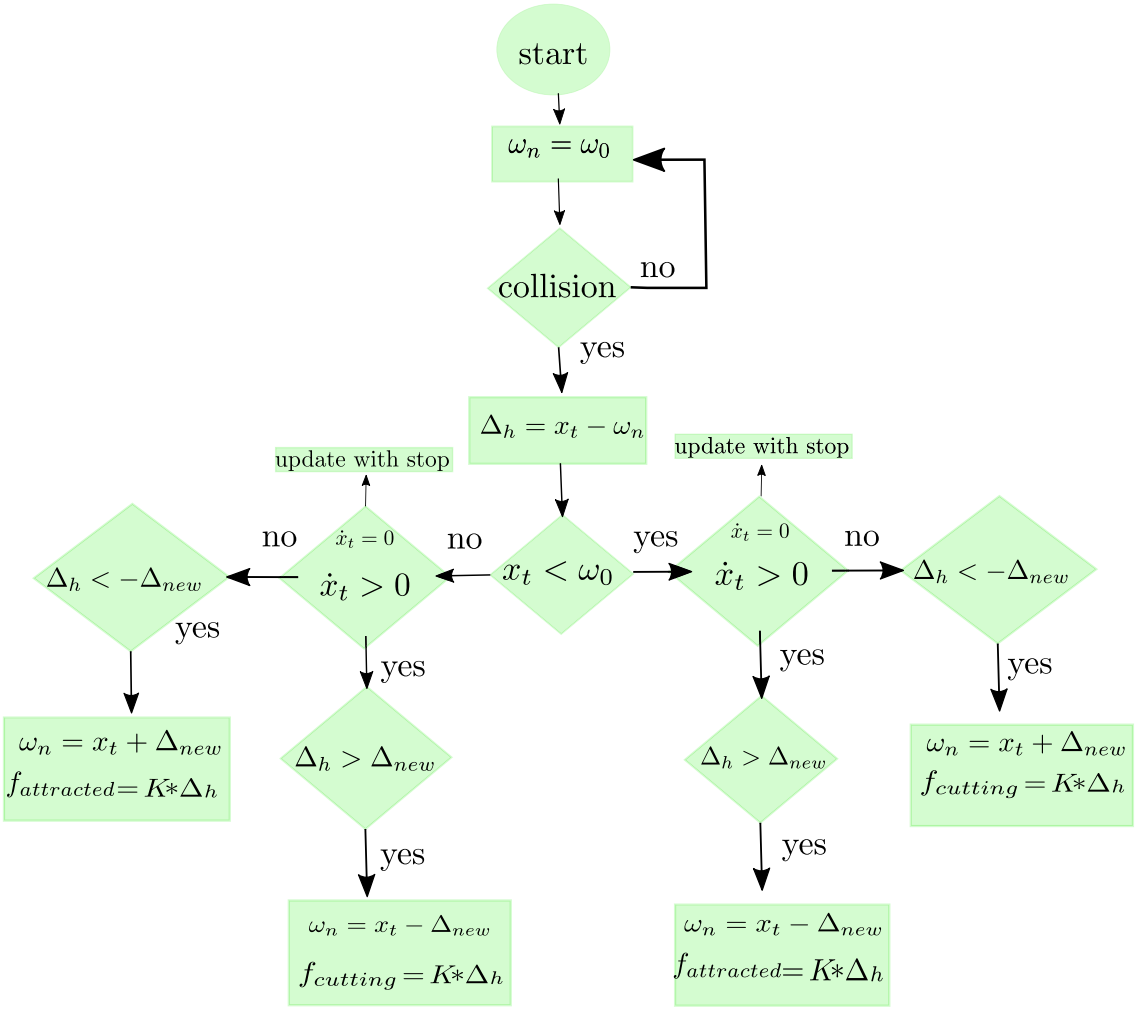

Figure 2-9 – Flow diagram to compute cutting force and attracted force.

This last test was performed (Fig. 2-10)to simulate a needle insertion and the withdrawal of the needle. $f_{cutting}$ and $f_{attracted}$ are computed based on the last proposed algorithm. Where the desired cutting force is equal to 1 N, and a desired attracted force equal to 0.5 N and ω_0 is equal to 7 cm. Concerning Δ_h and K_t they have the same values as the previous tests.

In the first instance, the user is free to move the tool in the free motion zone (FM) without generating any force. From $t = 24$s to $t = 27$s the needle is inserted and ω_n begin to update its position to ensure the desired force. During this displacement, the cutting force increases until reaching the desired cutting force at 1 N, while the tool is moving. From $t = 27$s

to 29.5s an intentional stop occurs, and when the algorithm reads that the needle's speed is zero, the wall begins to update until it reaches the needle's actual position. During the updating of ω_n, the force decreases until zero. When the intentional stop ends, the needle is withdrawn from the virtual tissue from $t = 29.5$ to $t = 31.5$ s, generating attracted force of 0.5 N. Finally, the needle is completely withdrawn from the tissue to the zone free motion, where the user can choose another point of insertion.

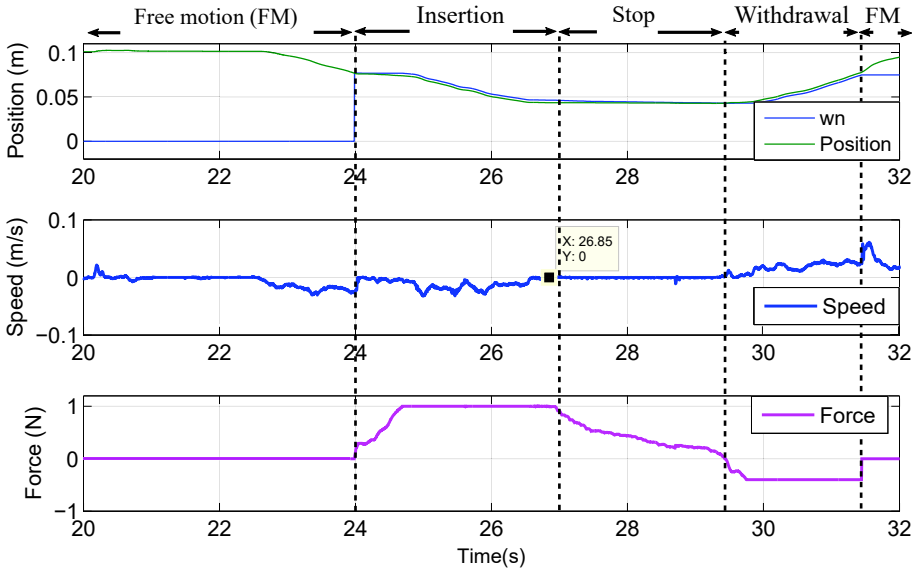

Figure 2-10 – Tracking wall $f_{cutting}$ and $f_{attracted}$ 1 DoF

2.3 Method for radial forces ($f_{clamping}$)

2.3.1 Virtual fixture "Orthogonal projection"

In the real procedure, once the needle has pierced the tissue, the trajectory is defined, allowing it to move along the main needle axis since the tissue that surrounds its body constraint the movements. This normal forces generated by the tissue, named clamping forces, will be implemented using a virtual fixture to represent them.

One of the objectives is to allow the doctor to choose the entry point on the virtual articulation. The trajectory and the clamping forces are recalculated every time that the

point of insertion changes. It is thus not possible to establish a predefined trajectory for every chosen case. Moreover, users can change its trajectory in order to reach the desired goal, and she/he should feel the forces involved while he modifies its trajectory.

This algorithm consists in creating a virtual guide in real time. The method is based on the computation of a line and finding the orthogonal projection of the current point onto a line (Fig. 2-11).

When the needle pierces the tissue for the first time, the current position is stored in P_0. The line is established by this point and the vector $\vec{u}_P$, which define the direction and sense of the needle.

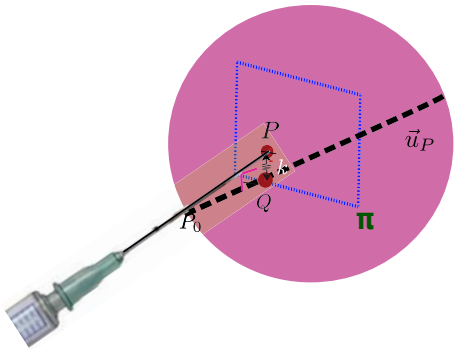

Figure 2-11 – Orthogonal projection of a point onto a line

For every time that the needle advances into the tissue the projection of the current point P onto the line defined by Q is calculated. To calculate this, it is necessary to find an orthogonal plane π that fulfills the following expression:

$$\pi \begin{cases} P \varepsilon \pi \\ \vec{u}_P \perp \pi \end{cases}$$

Q is then computed, which represents the intersection point between the plane π and the trajectory.

Once Q is obtained, a trajectory generator is applied, which will correct the user movement once he departs out from the desired path. The name of these orthogonal forces are *clamping forces* (Eq. (2.20)).

$$f_{clamping} = k * e \tag{2.20}$$

where e is the magnitude $||QP||$ and k is a tuning value that tends to restrain the needle's movement depending on the depth and the tissue stiffness.

2.3.2 Orientation Control

The clamping forces described aforementioned only limit the movement in 3 DoF. So, to fix the wrist orientation, a trajectory generator is implemented, using the quaternions.

When the tool pierced the tissue, the current quaternion is stored in q_0, which will be our reference to follow the orientation. So if the user changes the tool orientation, it will be necessary to determinate the error between the stored quaternion and the current quaternion to exert the forces at the user to correct his movement.

For that, the quaternion rotation is computed (Eq. (2.21)), which describes the rotation from q_0 to q_c the current quaternion.

$$\begin{aligned} q_r &= q_c^{-1} q_0 \\ q_r &= (q_{r0}, q_{r1}i, q_{r2}j, q_{r3}k) \end{aligned} \tag{2.21}$$

where the term q_{r0} is referred to as the "real" component, and the remaining three terms are the "imaginary" components.

Once calculated the rotation quaternions corresponding to the angle of the relative rotation is calculated (Eq. (2.22))

$$\theta_{qr} = 2 \cdot \arctan(q_{rnorm}, |q_{r0}|) \tag{2.22}$$

where q_{rnorm}, the euclidean norm, is calculated by the (Eq. (2.23))

$$q_{rnorm} = \sqrt{q_{r1}^2 + q_{r2}^2 + q_{r3}^2} \tag{2.23}$$

To finally get the orientation error denoted by the (Eq. (2.24))

$$\overrightarrow{\varepsilon_{qr}} = \{q_{r1}, q_{r2}, q_{r3}\}^T * \frac{\theta_{qr}}{q_{rnorm}} \tag{2.24}$$

The Fig.2-4b orientation generator is established by Eq. (2.25)

$$\overrightarrow{\tau}_{qr} = k\overrightarrow{\varepsilon_{qr}} - B\overrightarrow{v} \tag{2.25}$$

where k and B are parameters describing the nature of the tissue and $\overrightarrow{v}$ the velocity of the tool.

2.4 Experimental results

The previous presented models can be implemented in several haptic devices that can vary from characteristics to technology. In this case we use an electric haptic device for testing our methods and algorithms.

2.4.1 Work space

To establish a workspace and as a first approximation, a virtual semi-sphere is computed to set the virtual boundaries that represent the shoulder. The centre of the sphere is defined by the point (a,b,c), with a radius, denoted rd. This workspace is free to explore by the users when they are outside of it; it means no forces are exerting on the Haptic Interaction Point (HIP), so the system remains passive. When the HIP (needle tip) makes an interaction with the workspace, the system becomes active, exerting forces on the needle tip. To calculate the interaction force during the collision between HIP and the virtual shoulder (workspace)

the reaction forces (direction and magnitude) are calculated according to Eq. (2.26).

$$\begin{cases} Fx = (x/d_{cal}) * K \\ Fy = (y/d_{cal}) * K & d_{cal} < r_d \\ Fz = (z/d_{cal}) * K \\ Fx = 0 \\ Fy = 0 & d_{cal} > r_d \\ Fz = 0 \end{cases} \tag{2.26}$$

Where (x, y, z) correspond to the HIP, r_d the sphere radius, K the stiffness to represent the collision between the tool and the virtual sphere and d_{cal} is defined as the distance from the centre of the sphere to the HIP Eq. (2.27)

$$d_{cal} = \sqrt{(x-a)^2 + (y-b)^2 + (z-c)^2} \tag{2.27}$$

2.4.2 Tracking wall in 3-DoF

A test is performed in a 3-DoF case to prove the reliability of the tracking wall. For this test, a virtual shoulder is represented as a hemisphere with a radius of 0.15m (Fig. 2-12). It corresponds to the workspace defined early. In this virtual shoulder, nine inner layers represent the different tissues. The desired forces for each layer are 1.5 N, 1 N, 1.8 N, 2 N, 3 N, 3.5N, 2.5 N, 4 N, and 4.5 N, respectively. These values are arbitrarily chosen and can be easily customized to reproduce different patients' anatomy (such as the tissue stiffness and the layer width). The first layer represents the contact zone (skin, pink shaded area Fig. 2-13) that helps the user to feel the borders of it. As the user goes deeper and deeper, she/he feels the different forces applying on the needle while it penetrates each layer. When the user reaches the ninth layer, he/she withdraws it from the virtual tissue following the same trajectory as it was inserted.

To avoid any direction modification, a virtual fixture is implemented as proposed in section 2.3. It allows keeping the initial trajectory in applying normal forces on the needle.

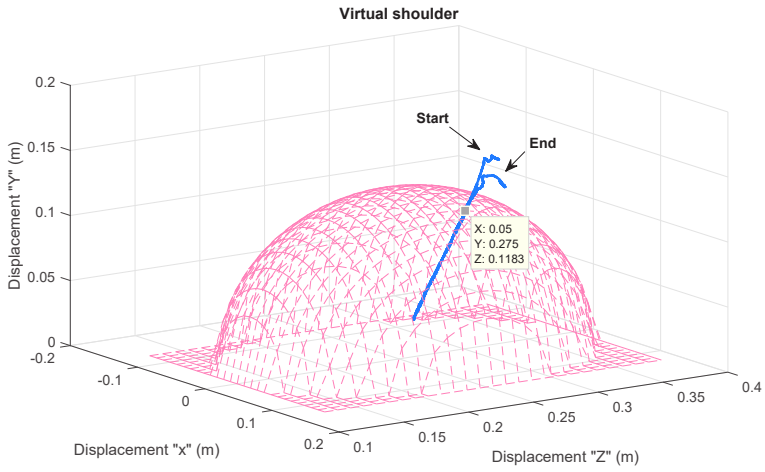

Figure 2-12 – Virtual shoulder and trajectory

The results are shown in Fig. 2-13 where it can be appreciated the needle displacement denoted by Px, Py, Pz in the framework of the haptic interface. Their corresponding tracking walls ω_{nx}, ω_{ny} ω_{nz} and the desired forces along $\vec{x}$, $\vec{y}$, and $\vec{z}$ axis. As can be seen, the force magnitude is computed to corroborate the desired forces (purple dot line).

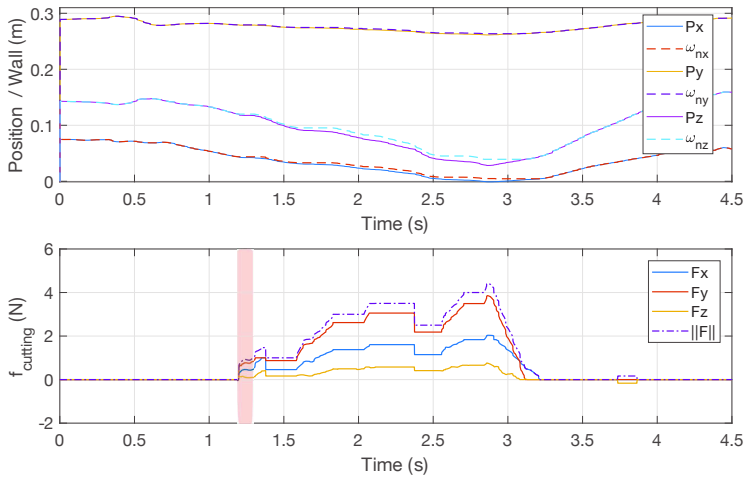

Figure 2-13 – Tracking wall $f_{cutting}$ 3-DoF.

2.4.3 Cutting force and attracted force

This section is dedicated to the introduction of the cutting and attracted forces computation based on a haptic device. The virtual environments are developed with CHAI3D [Conti et al., 2003]. In the final version of this simulator, it will be substituted by our partner enviroment.

Test in 3 DoF

The objective of this test is to compute the cutting forces and the attracted forces in 3 DoF. For this, a profile of seven different layers is set. Their respective cutting force values correspond to a progressive increase of the force, then a sudden decrease and finally by increasing it one last time. This is done by tuning K_t, to see if the tracking wall responses as desired during the change of force. The desired forces are 0.5 N (layer 1), 1 N (layer 2), 1.5 N (layer 3), 2 N (layer 4), 0.7 N (layer 5), 1 N (layer 6), and 1.5 N (layer 7) with a desired attracted forces of 0.7 N. This last is constant along all the layers for simplicity but this can be customized as the cutting forces.

Fig. 2-14 presents the needle position and the tracking walls along each axis when the tool is in free movement ($t = 0$ s to $t = 1$ s), during the tool insertion ($t = 1$ s to $t = 4.2$ s) and the tool withdrawal ($t = 4.2$s to $t = 5.1$s). As can be appreciated, the wall tracks the needle displacement during the tool insertion with a certain distance between the current position and ω_n to ensure the desired forces. In this case, as all the layers, have the same K_t value, it was proposed to set a large value of $K_t = 500$ N/m to reduce distance as much as possible without perturbing the haptic response.

The cutting and attracted forces are shown in Fig. 2-15, where the purple dot line represents the magnitude of the cutting forces ($t = 1.1$ s to $t = 4.2$ s), which increase and decrease according to the nature of the layer, pierced by the needle tip. As it is shown, the force response is almost instantaneous when this passes from 2 N to 1 N, and it is because Δ_{new} is smaller when the cutting force goes from a big force to a small one. The dotted line represents the attracted forces generated when the user withdraws the tool from the virtual articulation ($t = 4.2$ s to $t = 5.2$ s). In this case, the magnitude of the attracted force should

be negative because it is opposite to the cutting force. However, as it is a representation of the magnitude, this is plotted as positive.

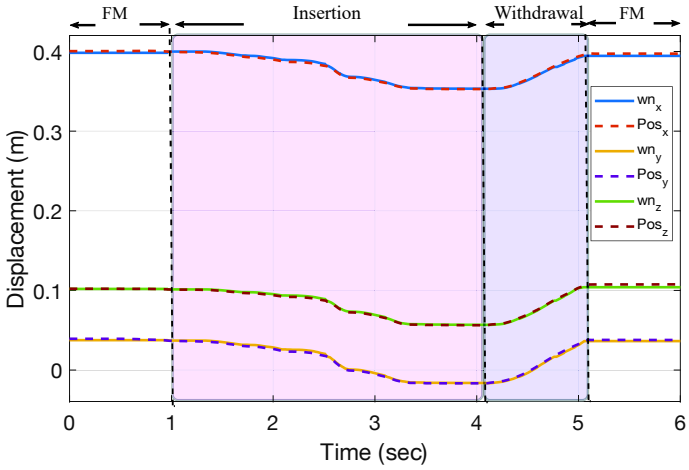

Figure 2-14 – Tracking wall - 3 Dof ω_n update

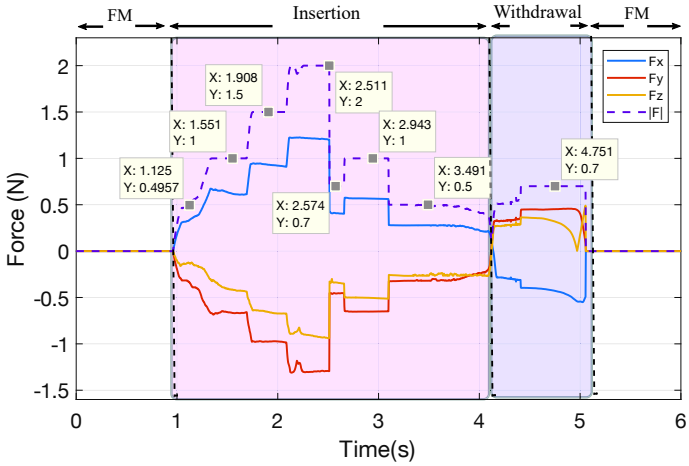

Figure 2-15 – "$f_{cutting}$ + $f_{attracted}$"- 3 DoF

2.4.4 Clamping forces + orientation control

The test performed in this section concerns the implementation of clamping forces and the orientation control previously described in section 2.3. Fig. 2-16 shows the tool displacement (blue line) and the clamping force's behaviour (pink arrows) during the needle insertion inside the articulation, while Fig. 2-17 shows the forces exerted by the simulator. In this test (Fig. 2-16) the user chose the point of insertion in the virtual environment (Start), then he inserted the needle until certain depth (1) but as he did not reach the objective he decided to withdraw the tool but not in its totality to then modified the needle's trajectory (2) in order to reach the desired target. Once it is done, the needle is completely withdrawn.

As can be seen in Fig. 2-16, at the beginning of the test, the user followed the desired trajectory. Consequently, this causes the force tends towards zero (pink zone). As the user kept moving deeper and deeper, the virtual force starts to rise due to the user trying to change the desired trajectory during the insertion (Fig. 2-17). Then the user withdrawn the needle until a certain position to change the trajectory (blue zone) to insert it again.

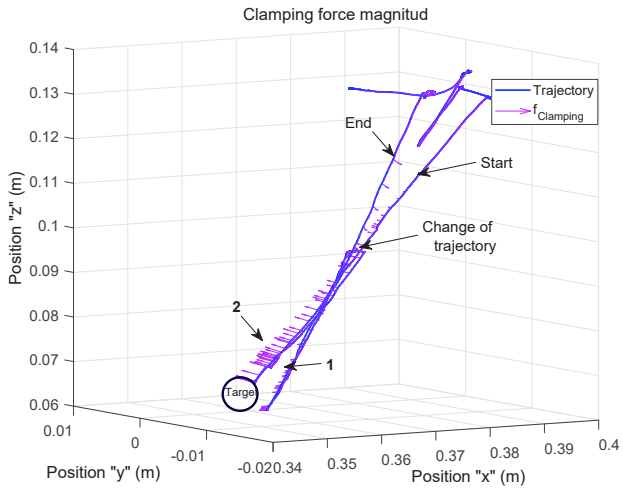

Figure 2-16 – Virtual fixture representation of "Clamping forces "

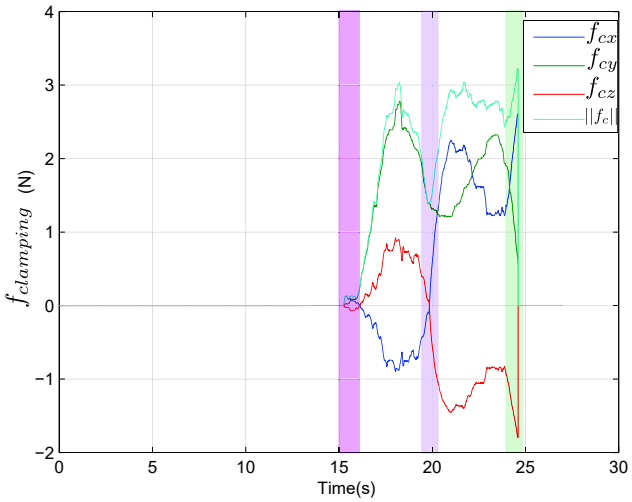

Figure 2-17 – "Clamping force responses", 3 DoF

2.5 Discussion

One of the main objectives is to render the cutting and clamping forces that surround the needle during the insertion.

For cutting forces, several methods are proposed in the literature, but the majority of this made use of FEM or complex models that are very computing consuming. As time computation is essential to represent a realistic behavior of the virtual environment

We proposed a new method approach called "Tracking wall". This method computes the cutting and the attracted forces when the needle is in $stage2$, and helps us to have a realistic haptic rendering without any chattering when large values of cutting force are set. However, it is necessary to take attention to the value of K_t, as high values can produce disturbances during the training.

The main advantages of this method are:

- No biomechanical models are used. So, the method is low computing resources.
- Ability to render the different tissues of the body. This is made by applying several tracking walls in serie or by changing the desired force in real-time.
- Ability to configure the rejection force.

The main disadvantages are:

- The lack of biomechanical model can reduce the realism of the process
- Can be only implemented in impedance haptic system, as the position of the system must be read
- The number of iterations "n" has been established for a device/language, if one of them change, the value of "n" must be set again. It all depends on device responsiveness and how the code is optimized during compilation.

Concerning the method implemented to compute the clamping forces, the proposed virtual fixture (Orthogonal projection) used to simulate the normal forces, helps to constrain the radial movements for following straight paths. For instance, it cannot be implemented to create different trajectories as curves or surfaces, which is one limitation of this virtual fixture. However, for our purpose, it fulfills our expectations since the user can only perform straight insertions. Computing the virtual fixture and the orientation control, allows us to render the forces generated by the tissue when a change of the trajectory occurs.

Chapter 3

Haptic feedback for the ultrasound probe interface

In this chapter, the solution to reproduce the feeling of using an ultrasound probe is presented. To represent the US probe it is desirable to have a tool that resembles at the real one, that reproduces the normal force (1 DoF) when the ultrasound probe is in interaction with the different tissues of the articulation (soft and hard surfaces), and also it must allow at the user to displace freely without mechanical constraints around of the needle insertion point. We present an US probe mock on which our control laws are tested. These control laws are PID, Intrinsically Passive Control and Backstepping, as well a discussion about their performance of each one is done.

3.1 Ultrasound probe

To design an ultrasound probe mock, an electric actuator can be used. However, their volume/power ratio are low and due to the dimension of US probe, these actuators do not fit inside of it. They are also very limited in the maximum force that can exert, which reduce the realistic haptic feedback.

For this reason, an optimal solution is to use a pneumatic actuator, despite the fact that this technology is complex to control as the air compressibility induces nonlinear behaviors

Type	Lineal
Frequency	6-18 MHz
Footprint	40x6 mm
Dimensions	105x56,4x25,8 mm
Main application	Rheumatology

Figure 3-1 – Linear ultrasound probe and specifications

[Herzig et al., 2016]. One of the principal reason to chose a pneumatic actuator to generate the acting forces of the ultrasound probe mock, is the facility to customize a tool that resembles at the same size of a real one (Fig. 3-1). The dimensions of the real US probe fits better with a pneumatic actuator (Fig. 3-2) and therefore increases the realism of the simulator. The advantage that these actuators provide, is higher power ratio without limiting the performances, to reproduce human body behavior, and thanks to the air compressibility in theirs chamber the actuators provide a natural compliance; as they are considered as Variable Stiffness Actuators(VSA), it is possible to reproduce the different tissue stiffness by modifying the pressures in both chambers.

Figure 3-2 – Pneumatic actuator

3.1.1 Mathematical model

Pneumatic cylinder

A pneumatic cylinder is an actuator which transforms the air pressure into mechanical movement. The cylinder has two isolated chambers denoted, P, and N. The mechanical move-

ment is produced by the difference of the air pressure between the chambers. The air flux is injected and vacuumed by two servo valves attached to each chamber. Fig. 3-3 shows a diagram of the pneumatic cylinder and its servo valves.

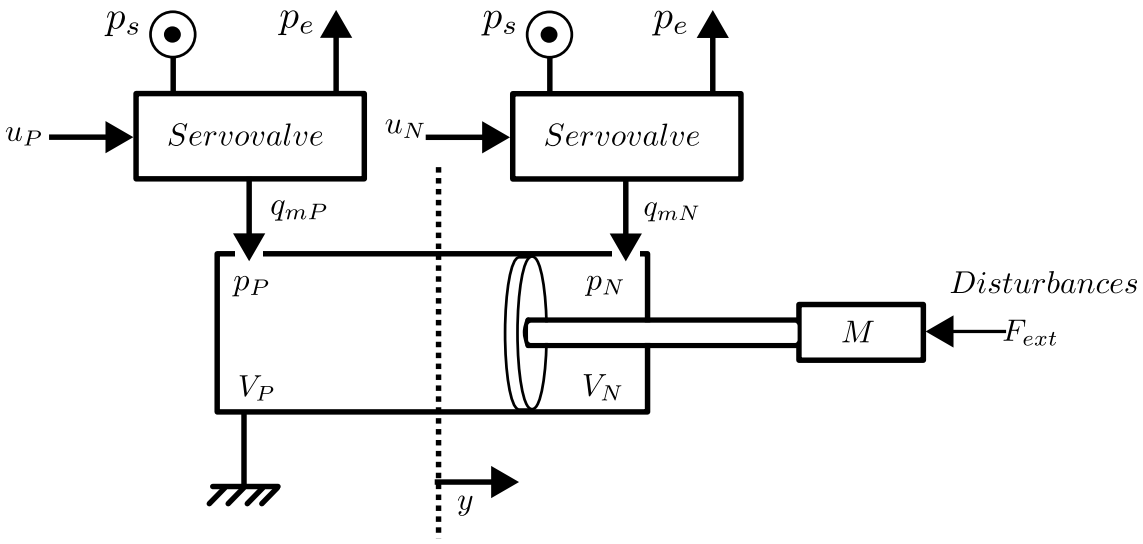

Figure 3-3 – Scheme of a pneumatic cylinder

Where q_{mP} and q_{mN} are the mass flow rates entering the chambers P and N. V_P and V_N are the volumes of chambers P and N. p_s is the source of air and p_e is the exhaust. M is the mass of the cylinder rod and its load. F_{ext} is an external force applied on the cylinder. Finally u_P and u_N are the controlled input voltage for the servovalves.

In the case of the pneumatic cylinder, it is necessary to consider two different mathematical models, a simple one that is in function of the air pressure and the force exerted, and a thermodynamic one that is in function of the polytropic behaviour of the supply air. This last is implemented for simulations to represent the cylinder and the first is used for the synthesis of the control laws.

Mechanical model

The mechanical model of the pneumatic cylinder implemented in the haptic mock probe is set by [Abry et al., 2013a]

$$M\frac{dv}{dt} = F_{pneu} - F_{vis} - F_{dry} - M \cdot g \cdot \cos\theta - F_{ext} \tag{3.1}$$

Where F_{pneu} is the force exerted by the pneumatic cylinder. F_{vis} and F_{dry} are the force exerted by the viscous friction and the dry friction respectively. g is the gravity acceleration and θ is the inclination of the haptic mock in reference to the vertical axis.

The F_{pneu} is calculated by the air pressure in each chamber by

$$F_{pneu} = S_P \cdot p_P - S_N \cdot p_N \tag{3.2}$$

Where S_P and S_N are the useful sections of the cylinder in the chambers P and N. And the F_{vis} is calculated by

$$F_{vis} = b \cdot \upsilon \tag{3.3}$$

Where b is the coefficient of viscosity and υ is the velocity of the cylinder.

Thermodynamic model

For this model, the assumptions are: gas perfect, the system is polytropic and leak of air is insignificant. Also, we consider that the ultrasound probe will work in a controlled environment where the ambient temperature does not change often. So as the system will remain in ambient temperature, the model is set as

$$\begin{cases} \frac{dp_P}{dt} = \frac{k}{S_P \cdot L_P(y)} \cdot (r \cdot T \cdot q_{mP} - p_P \cdot S_P \cdot v) \\ \frac{dp_N}{dt} = \frac{k}{S_N \cdot L_N(y)} \cdot (r \cdot T \cdot q_{mN} - p_N \cdot S_N \cdot v) \end{cases} \tag{3.4}$$

With

$$L_N(y) = \frac{1}{2} - y \quad L_P(y) = \frac{1}{2} + y \tag{3.5}$$

Where k is the polytropic constant, l is the length of the cylinder, T is the ambient temperature, r is the air constant and y the piston position.

3.2 Control laws for pneumatic systems

Once the ultrasound probe mock has been defined, we need to determinate the control that better fits our necessities. The control must allow to reproduce different stiffness, giving the user the sensation of pressing the patient's skin or bone during the exploration of the articulation with the probe.

Several control laws for pneumatic cylinders have been proposed like PID, Admittance PID, Backstepping, and in our contribution, an IPC. To determinate the best we conducted a comparative study between them.

3.2.1 PID

The Proportional Integrative Derivative control is the most known and used control law. This control uses the error between the desired and the actual state of the system and the control signal is given by

$$u(t) = K_p \cdot e(t) + K_i \cdot \int e(t)dt + K_d \frac{de(t)}{dt} \tag{3.6}$$

With

$$e(t) = y_{ref} - y_{act} \tag{3.7}$$

Where $u(t)$ is the control signal, K_p is the proportional gain, K_d is the derivate gain, K_i is the integrative gain, y_{ref} is the reference of the system and y_{act} is the actual state of the system. Fig. 3-4 show the diagram of a PID control with the system.

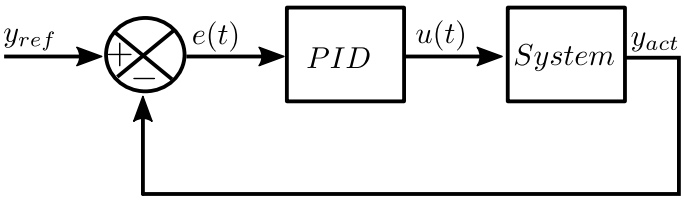

Figure 3-4 – PID diagram

In the case of the haptic mock, we separate it into the servovalve and the pneumatic cylinder, as it is shown in Fig. 3-5.

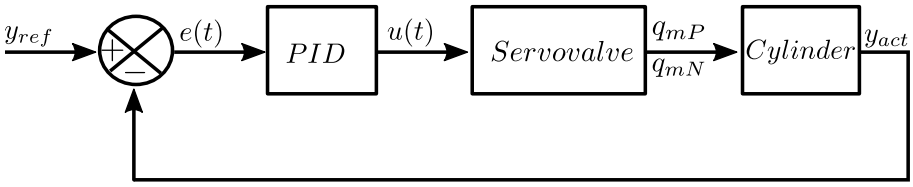

Figure 3-5 – PID diagram for haptic mock

Admittance PID

The admittance PID is a modification of the original PID adapted to work with a desired position and a stiffness. The adaptation is made by reading the force exerted by the haptic mock and then applying the stiffness and desired position. Fig. 3-6 shows the diagram of the admittance PID, where the control law is defined by Eq. (3.8)

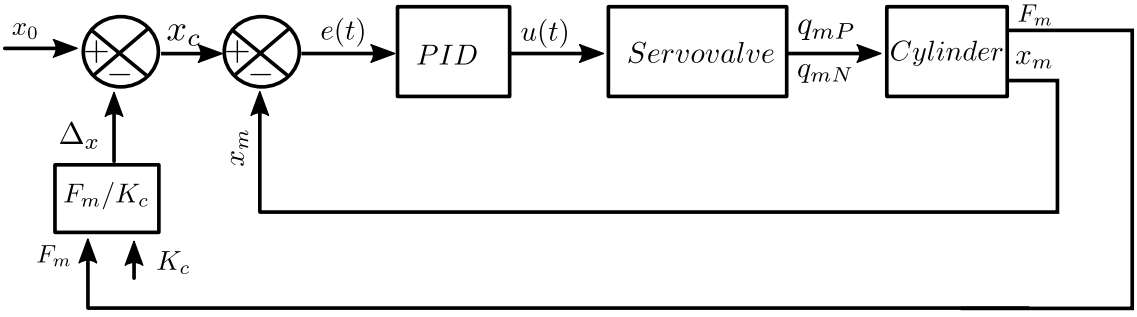

Figure 3-6 – Admittance PID diagram

$$u(t) = K_p e(t) + K_i \int e(t)dt + K_d \dot{e(t)} \tag{3.8}$$

with:

$$e(t) = x_c - x_m \tag{3.9}$$

$$x_c = x_0 - \Delta_x \tag{3.10}$$

$$\Delta_x = \frac{F_m}{K_c} \tag{3.11}$$

Where K_p, K_i, K_d are the proportional, integral and derivative gains from the control PID. x_0 is the reference position, x_m the position measured from the ultrasound probe, K_c is the desired stiffness of the tissue and F_m is the measured force obtained via a force sensor.

With this method it is possible to establish a desired trajectory and a desired stiffness. The system depends on two loops. The outer loop receives the desired position x_0 and an estimated position Δ_x from the inner loop. This latter depends on the measured force F_m and the desired stiffness K_c [Abdallah et al., 2019].

3.2.2 Intrinsically passive control

The Intrinsically Passive control (IPC), initially proposed by [Stramigioli, 1996], it is a Time Domain Passivity Control that utilizes the concept of passivity to provide stability. The main idea is that as long as the system remains passive, it will remain stable. The IPC model is a mass-spring-damper system, like the one shown in Figure 3-7

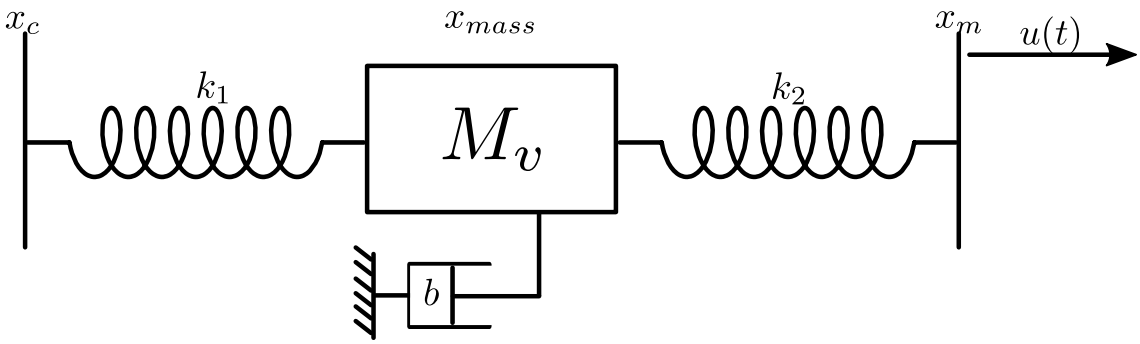

Figure 3-7 – IPC control law

The model of the IPC is given by

$$\begin{aligned} \ddot{x}_{mass} M_v &= -k_1(x_{mass} - x_c) - k_2(x_{mass} - x_m) - b\dot{x}_{mass} \\ u(t) &= -k_2(x_m - x_{mass}) \end{aligned} \tag{3.12}$$

Where k_1 and k_2 are stiffness factors, b is the damper factor, M_v is the inner virtual mass of the IPC, $u(t)$ is the control signal. x_c is the desired position of the user, x_m is the position of the device, $\ddot{x}_{mass}$ and $\dot{x}_{mass}$ are the acceleration and velocity of the inner mass respectively.

In the IPC control law, the system only requires the desired position and the device's position. Thanks to its passivity approach, the IPC provides stability to the system regardless of the device or user actions.

The IPC can be implemented in an admittance control with a desired stiffness as it is seen on Fig.(3-8).

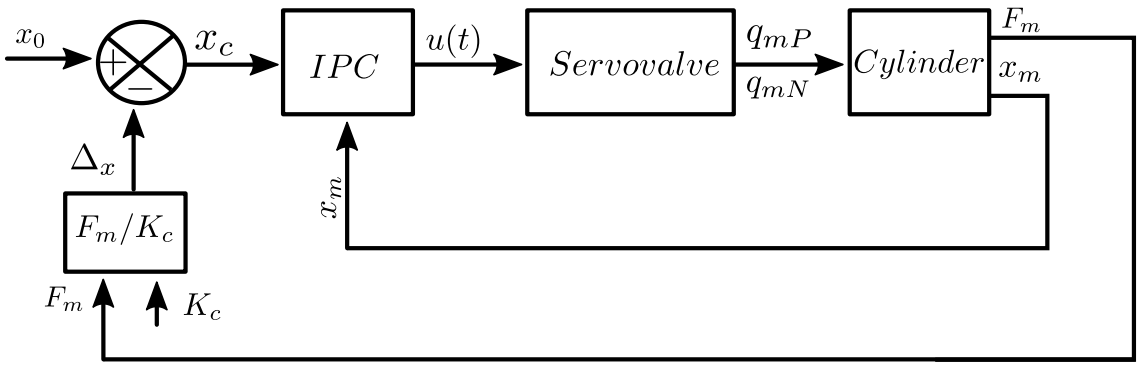

Figure 3-8 – Admittance IPC

Where the only required input values are the position of the rod, the desired position calculated by the desired stiffness and the measured force from the sensor.

3.2.3 Backstepping control

Backstepping is a nonlinear control law, this approach is established on the basis of Lyapunov's theory which consists in modeling the system in a strict-feedback form. This recursive method that minimizes effort control allows to follow a desired trajectory and also

ensure the asymptotic stability of the system. Authors in [Abry et al., 2016] developed a control law to control the position and the closed loop stiffness of an electropneumatic actuator. For that, authors propose a variable change which allows to obtain the electropneumatic model in a strict feedback form. This transformation, called A-T, helps to introduce two virtual inputs, q_{mA} the active mass flow rate and q_{mT} the pressurization mass flow rate [Herzig et al., 2015]. The stiffness manipulation is through the modulating of the control law gains [Herzig, 2016].

$$\begin{bmatrix} q_{mA} \\ q_{mT} \end{bmatrix} = \Lambda(y) \cdot \begin{bmatrix} q_{mP} \\ q_{mN} \end{bmatrix} \tag{3.13}$$

with the A-T transformation

$$\Lambda(y) = \frac{l}{2} \begin{bmatrix} \frac{1}{L_P(y)} & -\frac{1}{L_N(y)} \\ \frac{1}{L_P(y)} & \frac{1}{L_N(y)} \end{bmatrix} \tag{3.14}$$

For the implementation of the backstepping control, first a simpler model of the cylinder for synthesis is deduced, which also introduces the state vector as:

$$X = \begin{bmatrix} y & \upsilon & F_{pneu} & K_{pneu} \end{bmatrix}' \tag{3.15}$$

where pneumatic force (F_{pneu}) corresponds to the force applied by the piston due to the difference pressure in each chamber (Eq. 3.2).

And the pneumatic stiffness (K_{pneu}), describes the variation of pneumatic force during the movement (Eq. (3.16)).

$$\begin{aligned} K_{pneu} &= k\left(\frac{p_P S_P}{L_P(y)} + \frac{p_N S_N}{L_N(y)}\right) \\ L_P(y) &= \tfrac{l}{2} - y \quad L_N(y) = \tfrac{l}{2} + y \end{aligned} \tag{3.16}$$

The model for synthesis is

$$\begin{cases} \dfrac{dy}{dt} = \upsilon \\ \dfrac{d\upsilon}{dt} = (F_{pneu} - F_{visq} - F_{sec} - M \cdot g \cdot \cos(\theta) - F_{ext})(\dfrac{1}{M}) \\ \dfrac{dF_{pneu}}{dt} = \dfrac{2 \cdot k \cdot r \cdot T}{l} q_{mA} - K_{pneu} \cdot \upsilon \\ \dfrac{dK_{pneu}}{dt} = \dfrac{A_1 \cdot K_{pneu} \cdot y \cdot \upsilon - A_2 \cdot F_{pneu} \cdot \upsilon + B_1 \cdot y \cdot q_{mA} + B_2 \cdot q_{mT}}{L_P(y) \cdot L_N(y)} \end{cases} \tag{3.17}$$

Where

$$\begin{array}{cc} A_1 = 2 \cdot (k+1) & A_2 = k \cdot (k+1) \\ B_1 = \frac{2 \cdot T \cdot k^2 \cdot r}{l} & B_2 = k^2 \cdot T \cdot r \end{array} \tag{3.18}$$

As our objective is to control the position and the stiffness of the cylinder, we can see the control in position and stiffness of the cylinder, as it was made by authors of [Abry et al., 2013b]. We consider that the active mass flow rate q_{mA} is designed to track the desired position y_d, where the derivatives of this position are needed to define the trajectory (Eq. 3.19). q_{mT} ensures the track of the desired pneumatic stiffness.

$$\frac{dy_d}{dt} = \upsilon_d \quad \frac{d^2y_d}{dt} = a_d \quad \frac{d^3y_d}{dt} = j_d \tag{3.19}$$

Servovalve model

As it is not possible to control directly the mas flow rate of gas into the cylinder (q_{mP}, q_{mN}), we need to use as signal control, the input voltage of the servovalves to control the mass flow rate entering in the pneumatic cylinder. To convert the desired flow rate into input voltage, it is possible to define a polynomial function that are based on an experimental characterization to model the servovalves behavior [Bobrow and McDonell, 1998] or by using an experimental characterization map of the servovalve. The second technique is less time computing consuming and, therefore, optimal. This method consists of introducing the desired q_m and the gas pression into a look-up table and then obtain the value of the voltage. The parameters of the table have been previously obtained experimentally from the

characteristics of the servolvave in [Thomasset et al., 1999] and are shown in Fig. 3-9.

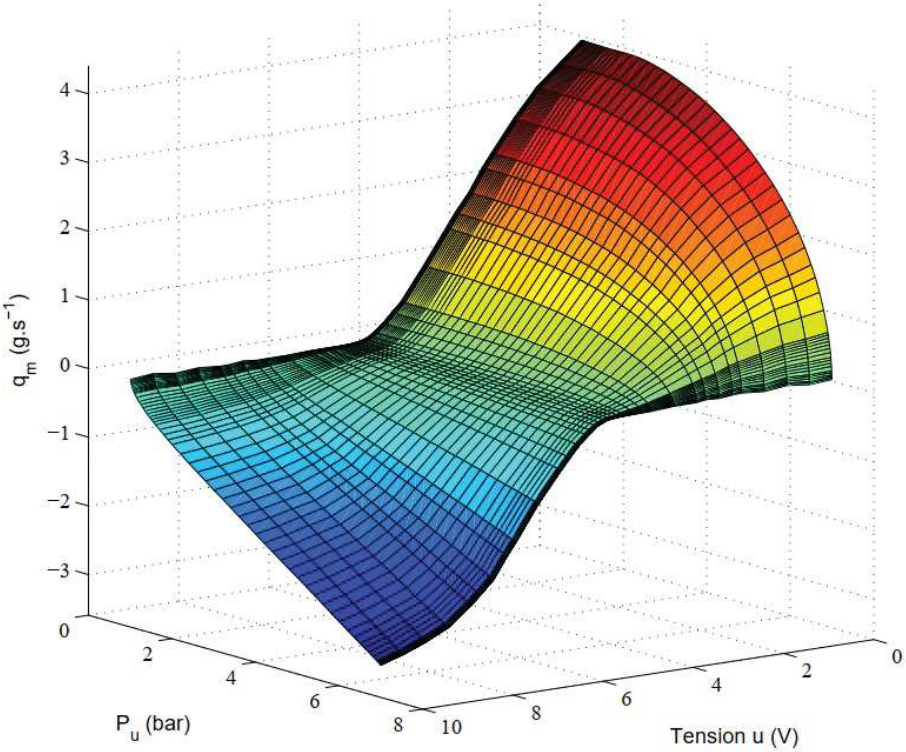

Figure 3-9 – Charateristic plot of a servolvalve MYPE-5-M5-010-B

Position tracking

To get the flow q_{mA} using the backstepping control defined in Eq. (3.17), three errors are determined.

Error 1: It is used to define the trajectory tracking and it is set as in Eq. (3.20), which define the error between the position and the desired one.

$$z_1 = y - y_d \tag{3.20}$$

With its derivative.

$$\dot{z}_1 = \upsilon - \upsilon_d \tag{3.21}$$

As the variable υ is seen as an input. To ensure the convergence of z_1 towards zero, a virtual υ^* is defined :

$$\upsilon^* = \upsilon_d - C_1 \cdot z_1 \tag{3.22}$$

Were C_1 is a strictly positive constant.

Error 2: z_2 allows to ensure the convergence of the state υ towards υ^*, thus the speed error is defined as:

$$z_2 = \upsilon - \upsilon^* \tag{3.23}$$

Which its derivative is:

$$\dot{z_2} = (F_{pneu} - F_{visq} - F_{sec} - M \cdot g \cdot \cos(\theta) - F_{ext})(\frac{1}{M}) - a_d + C_1 \dot{z_1} \tag{3.24}$$

On the other hand, in combination with equations (3.21), (3.22) and (3.23), we can obtain the position error.

$$\dot{z_1} = z_2 - C_1 z_1 \tag{3.25}$$

where F_{pneu_d}, is assumed to be a virtual input and it is chosen as:

$$F_{pneu_d} = F_{visq} + F_{sec} + M \cdot g \cdot \cos(\theta) + F_{ext} + M(a_d + z_1(C_1^2 - 1) - z_2(C_1 + C_2)) \quad (3.26)$$

with C_2 being also strictly positive and a_d the desired acceleration of the system.

Error 3: z_3 allows to converge F_{pneu} to F_{pneu_d} where it is defined the pneumatic force error is given by:

$$z_3 = F_{pneu} - F_{pneu_d} \quad (3.27)$$

also, the integration of this error variable is defined as:

$$z_{3i} = \int z_3 dt \quad (3.28)$$

The derivative of z_3 is:

$$\begin{aligned} \dot{z_3} = \dot{F}_{pneu} - (F_{pneu} + F_{visq} + F_{sec} + M \cdot g \cdot \cos(\theta) + F_{ext})(\frac{1}{M}) \\ - M(j_d + (C_1^2 - 1)(z_2 - C_1 z_1) - (\frac{z_3}{M} - z_1 - C_2 z_2)(C_1 + C_2)) \end{aligned} \quad (3.29)$$

And the derivative of z_2 is defined by:

$$\dot{z}_2 = \frac{z_3}{M} - z_1 - C_2 \cdot z_2 \quad (3.30)$$

So finally the active mass flow rate is:

$$q_{mA} = f_0 + f_1 \cdot z_1 + f_2 \cdot z_2 + f_3 \cdot z_3 \quad (3.31)$$

With

$$
\begin{aligned}
f_0 &= \frac{l(b(F_{pneu} - F_{visq} - F_{sec} - M \cdot g \cdot \cos(\theta) - F_{ext}) + MK_{pneu}\upsilon + M^2 j_d)}{2MkrT} \\
f_1 &= \frac{M \cdot l \cdot (-C_1^3 + 2 \cdot C_1 + C_2)}{2krT} \\
f_2 &= \frac{l \cdot (M^2 \cdot (C_1^2 + C_1 \cdot C_2 + C_2^2 - 1) - 1)}{2MkrT} \\
f_3 &= -\frac{l \cdot (C_1 + C_2 + C_3)}{2krT} \\
f_4 &= -\frac{K_{3i}}{2krT}
\end{aligned}
\tag{3.32}
$$

Where j_d is the desired jerk of the chosen trajectory and C_3 and K_{3i} are strictly positive constants. Until this part the control ensures the manipulation of the mass flow rate q_{mA}, which ensures that the cylinder follows the desired position tracking.

Pneumatic stiffness tracking

This part of the control is focused to control the pressurization mass flow rate q_{mT} to track the pneumatic stiffness. To get a control law that allows to set a desired stiffness to the system we get the error $z_4 = K_{pneu} - K_{pneu_d}$. Its derivative can be computed as

$$
\dot{z}_4 = \frac{A_1 \cdot K_{pneu} \cdot \upsilon \cdot y - A_2 \cdot F_{pneu} \cdot \upsilon - B_1 \cdot y \cdot q_{mA} + B_2 \cdot q_{mT}}{L_P(y) \cdot L_N(y)} - \dot{K}_{pneu_d} \tag{3.33}
$$

where the pressurization mass flow rate q_{mT} is defined by:

$$
q_{mT} = \frac{L_N(y) \cdot L_N(y)(\dot{K}_{pneu} - C_4 z_4) + A_2 \cdot \upsilon \cdot F_{pneu} - A_2 \cdot \upsilon \cdot y \cdot K_{pneu}}{B_2} + \frac{2 \cdot y \cdot q_{mA}}{l} \tag{3.34}
$$

where C_4 is strictly positive. The pneumatic stiffness trajectory tracking leads to a virtual mass flow rate q_{mT} control which depends on q_{mA}. Once the value of these two virtual mass flow rates are computed, the actual mass flow rate are calculated using the inverse A-T

transformation defined in 3.2.3.

$$\begin{bmatrix} q_{mP} \\ q_{mN} \end{bmatrix} = \Lambda^{-1}(y) \cdot \begin{bmatrix} q_{mA} \\ q_{mT} \end{bmatrix} \tag{3.35}$$

Fig. 3-10 shown the diagram of the control law, where the measurements of position (y) and speed (υ), as well as p_p and p_N (the pressures of each chamber) required to compute F_{pneu} and K_{pneu}. It is necessary to mention that the pressure of each chamber are obtained from two pressure sensors that are set in each chamber.

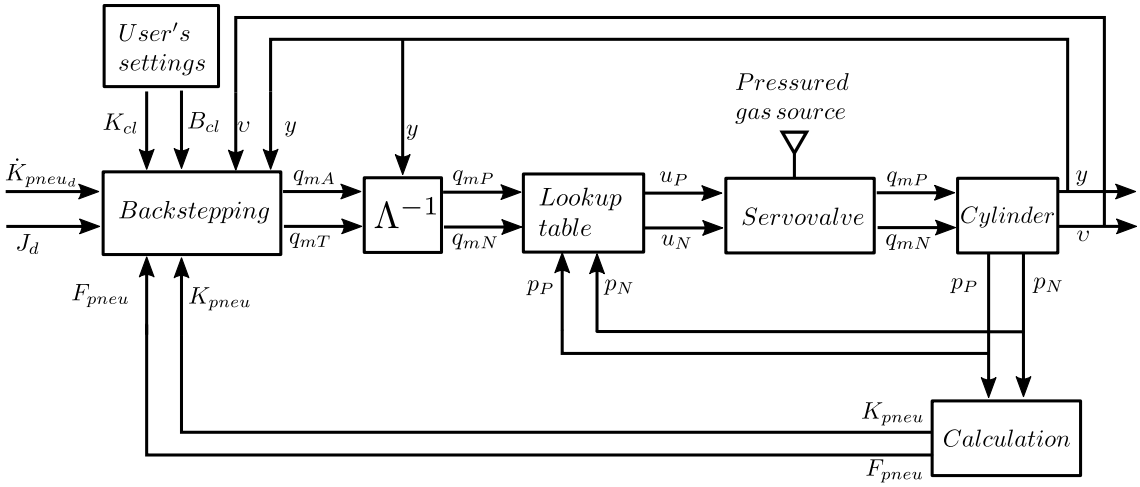

Figure 3-10 – Backstepping implementation

Tuning of gains C_1 and C_2

The parameters of the control law can be made by trial and error, which is time-consuming, inaccurate or complex. Authors in [Abry et al., 2013b] provide a linear method to estimate the parameters C_1, C_2. For that, first we introduce two terms: K_{cl} (closed-loop stiffness) and B_{cl} (closed-loop damping). The close-loop stiffness, is defined as the actuating system response in close-loop to respond an external disturbance defined by Eq. (3.36)[Abry et al., 2013a].

$$K_{cl} = -\frac{dF_e}{dz_1} \tag{3.36}$$

Where F_e is the disturbance force by the user. which leads to

$$K_{cl} = M(C_1C_2 + 1) \tag{3.37}$$

Then, we define the closed-loop damping of the system which is defined as the actuating system response to a velocity error.

$$\begin{aligned} B_{cl} &= -\frac{dF_e}{d\bar{v}} \\ &= M \cdot (C_1 + C_2) \end{aligned} \tag{3.38}$$

So with the closed-loop stiffness (Eq. 3.37) and closed-loop damping (Eq. 3.38), we can obtain a system of second order:

$$MC_1^2 - B_{cl}C_1 + K_{cl} - M = 0 \tag{3.39}$$

Resolving the previous equation we obtain C_1 and C_2.

$$\begin{cases} C_1 = \frac{B_{cl} + \sqrt{B_{cl}^2 - 4 \cdot M \cdot (K_{cl} - M)}}{2 \cdot M} \\ C_2 = \frac{B_{cl} - \sqrt{B_{cl}^2 - 4 \cdot M \cdot (K_{cl} - M)}}{2 \cdot M} \end{cases} \tag{3.40}$$

So, the global stability of the system requires that B_{cl} and K_{cl} respect the next expression.

$$\begin{cases} B_{cl} \geq 2\sqrt{M(K_{cl}-M)} \\ K_{cl} > M \end{cases} \tag{3.41}$$

Until now, the proposed backstepping control is used when the system is provided with two servovalves. However, this leads to a more expensive simulator, so a practical solution is to discard one servovalve and adapt the control law. Besides, our main purposes is to control the position and compute the human tissues behavior, the position tracking and the closed-loop stiffness tuning are thus enough as was corroborated by the work developed by [Herzig, 2016].

The compromise of converting the control law from using two servovalves to one (Fig. 3-12), is the loss of the trajectory tracking (q_{mA}) or the pneumatic stiffness (q_{mT}), as only one servovalve can not satisfy both demands of flux at the same time. For this application, it has been chosen to preserve the trajectory tracking, as based on the patient articular profile, the ultrasound probe head must adapt to the considered stiffness according to the probe position.

As the trajectory tracking has been chosen, the flow q_{mT} is not controlled and therefore the inverse transformation A-T from Eq. (3.14) is not used. So, to provide a calculation of q_{mA} and the voltage applied to the servolvalve, an algorithm developed in [Herzig, 2016] is proposed.

The first step of the algorithm is to determinate the flux q_{mP} of the servovalve by measuring the pressure of chambers P and N. This made using a projection of the characteristic plot, Fig. 3-11, of Fig. 3-9.

From the projection, it is obtained $\tilde{q}_{mA,p_P}(u)$ and $\tilde{q}_{mA,p_N}(u)$ from the closest point and with an inverse weighting of the distance. Once this is made, with current position of the cylinder the active flow is calculated for the operation point as

$$\tilde{q}_{mA,p_P,p_N}(u) = \frac{l}{2}\left(\frac{\tilde{q}_{mA,p_P}(u)}{\frac{l}{2}+y} - \frac{\tilde{q}_{mA,p_N}(u)}{\frac{l}{2}-y}\right) \tag{3.42}$$

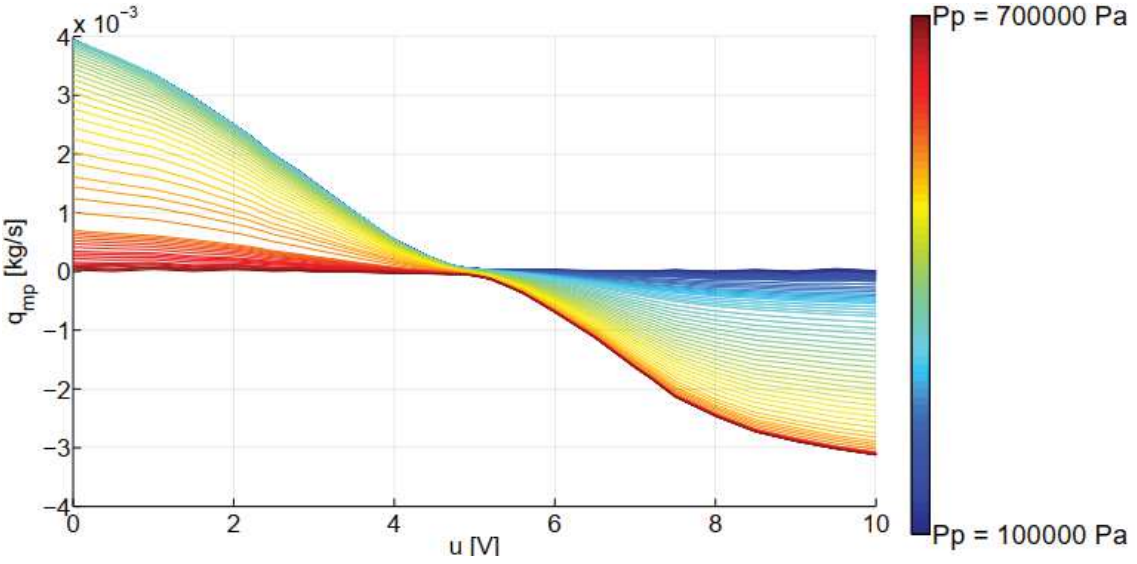

Figure 3-11 – Projection of the characteristic plot for servovalve

Once this is get, the tension to be applied to the servolvalve can be get by inverting $\tilde{q}_{mA,p_P,p_N}(u)$. Due to the bijection of $\tilde{q}_{mA,p_P,p_N}(u)$, for a fixed p_P that increases, its corresponding p_N must decrease and vice-versa. Thanks to the bijection property of $\tilde{q}_{mA,p_P,p_N}(u)$, one unitary solution is assured for the voltage u.

Until now, PID, IPC and Backstepping control laws are shown as an alternative to render the different tissue's stiffness.

Our main study in this section is to evaluate the PID, IPC and Backstepping control to render the different forces generated when the ultrasound probe is in interaction with the articulation. As the articulation is composed by soft tissue and a bone, we need to be able to render a wide range of stiffness that varies from soft to hard surfaces.

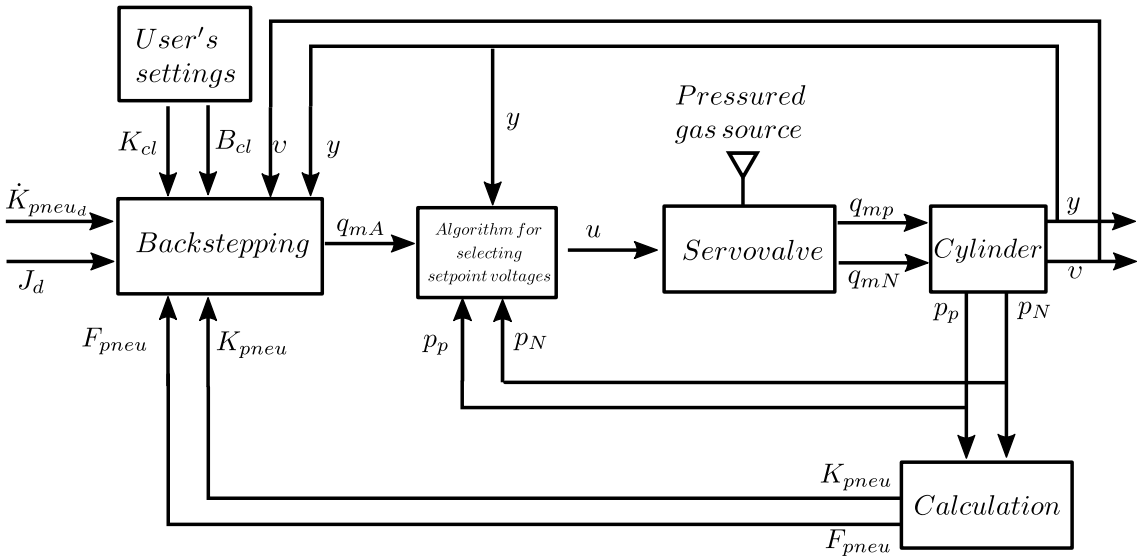

Figure 3-12 – Backstepping- one servovalve

3.3 Implementation

For our implementation, we have four elements connected between them, as it is seen in Fig. 3-13. Where the blue lines represent the pneumatic connections and the rest of the lines the electrical connections. The description of the connections are depicted in Table (3.1). The controller board is a dSPACE DS1104.

Table 3.1 – Ultrasound probe: element connections

Devices	a	b	c	d	e
Ultrasound Probe (1)	Fixed part (shell)	Pneumatic cylinder	Mobile head	Upper chamber pressure sensor	Position sensor
dSPACE Card (2)	Servo control voltage output port (0-10 Volts)	Output port to power the position sensor	Input port for position measurement	Input port measure (pressure lower chamber)	
Servo valve (3)	Power supply (4 bars)	Pneumatic output to the upper chamber	Pneumatic output (lower chamber)		
Power supply (4)	Servovalve power supply (24 Volts)	Position sensor power supply (5Volts)			

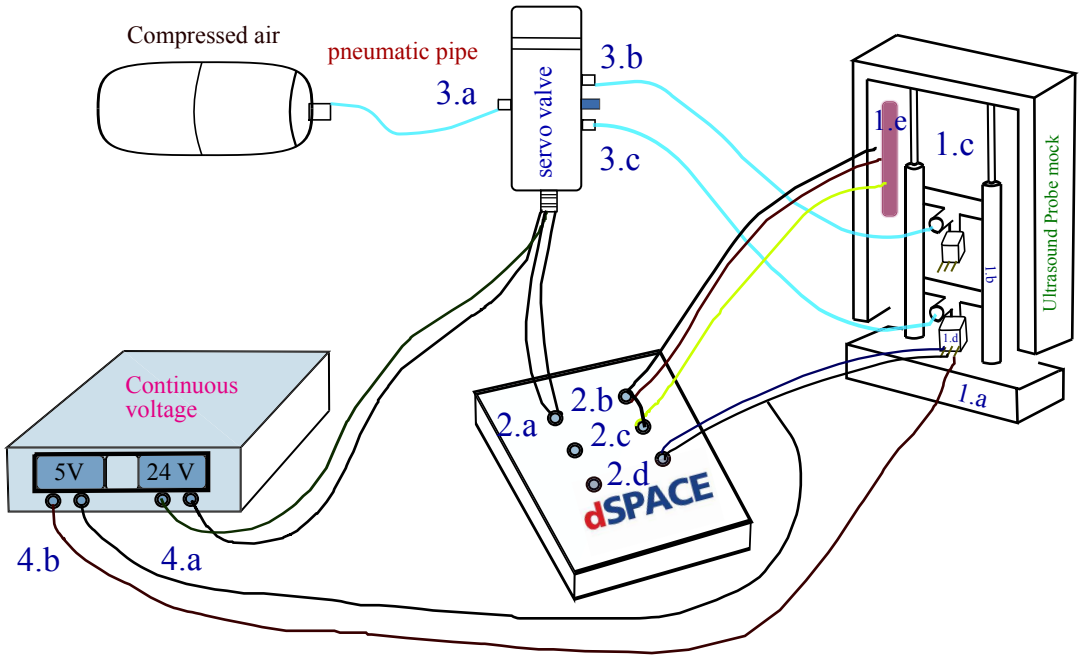

Figure 3-13 – Pneumatic implementation

3.3.1 Evaluation criteria

The evaluation criteria with the three controls laws are the position error, the level of the control voltage and the chattering caused during the performance. With this test bench, we can add a wide range of stiffness to simulate the different tissues. Nevertheless, the relevance of this test is more qualitative than quantitative, as the haptic sensation is a more crucial factor to evaluate in each control which will be evaluated by our medical partner and in a campaign test.

In this test, as we do not have the real value of the stiffness that we need to render with our haptic device, we propose the following profile of stiffness (Fig. 3-14). Which can be modify easily in our test bench once the real values are obtained.

This profile is a close approach of what occurs during the ultrasound inspection process. We are going to suppose that the needle is inserted as can be seen in the Fig. 3-14. During the performance, as the needle tip is visible in the ultrasound 2D image, the user should displace the probe around of the insertion point. The ultrasound probe is displaced by the user on the soft surface, where the stiffness he/she feels can be low, medium or high, as this

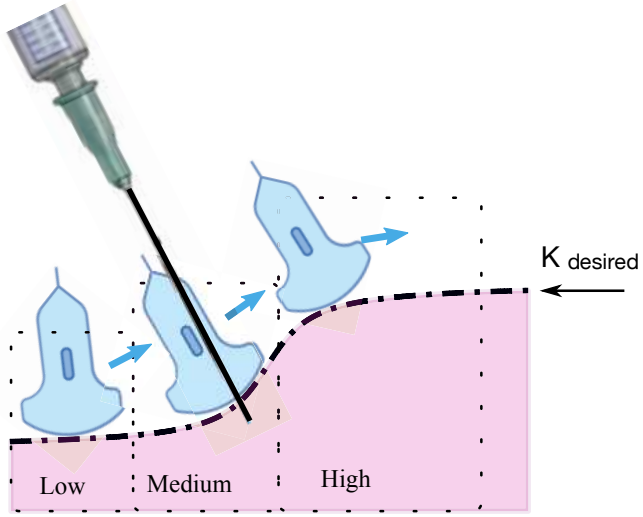

Figure 3-14 – Consideration of stiffness profile.

can be composed of skin, fat or bone. All of this depends of the part of the articulation in contact. We consider that the higher stiffness is when the US probe is touching part of the bone.

3.3.2 Control laws comparison

We perform two different tests using each one of the three previously proposed controls. The two tests consisted of two different profiles: the first, an Increasing Stiffness Profile (ISP), and the second a Step Stiffness Profile (SSP).

The parameters of the PID and IPC controls are in Table 3.2, and for the backstepping control they are in the Table 3.3.

Table 3.2 – Control law parameters

PID parameters		IPC parameters	
K_p	60	k_1	55
K_i	5	k_2	100
K_d	20	M_v	0.4 kg

Table 3.3 – Backstepping parameters

Mechanical parameters			
M	Load mass	0.37	Kg
S_p	Cylinder section area superior	78.540×10^{-4}	m^2
S_n	Cylinder section area inferior	65.974×10^{-4}	m^2
F_{sec}	Stiction force	5.2	N
b	Viscous friction coefficient	67.9	$N \cdot s/m$
l	Stroke of the rod	0.05	m
Thermodynamic parameters			
k	Polytropic coefficient	1.2	-
r	Perfect gas constant	287	$J/(kg \cdot K)$
T	Temperature of the supply air	298	K
Gains parameters			
C_1	-	780	
C_2	-	280	
C_3	-	2100	
C_4	-	100	

The procedure of this test is a follows. First, all the control laws begin with the same initial conditions ($x_0 = 0$ m and no acting force applied on the sensor) and after a few seconds, a load of $1kg$ is charged over the force sensor that acts as our acting force. Then, the desired stiffness profile is established and remains during the rest of the test.

Increasing Stiffness Profile (ISP)

The Increasing Stiffness Profiles used for the PID and IPC is shown in Fig. 3-15a. In the case of the backstepping control, the profile is shown in Fig. 3-15b.

The limits of the stiffness profiles were chosen empirically, by testing the maximum and minimum values where a difference of stiffness is felt by the user. For the PID and IPC the profiles go from 500 to 1000 N/m and for the backstepping control from 800 to 3000 N/m.

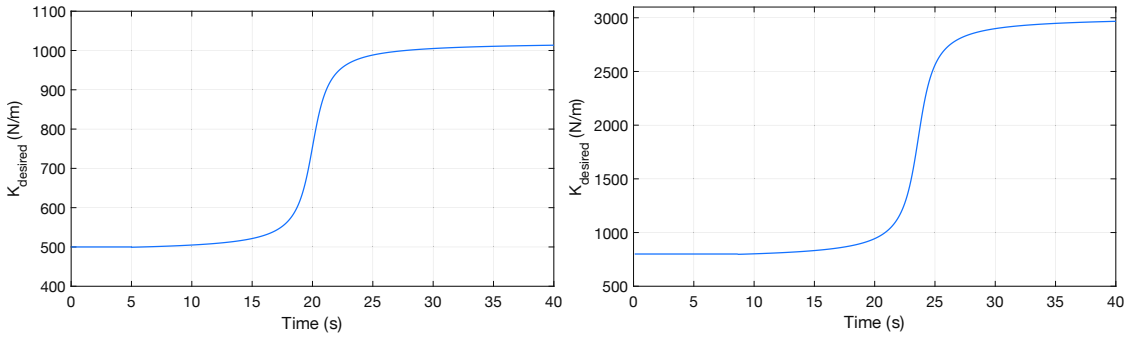

(a) Increasing Stiffness Profile (b) BS-ISP: profile stiffness

Figure 3-15 – Stiffness profiles

Fig. 3-16a, Fig. 3-16b and Fig. 3-16c show the initial position of the system (x_0), the expected position (x_c) and the measured position (x_m) for the PID, IPC and Backstepping control respectively. All the controls begin with the same initial conditions. Then the load of $1kg$ is charged on the sensor at $t = 10$s (PID and IPC) and $t = 8.5$s (Backstepping) and the desired ISP is activated, which increases the desired stiffness in function of time. From this point the position changes its value as the desired stiffness increases over time. At $t = 25$s the stiffness reaches its maximum value.

As can been seen, PID and IPC have similar behavior and both react faster than the Backstepping. In the case of the Backstepping control, this does not reach the expected position at first and although this can be considered a drawback, it presents a smoother trajectory tracking of the expected position x_c, once the desired stiffness overpass the 1000 N/m.

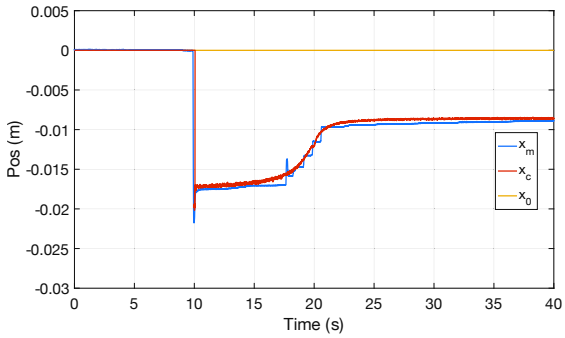

(a) PID-ISP: position

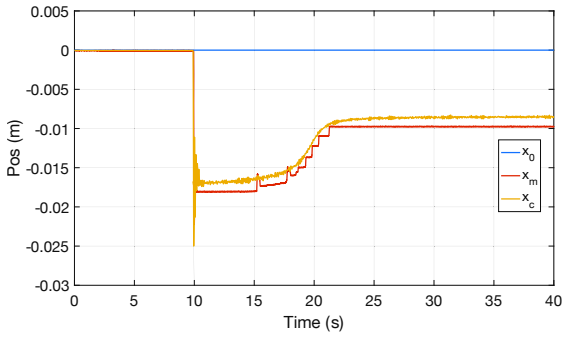

(b) IPC-ISP: position

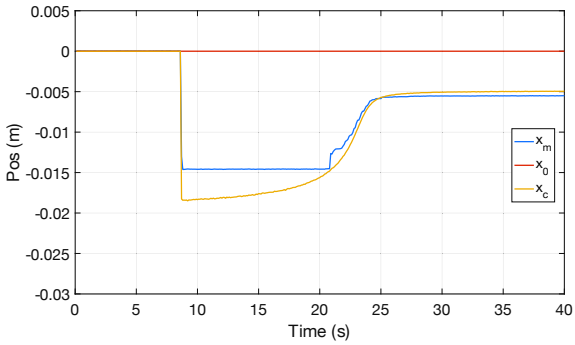

(c) BS-ISP: position

Figure 3-16 – ISP positions

From this, we can deduce that when the force is constant and the desired stiffness increases, the system compensates the stiffness by taking out the rod in all the control laws. In Fig. 3-17a, Fig. 3-17b and Fig. 3-17c it is shown the position error. As can been seen, it exists an overshoot when the load is charged on the sensor in all the control laws. After that, the position errors are around 3*mm* for the PID and IPC during the transition, and it almost tends to zero in steady-state. In the case of the Backstepping control, the error is greater than the others having a maximum error of 5*mm* but during the transition the error decrease quickly. In steady-state, the error tends also to zero, as it happens with PID and IPC.

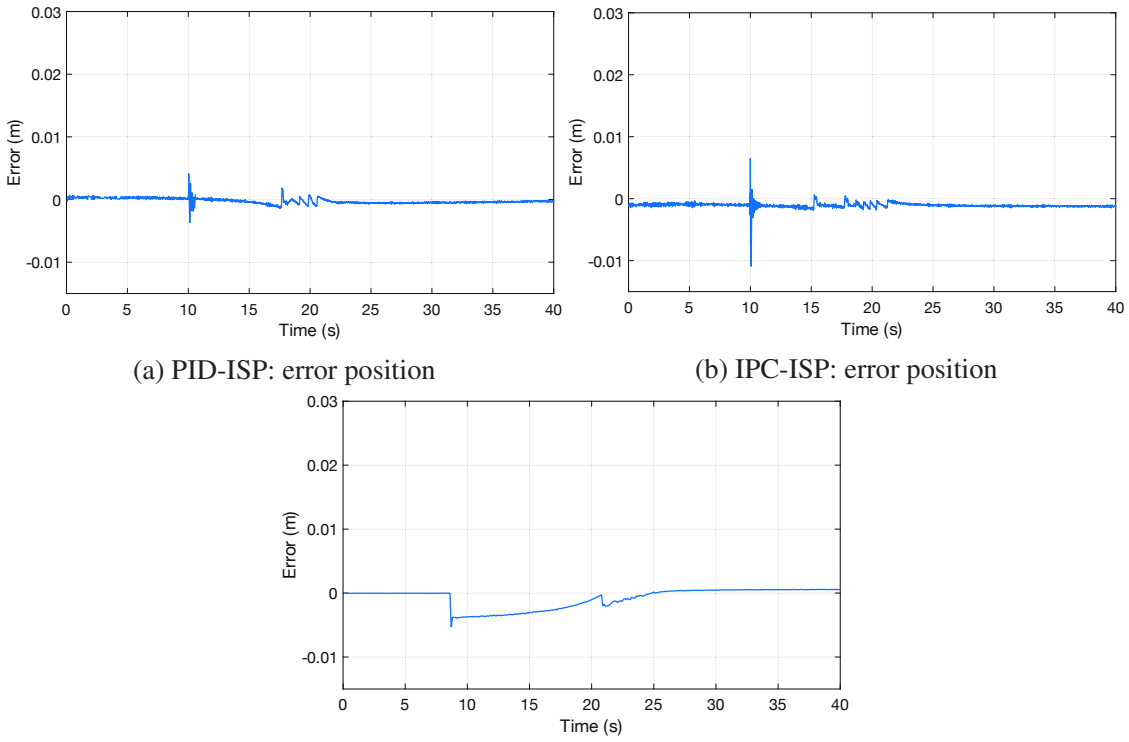

(a) PID-ISP: error position

(b) IPC-ISP: error position

(c) BS-ISP: error position

Figure 3-17 – ISP error position

In Fig. 3-18a, Fig. 3-18b and Fig. 3-18c it can been seen the control voltage for the three controls. In this case, it also exists a peak of voltage when the load is charged. After this point, the voltage remains between 5.3 and 4.4 for the three control laws. The voltage control for the IPC is smoother and with fewer variations. The voltage of the IPC presents a step behavior, while the backstepping voltage the changes are abrupter.

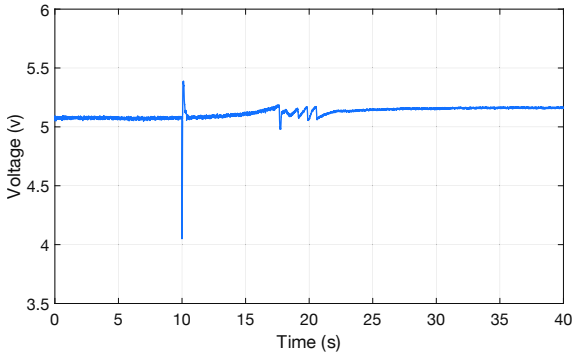

(a) PID-ISP: control voltage

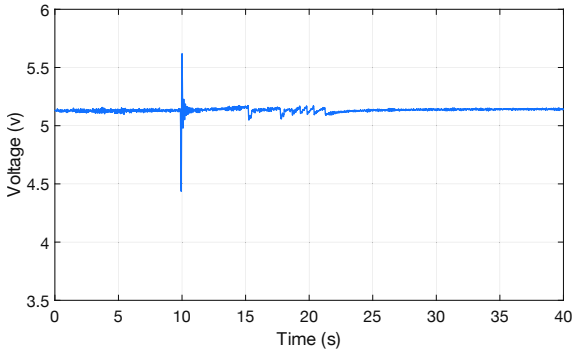

(b) IPC-ISP: control voltage

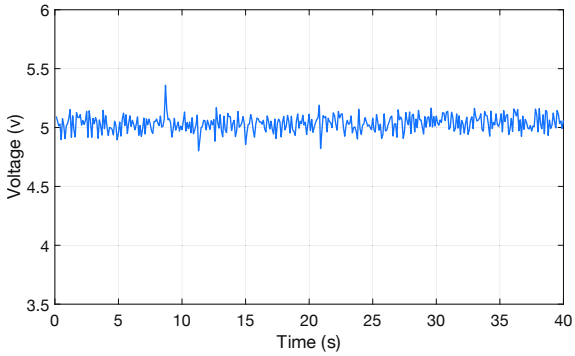

(c) BS-SSP: control voltage

Figure 3-18 – Control voltaje for ISP profile

As the backstepping control is implemented by using one servolvalve instead of two, the pneumatic stiffness is no longer controlled. Because of this it is necessary to verify that its evolution is limited and does not diverge, to ensure the global stability of the system ([Herzig, 2016]). For this we calculate the $K_{pneu_{min}}$ and the $K_{pneu_{max}}$ as

$$\begin{aligned} K_{pneu_{min}} &= \kappa \cdot P_{atm} \frac{(\sqrt{S_{Pi}} + \sqrt{S_{Ni}})^2}{l_i} \\ K_{pneu_{max}} &= \kappa \cdot P_{max} \left(\frac{2S_{Pi}}{l_i + 2y_{imax}} + \frac{2S_{Ni}}{l_i - 2y_{imax}}\right) \end{aligned} \tag{3.43}$$

This aids us to determinate the maximum and minimum stiffness on which the system can work. For our case the maximum and minimum stiffness are 692.14 and 14155 N/m. In Fig. 3-19 it is shown the pneumatic stiffness.

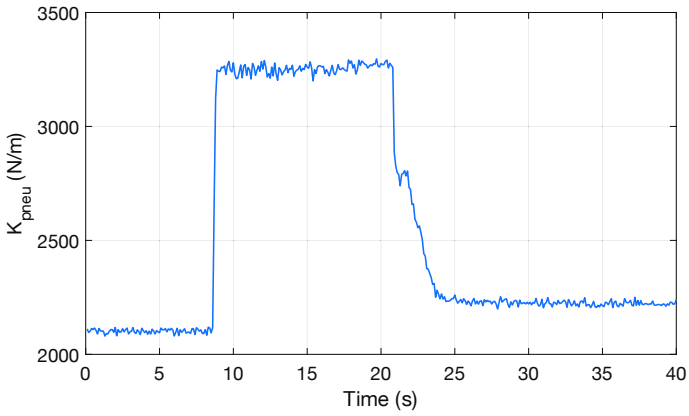

Figure 3-19 – BS-ISP: K_{pneu}.

The pneumatic stiffness is set from 2100 N/m to 3300 N/m, which are between the maximum and minimum values, and therefore the system is globally stable.

Step stiffness profile (SSP)

The Step Stiffness Profiles are established as a changing step that simulates a case where the stiffness changes suddenly. This test is to prove the robustness of the control laws in a case of abrupt changes of stiffness. In real tests with patients, this case is very unlikely to happen, as the practitioner moves the ultrasound probe smoothly over the articulation while he/she searches for the needle. For the PID and IPC, the SSP used is shown in Fig. 3-20a. In the case of the backstepping control, the profile is shown in Fig. 3-20b

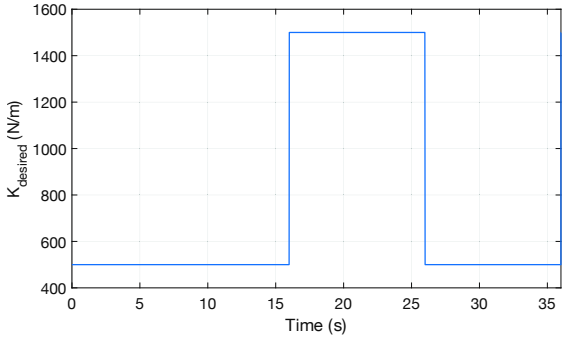

(a) PID and IPC: Step Stiffness Profile

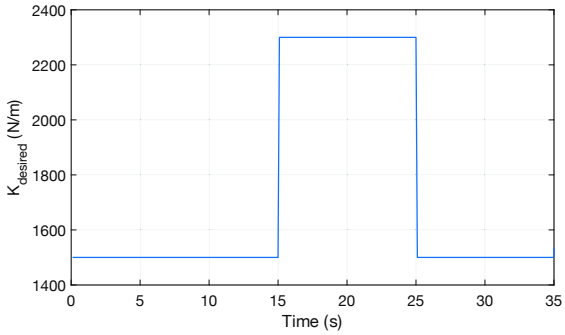

(b) Backstepping: Step Stiffness Profile

Figure 3-20 – SSP profiles

Fig. 3-21a, Fig. 3-21b and Fig. 3-21c show the x_c position of the PID, IPC and back-stepping control during the abrupt stiffness change. As it was made with the ISP test, at $t = 9$ s, the load was charged on the force sensor.

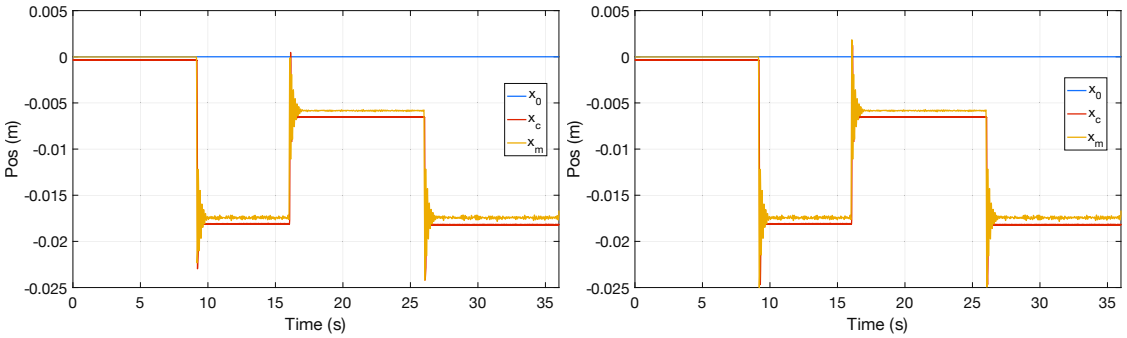

(a) PID-SSP: position.

(b) IPC-SSP: position.

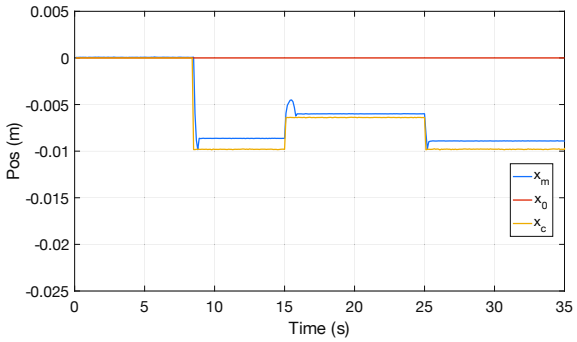

(c) BS-SSP: position.

Figure 3-21 – Control law positions

Fig. 3-22a, Fig. 3-22b and Fig. 3-22c show the position errors for the SSP profile. As it is noticed in the position plots, the PID and IPC control present similar behavior. A drawback presented by this backstepping is an increase around 10% of steady-state error in comparison with the PID and IPC. So, the backstepping control is robust to the sudden change of stiffness but with the cost of position precision.

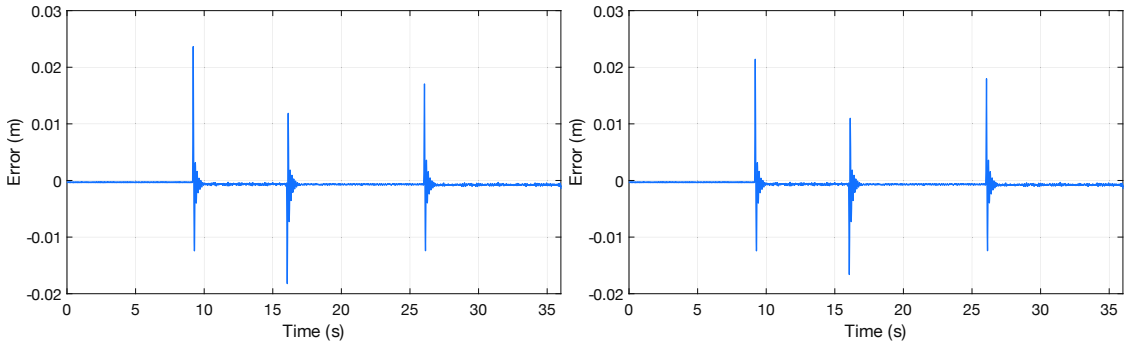

(a) PID-SSP: error position

(b) IPC-SSP: error position

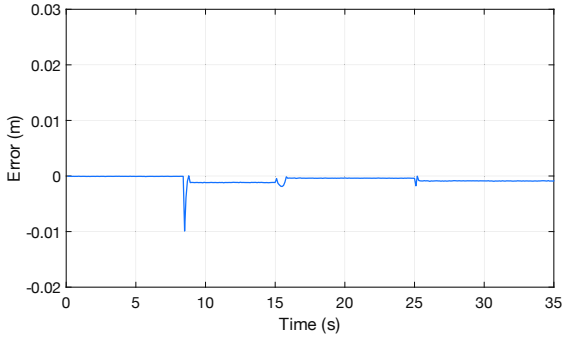

(c) BS-SSP: error position

Figure 3-22 – Control laws error position

For the control voltage, Fig. 3-23a, Fig. 3-23b and Fig. 3-23c show the voltage control. The control voltage of the three control laws shows only overshoot during the abrupt change of stiffness. The backstepping control presents a similar behavior from the ISP profile, proving the consistency of the control during the change of stiffness.

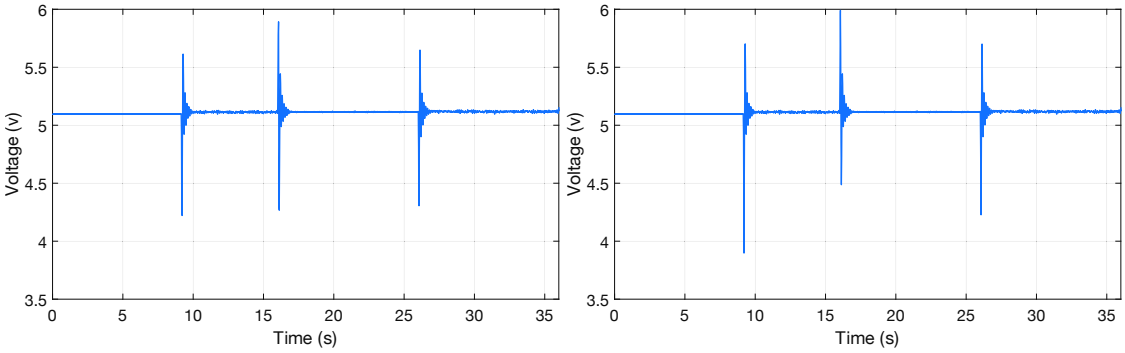

(a) PID-SSP: control voltage

(b) IPC-SSP: control voltage

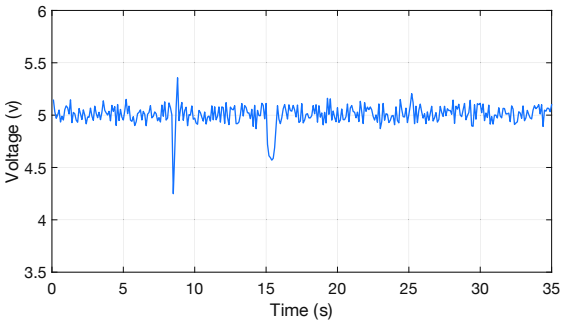

(c) BS-SSP: control voltage

Figure 3-23 – Control voltage for SSP profile

Finally, the k_{pneu} of the backstepping control for the SSP is shown in Fig.3-19. In this case, the values of the stiffness remain between 2100 and 2450 N/m, proving that the system remains globally stable with the values calculated in the ISP profile.

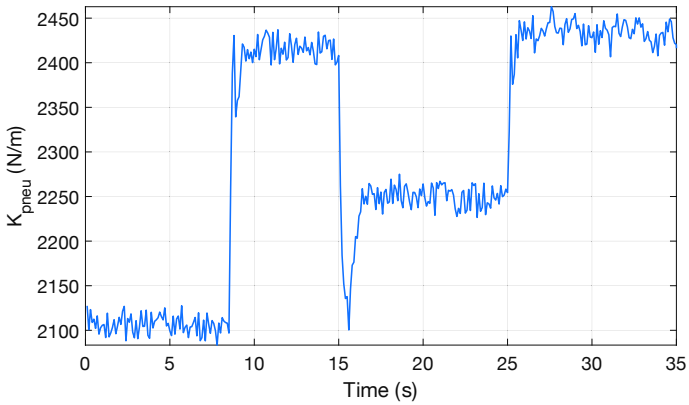

Figure 3-24 – BS-SSP: k_{pneu}

3.4 Discussion

To implement the ultrasound probe, we opted for using a single servovalve with a cylinder to reduce the cost of the prototype. By changing the position of the rod, it is possible to manipulate the stiffness of the system from the desired input stiffness. We compare three different control laws to find the best that fits our necessities. These control laws were PID, Backstepping and the IPC.

Two stiffness profiles were proposed, ISP and SSP, to help us to find the different advantages and disadvantages of the three control laws. For instance, the PID and IPC behave in a similar way for the ISP and SSP, with some minor differences between the steady state-error and the control voltage. In the case of backstepping, this control presents, in the two tests, a greater steady-state error, but this also does not offer chattering in the SSP test (contrary to the PID and IPC). This indicates that the control is more robust to the sudden changes of stiffness. This is because the backstepping is a non-linear control law that better fits with the non-linear behavior of the cylinder and the servovalve. Also, it is not necessary to implement a force sensor to measure the acting force on the ultrasound probe, since in the

backstepping control the force applied by the user is considered as a perturbation and can be estimated. This is considered an advantage for backstepping control against PID and IPC, as the implementation of a force sensor increases the cost of the systems.

From a quantitative point of view, the PID and IPC are probably the best options, due to its precision. However, as our final objective is to deliver a realistic render of the acting force on the ultrasound probe, so the robustness of the backstepping have greater advantages over the other two, as the stiffness profiles can vary from patient to patient, as well the examination surface. To determine the more optimal control, a campaign of test with expert practitioners must be done so their qualitative feedback help to determinate the best control to render the acting force.

Chapter 4

Global design and communication with virtual environment

4.1 Introduction

The objective of SPARTE project is to create a simulator of puncture for articulations under echography. To reach this, it is necessary to choose a haptic device that reproduce the haptic feeling of puncturing with a needle, as well as we need to offer a haptic device that provides the force feedback of an ultrasound probe when it is in interaction with the articulation.

Different mechanical designs are proposed to represent the syringe/needle with the haptic device as well as the ultrasound probe. For all the mechanical design and implementations, the aim limb to perform the tests is the shoulder. However,the articulation can be changed in future tests and implementaions, as there is no limit to the possible number of scenarios in which the simulator can be used.

The assembly of the simulator is introduced in this chapter. We collaborated with LIRIS laboratory to join its numeric model to render the 2D ultrasound image with our virtual environment and mechanical design. In this chapter, we also present the results of one test performed by our medical partner from HCL.

4.2 Choosing the haptic device for needle insertion

To implement the syringe/needle in our simulator we make an evaluation of three commercial haptic devices, where three points are evaluated to implement our tools. These three principal points to evaluate are:

- **Tool Adaptation:** it means that the needle's mock can be attached to the haptic device in an easy way.
- **Force limitation:** the haptic systems must be able to exert enough forces to render hard contact.
- **Work space:** the haptic device allows to insert the needle in any part of the articulation in the virtual environment.

Table 4.1 gives the specifications of some commercial haptic devices and theirs limitations to implement them to simulate the syringe (Fig. 4-1).

Table 4.1 – Haptic devices

Device	Specifications	Syringe adaptation
Omni Geomagic Touch	6 DoF 3 Active translation 3 Passive rotation 3 N translation work space 16 cm x 12 cm x 7 cm	Easy adaptation Force limitation Free manipulation of tool No rotation active
Haption Virtuose desktop	6 DoF 3 Active translation 3 Active rotation 10 N translation 0.8 Nm rotation work space 52 cm x 37 cm x 40 cm	Easy adaptation Force acceptable Free manipulation of tool All the Dof motorized
Delta Force dimension	3 DoF 3 Active translation 12 N translation Work space 16 ϕ x 11 cm	No easy adaptation Force acceptable Restriction of natural tool movements

(a) 3 DoF Geomagic Touch (b) 6 DoF Virtuose desktop (c) 6 DoF Delta

Figure 4-1 – Commercial electrical haptics systems

Most of these devices fit our needs to represent the syringe with the haptic device. For our study case, we choose the Virtuose 6D Desktop haptic device from Haption, since it is the one that offers enough workspace, it has acceptable force feedback, the syringe can be adapted on the haptic device's tool, and also respect the natural movements that the doctor needs to perform during the needle injection.

4.3 Ultrasound probe design

For the ultrasound probe, as has been mentioned in section 3.1, the electric haptic actuators are not suitable for implementing the ultrasound probe. Due to this, the appropriated actuator that best fits, is a pneumatic actuator.

The first pneumatic ultrasound probe was designed by [Abdallah et al., 2019] (Fig. 4-2), and was implemented to be used as a remotely control of an echographic robot. The US probe is composed by two principal parts: one part called mobile head, which is attached at the end of the cylinder rod, providing one degree of freedom. And the other fixed part where the components are set on it, is named shell. The component specifications that conform the US probe are enlisted below.

- Pneumatic actuator: CS 10 E from Pneumatic UnionR.
- Pressure sensor: 40PC100G2A from honeywell.
- Position sensor : LP804-2 by Omega Engineering

- Mobile head.
- Shell

This ultrasound probe was designed to be robust but serve to our test in the search of the optimal control law. In future implementations, the probe will be built to resemble a more real ultrasound probe.

To reproduce the haptic feedback, the user holds the US probe from the shell and applying force on a hard surface as he will do in real. The pneumatic actuator will generate force feedback to the user according to the virtual environment, which can be, in our case, any articulation.

To control the pressure of the cylinder, a servo distributor MPYE-5-M5-010 B from Festo is used. To measure the acting force exerted on the surface we use a force sensor ELPF-T2M-100N from Meas instrument.

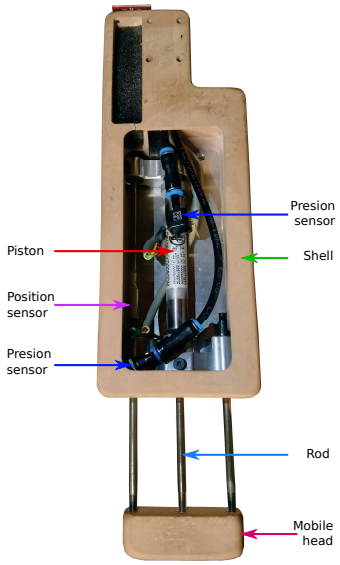

Figure 4-2 – Pneumatic ultrasound probe

4.4 Mechanical design

To adapt the syringe with the haptic device, different mechanical designs were proposed and tested by a specialist who validates them and provides us qualitative feedback. Fig. 4-3

shows on the left side the real syringe, and in the right side the syringe mock which is adapted in our mechanical design. The syringe was built using additive fabrication to resemble to its real counterpart. As our main objective is to compute the forces during the needle insertion in tissue, we focus on the needle motion, thus the syringe's piston can not move during the test.

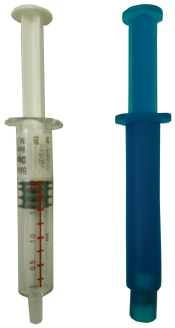

Figure 4-3 – Real syringe and mock syringe

4.4.1 Design one "Tool-Down"

The first design proposed, consisted in changing the tool configuration of the haptic device from "tool- up" default configuration (Fig.4-4) to "tool-down". This configuration helps to adapt the syringe with the haptic device's tool.

Figure 4-4 – Standard configuration Virtuose™6D Desktop

The prototype consisted in adapting the syringe at the end of the tool device, as it is seen in the Fig.4-5. A retractable needle is set inside the syringe which displaces when it collides

against the shoulder. This helps to give a visual perception of piercing it, and also when the syringe is removed from the point of insertion, the needle moves out returning at its original position. With this configuration, the user can hold the syringe's position according to his/her necessities when he/she is choosing the insertion point.

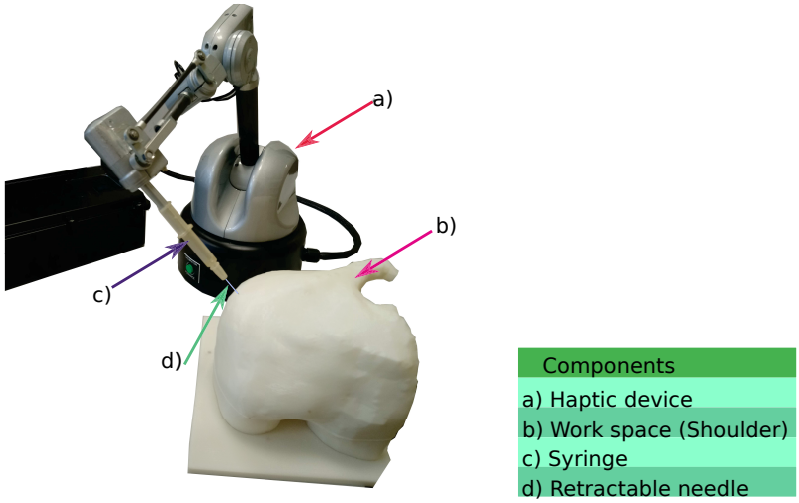

Figure 4-5 – Design 1:"Tool-down" configuration

The advantages of this design are:

- Free movement of the syringe around the space work
- Ability to choose the point of insertion
- Simplicity to change the articulation's position and to interchange the needle's length

Despite this, some disadvantages were found by the medical staff. The main problem relied on how the forces are exerted by the haptic device, due to its mechanical configuration. Since the device exerts the force at the top of the syringe, and not at the needle tip, the doctor feels a pulling force instead of a pushing one, reducing the realism and feeling sensation of piercing the shoulder. Another problem was the functionality of the retractable needle as this only returns at its starting position when the injection is in diagonal and vertical, but not when in a horizontal position. One way to solve this problem is to add a spring to help it

to return to its initial position, but because of the main disadvantage mentioned above, we focus on solving the main problem, and we did not investigate further this solution.

4.4.2 Design two "Tool-Up"

Taking into account the commentaries of the first design, the tool's configuration was changed from tool-down to tool-up. In this way, it is assumed that the force is exerted on the needle tip.

The objective of this design is similar to the first one, which consists in creating an environment where the user can manipulate the syringe to choose the insertion point onto the articulation.

In this case, the syringe is set parallel at the tool's device, to ensure that the forces are exerted by the haptic device at the end of the needle. An outer shell was built using adding fabrication and was screwed at the device as can be seen in Fig. 4-6. Two supports are added to hold the syringe. In this way, a space where the user is allowed to grasp is left. Inside the hollowed syringe, it is set the retractable needle that moves inside it when this collides with the shoulder. It returns at its initial position when the needle is withdrawn from the shoulder.

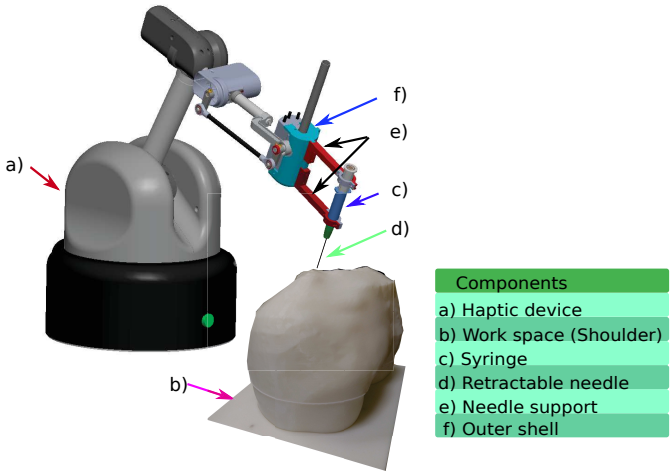

Figure 4-6 – Desing 2:"Tool-Up" configuration

The feedback given by the medical staff concerning this design, relies more on the needle's movement, as the syringe's body must not be constrained, and in this case, the needle was constrained by the supports. Hence, when the user wants to change the trajectory inside of the articulation, the wrist mechanical movement limits it and therefore, it feels unrealistic.

4.4.3 Design three: "Needle tip constraint"

For this design, it has been proposed to constrain the needle tip as can be appreciated in Fig. 4-7 letting free the syringe's body, which allows free movement during its interaction with the user.

The design consisted of a base where the haptic device relied on it. In the front part of the base, a support is used to guide the needle during the insertion. A spherical groove is placed inside this support (Fig. 4-8) to allow the three rotations of the needle and its translation (forward/backward movement), giving the perception of piercing the articulation. Also, this needle support was built to limit the angle α to a maximum of 45 °.

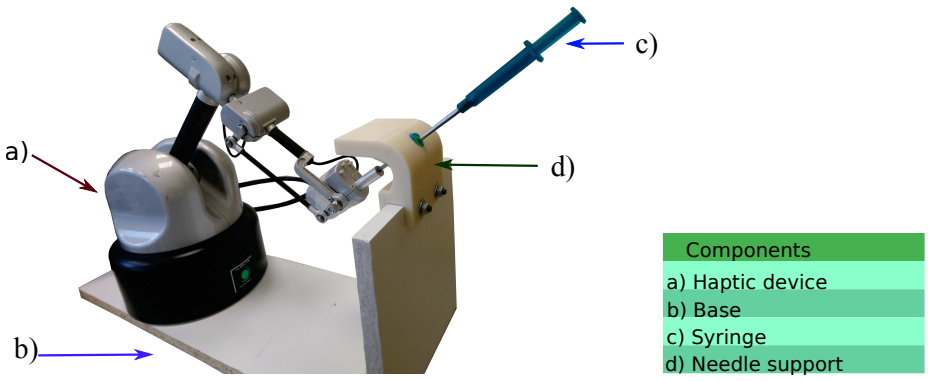

Figure 4-7 – Design 3: "Needle tip constrain"

The medical staff's feedback has considered that this design allows feeling more realistic cutting forces, as they are exerted at the end of the tool giving the correct sensation. Also, the needle support was accepted, but with certain modifications considering two issues.

- The support lacks enough space to let the user lays his hand onto the needle support. Since in real procedures they lay it on the body, so the fist can obtain stability at the moment of the needle pierces the tissue.

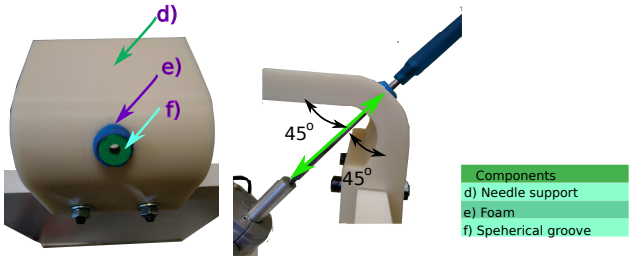

Figure 4-8 – Point of insertion limited to move 45°

- The second problem is related to the change of trajectory because the hole that supports the spherical groove does not respect the natural rotation of the needle causing that the change of trajectory feels constrained.

4.4.4 Design four: "Needle tip constraint with conical hole"

In the fourth design (Fig. 4-9) more space has been added to the needle support, allowing the user to rest the fist onto it. It is also added a tapered hole in the needle support (Fig. 4-10) that allows rotating the syringe's body to change the trajectory. With these modifications, the design has fulfilled the requirements needed to perform the needle insertion.

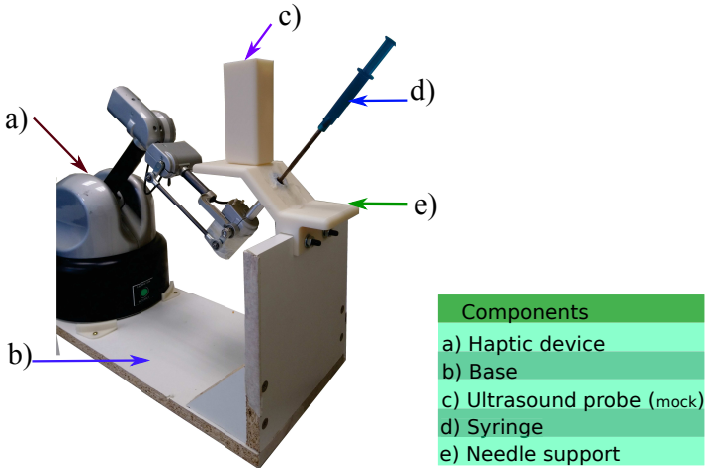

Figure 4-9 – Design 4: "Needle tip constrain with conical hole"

However, while working with the ultrasound mock probe (Fig. 4-9), it can be appreciate

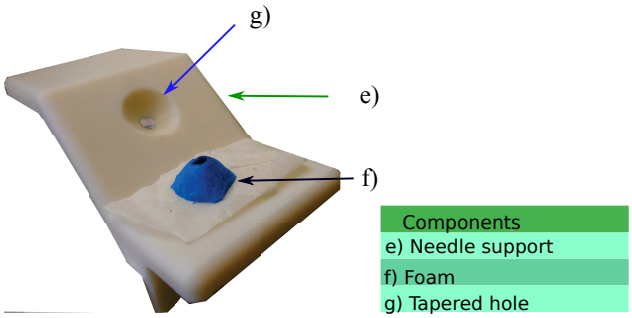

Figure 4-10 – Needle support "tapered hole"

that the point of insertion is not in the same plane where the ultrasound is placed, causing a problem of realism, since in real performance the probe must be in the same plane of the needle.

4.4.5 Design five: Implementation of a support surface

This last design was manufactured to improve the previous one's restriction. More surface was added to allow placing the students' fist on the articulation, as well as enough space to let free exploration with the ultrasound probe, around the articulation's working plane (Fig. 4-11).

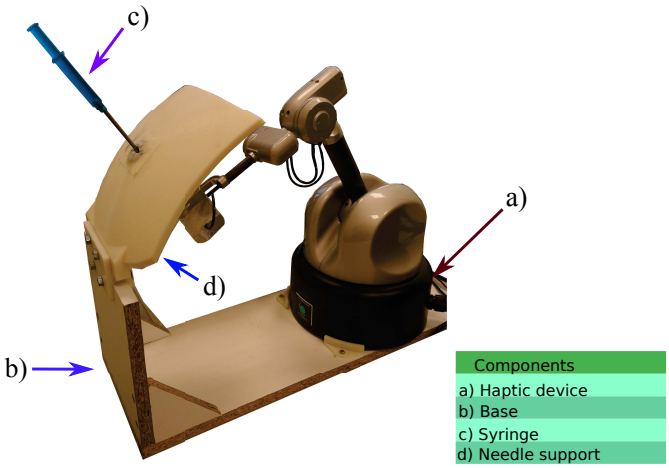

Figure 4-11 – Design Five: support surface

Despite the improvements made, we still have one main issue unresolved, the fixed insertion point. This problem is carried out since design three.

To solve this issue and after discussion with the different SPARTE partners the proposed solution is to split the gestures into two parts:

1. First, the user is free to explore with the US probe the joint surface to determine its insertion point.

2. Once the point is chosen, the numeric model is calibrated according to this point and the user can start to insert the needle.

This last version complies with all the requirements demanded by the medical staff. A test to prove its efficiency was performed, where the objective was to compute the forces during the needle insertion and render the ultrasound probe image, which helps to guide the needle inside the tissue. The rendering of the image is the work developed by one of the partners of the SPARTE project: the laboratory LIRIS.

4.4.6 Ultrasound probe considerations

As was discussed in section 4.2 the best way to render the acting forces for the ultrasound probe is by implementing a pneumatic actuator (Fig. 4-12a).

The main idea is to use a position sensor (for instance a magnetic sensor such as trakSTAR) by Ascension Technology corporation to localize the ultrasound probe in the space work that simulates the articulation. However, this sensor can not be yet implemented in our partner software. For this reason, the ultrasound probe is simulated by implementing a haptic electric device (Geomagic Touch), without force feedback (Fig. 4-12b). The only parameters used are the position and the quaternions to localize the ultrasound probe position in the space work of LIRIS software.

(a) Pneumatic ultrasound probe

(b) Electric ultrasound probe

Figure 4-12 – Ultrasound probe

4.4.7 Discussion about the prototype

Different designs have been built in collaboration with the SPARTE project partners and in particular with the medical expert. To accomplish the criteria mentioned previously in subsection 1.5.2 different designs have been tested. After different tests, the last design has been accepted and validated by our medical experts. They consider it that the system's realism (in conjunction with the environment detailed in the following section) is enough to immerse themselves in the simulation. For practical issues, the complete simulator that is compound by the needle and the US probe (two different haptic interfaces), has not been implemented together for the following tests. But the complete simulator should be ready for the measurement campaigns which will be tested by several junior and senior doctors to evaluate it.

4.5 Virtual Environment

4.5.1 CHAI3D framework

The deformable wall algorithm, the virtual fixture, and the orientation control were rewritten in C++ and a user-friendly interface was implemented using the framework CHAI3D [Conti et al., 2003]. The virtual environment consisted of a virtual articulation that helps the user to have more immersive experience due to its similarity to the real workspace (Fig. 4-13).

To connect the haptic device, it was created a library that communicates the CHAI 3D framework with the Virtuose API, since CHAI3D natively does not support our haptic device (Virtuose 6D desktop). The virtual environment was compiled in Visual Studio 2017 for the creation of Windows binary and in QT creator for UNIX like operating systems.

Creating this virtual environment allows us to establish different force profiles during the needle piercing. It also allows the user to rotate the virtual articulation freely and to choose freely the point of insertion. For all of our tests, a shoulder was set as the interest body's articulation. Fig. 4-13 shows the virtual environment created in CHAI3D, and the complete.

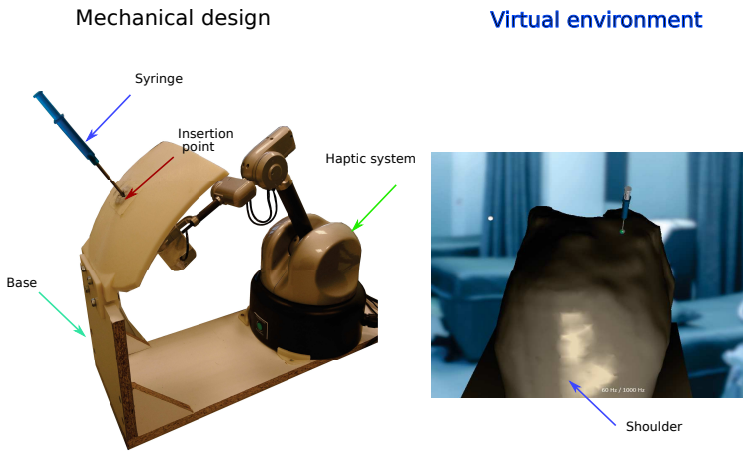

Figure 4-13 – Test bench

4.5.2 Memory sharing

It should be noticed that the algorithms were tested by setting randomly desired forces, in order to get force feedback. This was made in this way, because of the lack of having any real profile of forces during the needle insertion.

To have the real forces during needle insertion a collaboration between Ampere and LIRIS was performed. LIRIS created an environment [Barnouin et al., 2018], which recreates the ultrasound 2D image and can send us the actual working layer. From this, we can determine the desired forces and apply them to the needle's haptic device. However, as each partner use different development environment and frameworks, there is no official support

to communicate all of them with the haptic system. Because of this, the chosen solution was to implement a memory sharing method to run both software in parallel to share the position and the quaternion orientation of the haptic device with the model simulation software. In return, we read the desired forces depending on the layer where the needle is. Memory sharing is considered as a fast interprocess of communication mechanism, where the operating system helps to map a memory segment in the address space where a process can read or write in this memory segment, thanks to the Boost libraries. [1]

Fig. 4-14 shows a schematic of the data that are shared during the simulation. The haptic device that represents the syringe is running implementing the CHAI3D framework through the developed library previously mentioned. The data transmission occurs with the start of the simulation. In our case, we reserve a memory space named "POS", and share one named "FORCE". In our memory space, we are going to write the position and the quaternions of the haptic device for our partners' software. As it is running in parallel, LIRIS' environment can read it and use it for their model to recreate the corresponding 2D ultrasound image and the needle position in it. Knowing these information, they can determine the layer that the needle tip is in interaction and write the data in the memory space named "FORCE". With our algorithms we retrieve this information and then the force is computed to be sent to the user as long as it exists a collision between the needle tip (tool) and the articulation (virtual environment).

The next scheme (Fig.4-14) shown the data sharing between CHAI3D, the virtual environment developed by LIRIS and the communication established with boost libraries.

[1] The BOOST libraries-https://theboostcpplibraries.com/

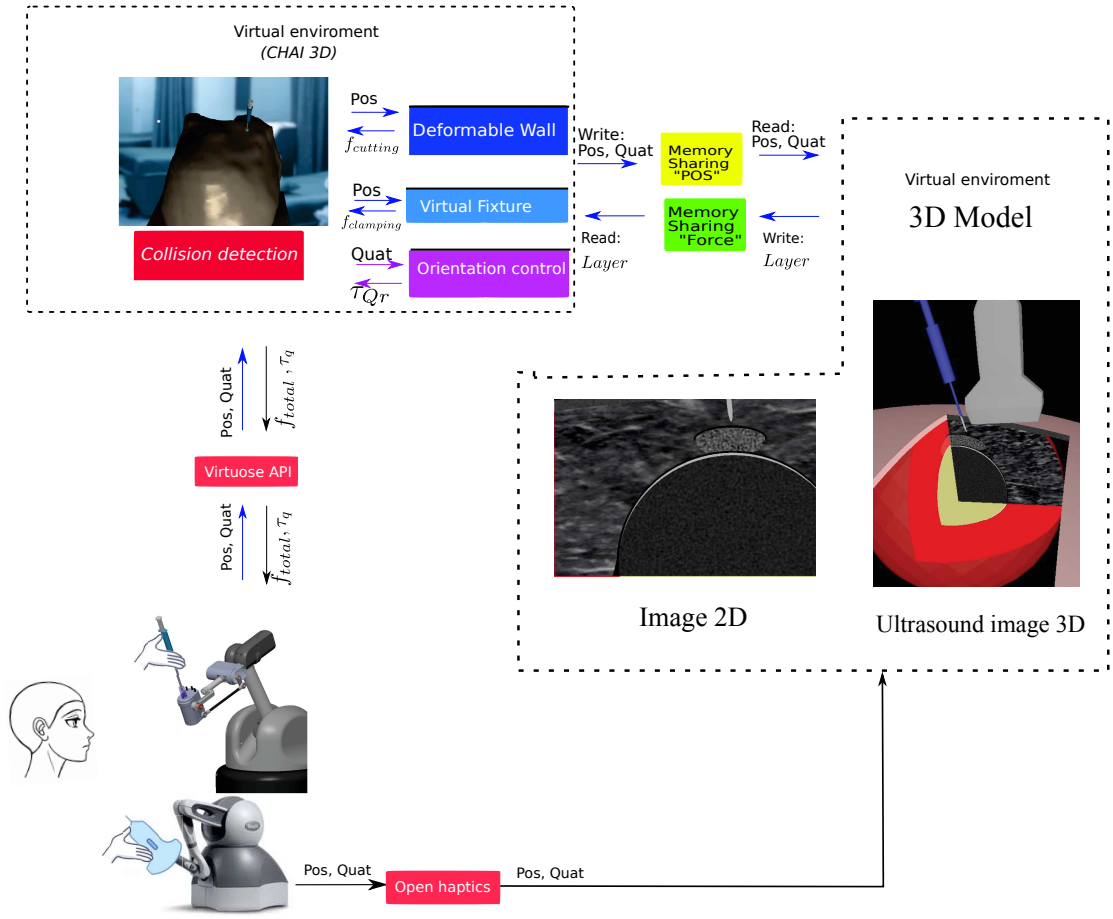

Figure 4-14 – Sharing data scheme

4.6 Experimental results

A test was performed by an experienced doctor (our medical partner from HCL), which consisted in testing the forces exerted by the haptic device during the needle insertion, as well as test the visualization of the ultrasound image during the performance.

Part of the shoulder anatomy is developed by LIRIS where they include almost all the inner layers and elements except for the tendons (Fig. 4-15). This anatomy is based on a model developed by LBMC.

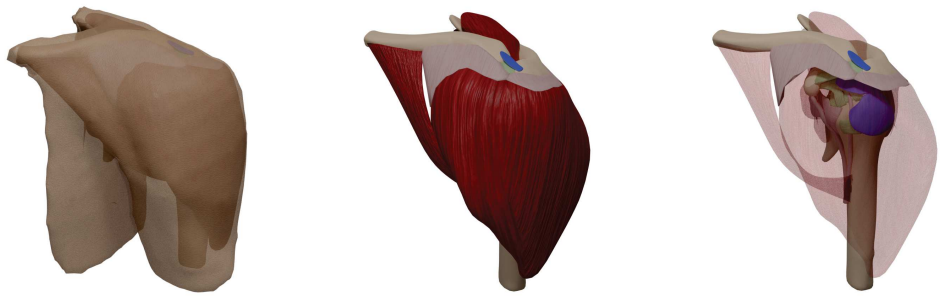

(a) Shoulder: skin (b) Shoulder: Muscles (c) Shoulder: inner elements

Figure 4-15 – Shoulder: complex model [Barnouin et al., 2020]

However, as the model is not complete it is no possible to proceed to experiments with the medical partner. In agreement with them, we choose to use a simpler model for the articulation. In our articulation's model, we set layers such as skin (as the first layer), muscle, bursa, tendon, cartilage, and as final layer, the bone (Fig. 4-16).

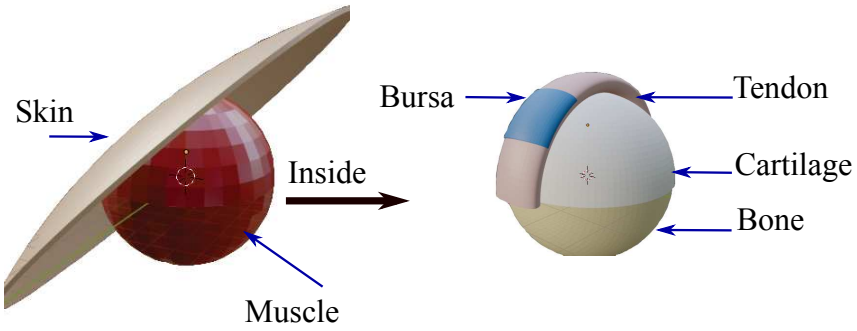

Figure 4-16 – Simple representation of the articulation [Barnouin et al., 2020]

This model was loaded in both virtual environments created in Chai3D (Fig. 4-17) and in the software that will recreate the 2D ultrasound image. The environment created in Chai3D includes a force plot that indicates the user the force exerted during the simulation, and frequency indicators to supervise that the image and force feedback are rendered at least at 30 Hz and 1000 Hz respectively.

During the simulation, it was mandatory to have the same model loaded since CHAI3D needs to determine the collision point to start computing the injection's forces (Fig. 4-17 and Fig. 4-18a).

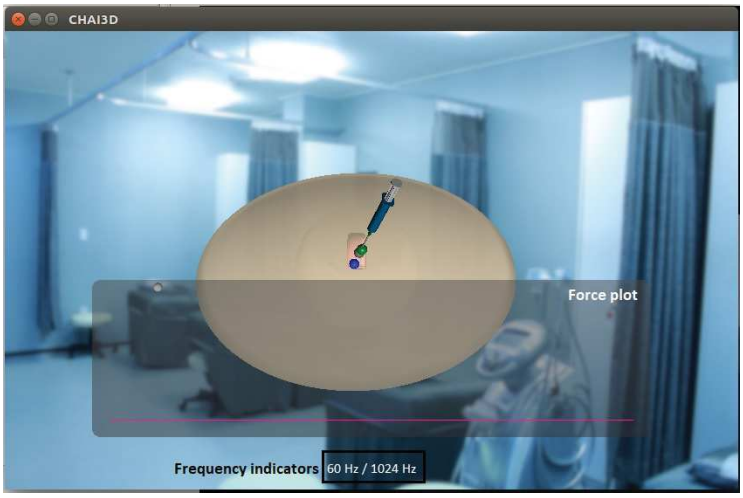

Figure 4-17 – Chai3D + simple articulation

In this part of the test, as was previously mentioned the ultrasound probe is represented by the Geomagic Touch (Fig. 4-18c), but during this tests the device does not offer haptic force feedback. As our objective in this part is only to render the forces during the insertion and display the 2D ultrasound image (Fig. 4-18b), therefore only reading the device's position fulfills our requirement. In a future test, the ultrasound probe will be implemented using a pneumatic technology to supply enough force in order to render the forces involved during the contact ultrasound probe-tissue.

Fig. 4-18b shows that both haptic devices (Haption and Geomagic) running in the software developed in LIRIS, thanks to the Boost libraries. Geomagic Touch can be running directly from this software since it has a native library to run the haptic device. Nevertheless, as LIRIS's environment does not officially support Haption devices, the communication is established through memory sharing.

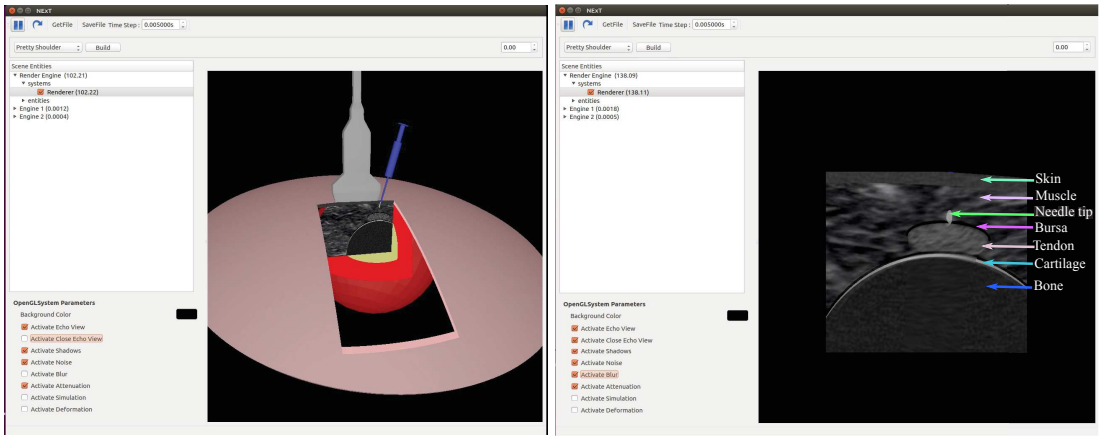

(a) A real-time ultrasound rendering.

(b) 2D ultrasound image.

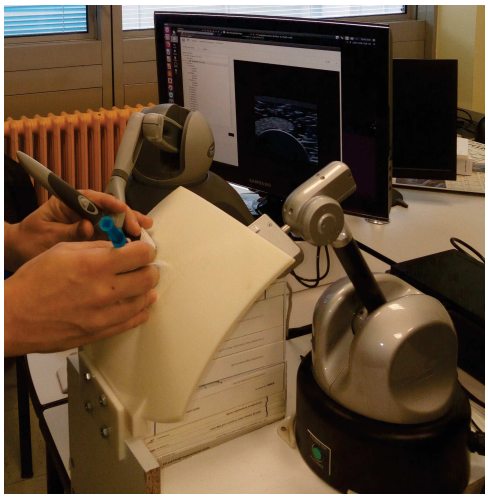

(c) Ultrasound probe and syringe represented by two haptic devices OMNI and Haption

Figure 4-18 – SPARTE project simulator; collaboration AMPERE and LIRIS laboratories

Test specifications

The test consisted in inserting the needle and trying to follow its trajectory on the ultrasound image, using the ultrasound probe to check the needle trajectory towards the bursa. Once the doctor reaches the bursa, we asked him/her to withdraw the needle a few centimeters to change the trajectory inside of the tissue to reach another part of the bursa. During the performance, the doctor must localize the needle tip with the help of the ultrasound probe. The 2D image is rendered in real-time, letting the user to visualize the different parts of the articulation. The main difficulty for doctors relies on manipulating the needle and the ultrasound probe at the same time in order to visualize the needle during its trajectory to the bursa. The cutting force profile during the needle insertion was established empirically by our medical partner. For future tests and validation, these forces, will be given by our partner from LBMC.

Table 4.2 – Cutting force values

Layer	Tissue	Cutting force
1	Skin	1 N
2	Muscle	2 N
3	Bursa	1.5 N
4	Tendon	2.5N
5	Cartilage	3 N
6	Bone	4 N

Results

In this test three injections were performed, they are denoted as injection 1, 2 and 3 in Fig 4-19. The first and second injection consisted of reaching the bursa and keep the needle visible all the time. The doctor changes the trajectory of the needle, by withdrawing the needle a few centimeters, and then proceed to change its orientation. The last injection consisted of puncturing and retrieving the needle without changing the trajectory, but in a quick movement to see the hard contact force behavior.

In Fig. 4-20 it can be appreciated the user's displacement in x, y and z and the desired needle's trajectories. The blue zones represent when the needle is inserted and the desired

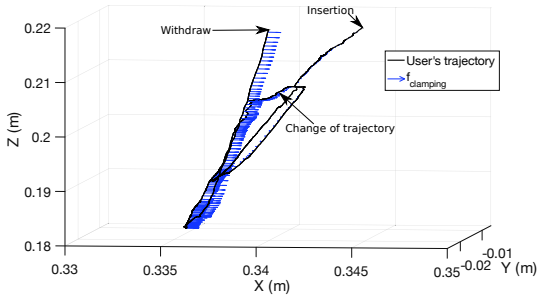

(a) First injection.

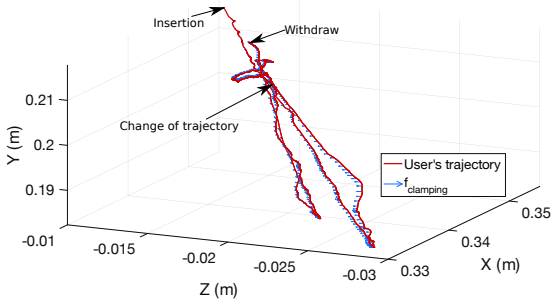

(b) Second injection .

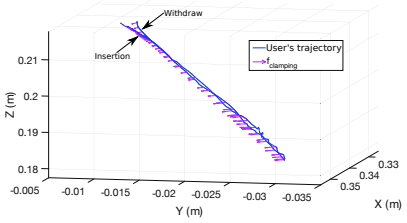

(c) Third injection

Figure 4-19 – Needle's trajectories

trajectories and interaction forces are calculated. The white zones represent when the needle is located outside of the articulation. In this case, the trajectories and desired forces are no longer calculated. From $2 < t < 7$ s it occurs the first injection (Fig. 4-19a), from $11 < t < 16$ s it occurs the second injection (Fig.4-19b) and from $20 < t < 22$ occurs the third injection. For the three injections the clamping forces and cutting forces are calculated are shown in Fig. (4-22) and Fig.(4-21).

During the injections and withdrawals (Fig.4-20) we can appreciate the evolution of the angle α and the modification of the trajectory which is in accord with the needle's depth and the angle. If $\alpha \to 0$ the user is not able to change the trajectory because the needle is completed inserted into the articulation, and also the needle becomes constraint in its normal displacements. Because of that, Fig.4-22 shows how the clamping forces increase. In case the user needs to modify again the trajectory, such as the case in $t = 3$ s and $t = 13$ s, the needle must be withdrawn a few centimeters to ensure that the angle α increases.

During injections 1 and 2, one can appreciate how the user almost follows the initial trajectories at the beginning ($2 < t < 3$ and $11 < t < 13$ s). But when the needle is withdrawn in both cases, the user does not respect the trajectory, and in this point, the clamping forces

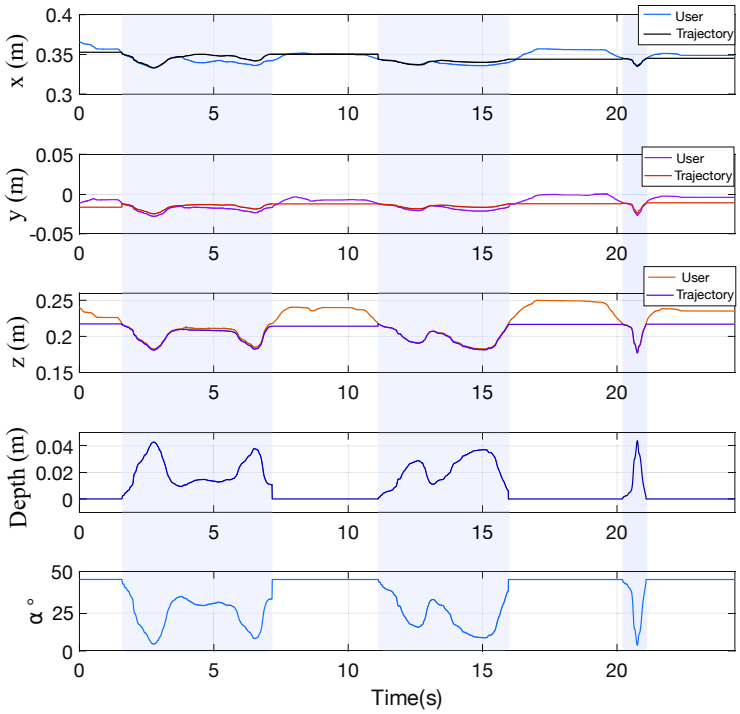

Figure 4-20 – Desired trajectory and user trajectory

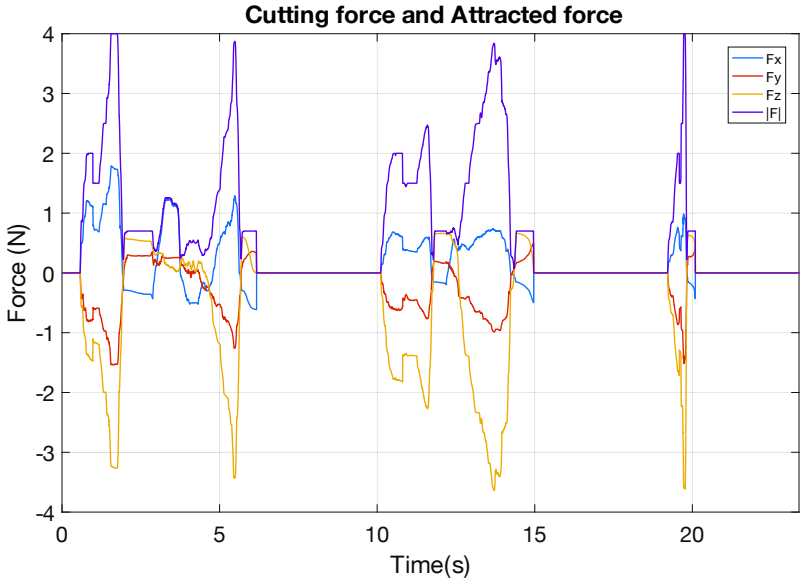

Figure 4-21 – Cutting forces and attracted forces

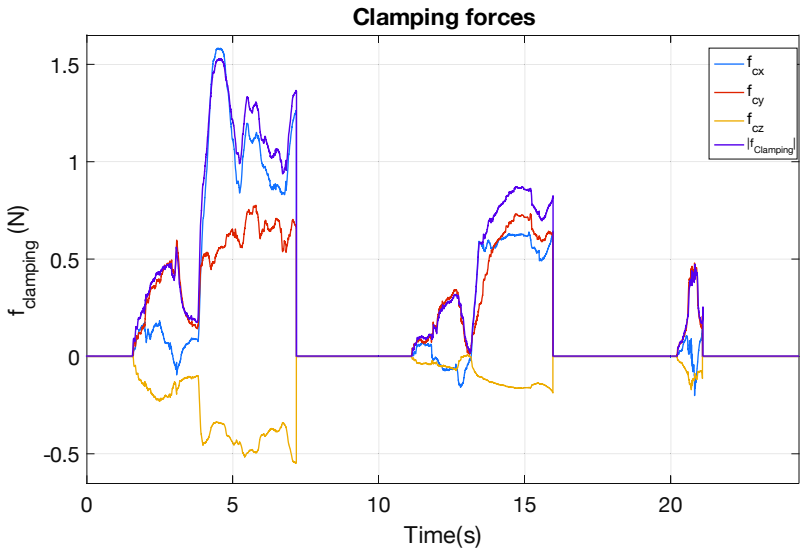

Figure 4-22 – Clamping forces

are exerted on the tool to correct the user trajectory.

One case that is also important to evaluate is the force response when the needle collides with a bone (Fig. 4-23). As can be seen during the injection 1 and injection 2, the user collides with the bone but the force is not high enough to retract the user movements as the incoming speed is low as it is seen in Fig. 4-23. However, the value of the force is higher when the user inserts the needle at a higher speed as it is the case of injection 3. For a better appreciation, Fig. 4-24, shows a zoom of the hard contact force "Decaying sinusoid" (as it is detailed in section 2.1.1) that occurs from $20.65 < t < 20.85$ s, and has a duration of 0.055 s, that avoids disturbing the haptic rendering. The objective of this force is only to send a small pulse that helps the user to identify when he/she collides with bone.

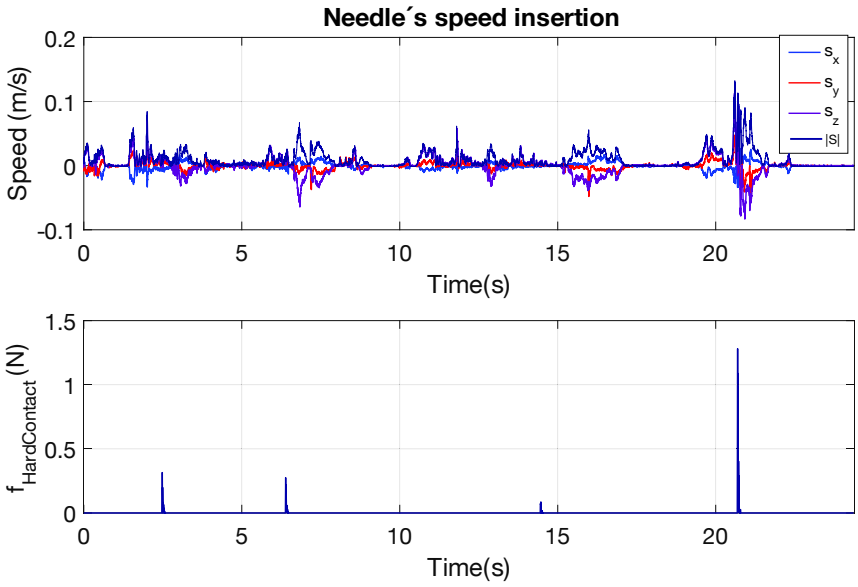

Figure 4-23 – Hard contact force response

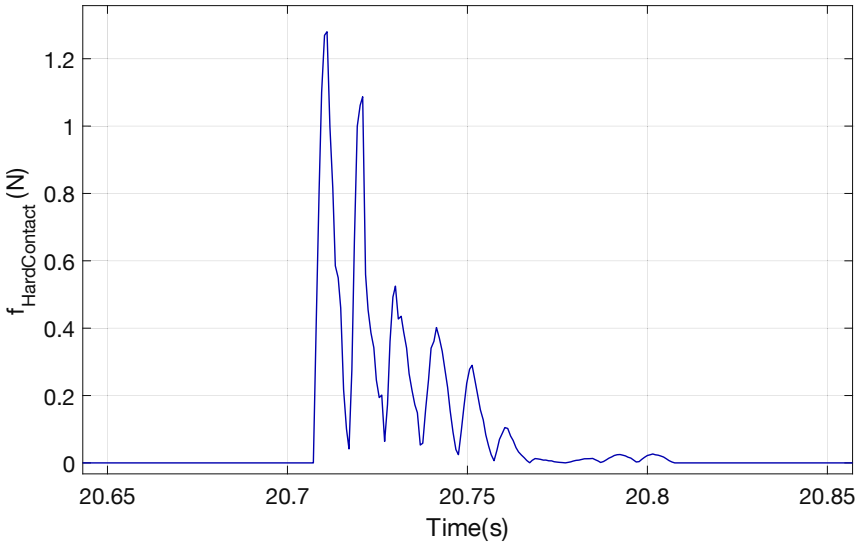

Figure 4-24 – Zoom of the hard contact force "Decaying sinusoid"

4.7 Discussion

In this section the different mechanical models to represent the syringe with the haptic device were presented. The insertion point was limited in one point of entry to prohibit the user to modify the trajectory since the device does not offer enough force to counter his/her movement. However, the simulator allows the user to rotate the virtual environment, so he/she can freely choose a point of injection in the articulation.

Concerning the design, a surface was added, as it was requested by the medical staff, that supports the users' fist during the needle insertion, providing comfortability and improving the realism during the training.

Using the Boost libraries it was possible to share the position of the haptic device with the user interface developed by LIRIS laboratory. With this method, we could determine the layer on which the needle was interacting, and compute the desired forces during the test.

According to the evaluation of our specialist, the mechanical part needs to be modified so it can allow changing the inclination of the support, where the user's fist lies. Respecting the part developed by LIRIS, it is necessary to modify the model that represents the articulation, as this does not resemble a real bursa.

Conclusions and future work

The use of simulators for training medical students is beginning to be the new standard in medical schools and training centers. These simulators begin to offer a more realistic and immersive experience, that helps students to practice and easily interpolates their newly developed skills when working with patients.

In this PhD thesis, we proposed a prototype for an intraarticular injection simulator. To render the forces during the needle insertion we proposed a new method approach called "Tracking wall", that compute the cutting forces and the attracted forces and helps us to have a good haptic rendering without any chattering when large values of cutting force are set. The advantages of this method are that it is simple to compute, it has the ability to render the different tissues of the body, and it has the ability to configure the rejection force. The disadvantages are that the lack of biomechanical model can reduce the realism of the process, also this method can be only implemented in impedance haptic system; and the number of iterations for a proper simulation has to be determined according to the chosen devices or languages.

Concerning the method implemented to compute the clamping forces, we proposed the use of a virtual fixture (Orthogonal projection) to simulate the normal forces, and to constrain the radial movements for following straight paths. The disadvantages of this method are that this cannot be implemented in case of curved trajectories.

To implement the ultrasound probe, we opted for using a single servovalve with a pneumatic cylinder to reduce the cost of the prototype. We compare three different control laws to find the best that fits our necessities. For instance, the PID and IPC behave in a similar way for the ISP and SSP profiles, with some minor differences between them. In the case of the backstepping control laws, this control technique presents, a greater steady-state error in general, but it also limits the chattering, contrary to the PID and IPC. From a quantitative point of view, the PID and IPC are probably the best options, but from a qualitative point of view, it is necessary to carry out a campaign of test with expert practitioners that their feed-

back help to determine the optimal control to render the desired stiffness tissues. However, it is noteworthy that PID and IPC need a force sensor between the probe and the surface whereas a backstepping control does not need one.

A new ultrasound probe is currently under development. The new version will be smaller and lighter in order to look like more a real US probe, which would increase the realism of the simulator. Similar control laws will be then implemented.

To avoid any communication problems with LIRIS interface in case another haptic device is used, we opted to use the Boost libraries to create a memory sharing space. This option helps us to share the position of the haptic device with their user interface. With this method, we could determine the layer of which the needle was interacting and compute the desired forces during the test.

We also developed different mechanical models to represent the syringe with the haptic device. The insertion point was limited to one point of entry. However, the simulator allows the user to rotate the simulator's virtual environment, so he/she can freely choose a point of injection in the articulation. By doing this, different cutting forces can be represented in each needle insertion. A surface was added, as it was requested by the medical staff, that supports the users' fist during the needle insertion.

The proposed system is the first partially functional prototype of the desired injection simulator proposed by the project SPARTE. This simulator can be implemented for study and tests with expert practitioners, in order to get qualitative feedback to improve the realism and immersion of the system.

As future work for the next prototype we propose:

- The modification of the mechanical support so it allows changing its inclination in order to improve the needle's insertion. This mechanical modification will not affect the tracking wall and virtual fixture algorithms.
- A connection between the pneumatic ultrasound probe and the LIRIS interface must be made, to allow the rendering of force on it.
- An assembly between the biomechanical model developed by the LBMC, the user

interface of LIRIS and the work presented in this PhD thesis, must be done thought running all the software in a single process, or by interchanging data between processes using memory sharing methods, so the final computational interface will be finished.

- A test campaign with expert practitioners from HCL must be done to get qualitative feedback for the mechanical design, rendering forces and general appealing of the final simulator.

- Pedagogic scenarios have to be implemented and a reflection has to be done on how to insert this learning tool during medical doctors training course.

- Once the pedagogic scenarios are chosen, it is necessary to determine the criteria to evaluate the user's gesture in order to distinguish the different levels of expertise and determine the learning curves for each task.

Publications

The PhD thesis leads to three publication.

The first one presents the Tracking wall method developed during this PhD work (section 2.2). It is used to compute the Cutting forces during the needle insertion in 3 DoF. (Status: accepted)

- Ma. de Los Angeles Alamilla Daniel, Richard Moreau, Tanneguy Redarce. "A New Method to Render Virtual Walls for Haptic Systems: Tracking Wall. Application to Needle Insertion Simulation". *3rd International Conference on Virtual and Augmented Reality Simulations (ICVARS '19)*, Feb 2019, Perth, Australia. Presented during ICMCE 2018 conference.

The second publication presents an enhanced version of the Tracking wall method. With this improvement we were able to compute the Cutting forces and Attracted forces in 3 DoF. Also a method is proposed to compute the Clamping forces implementing a virtual fixture. (Status: under review).

- Ma. de Los Angeles Alamilla Daniel, Richard Moreau, Tanneguy Redarce. "Enhanced tracking wall: A real-time computing method for intraarticular needle injection on robotics and Automation". *International Conference on Virtual and Augmented Reality Simulations (ICRA 2020)*

The last publication presents the complete simulator, the tested and implemented methods to compute the forces during the needle insertion and exploration with the ultrasound probe. This also shows the current state of the user interface and the results obtained during the evaluation with our medical partner. (Status: in progress).

- Ma. de Los Angeles Alamilla Daniel, Richard Moreau, Tanneguy Redarce. " INIHS : Haptic simulator for practicing the intraarticular needle injection under echography". *IEEE Transactions on Biomedical Engineering*

Bibliography

Abdallah, I., Gatwaza, F., Morette, N., Lelevé, A., Nouaille, L., Brun, X., and Vieyres, P. (2019). A Pneumatic Haptic Probe Replica for Tele-Robotized Ultrasonography. In *First International Conference on Smart Multimedia*.

Abolhassani, N., Patel, R., and Moallem, M. (2007). Needle insertion into soft tissue: A survey. *Medical Engineering and Physics*, 29(4):413–431.

Abry, F., Brun, X., Sesmat, S., and Bideaux, E. (2013a). Non-linear position control of a pneumatic actuator with closed-loop stiffness and damping tuning. In *2013 European Control Conference, ECC 2013*, pages 1089–1094.

Abry, F., Brun, X., Sesmat, S., Bideaux, E., and Ducat, C. (2016). Electropneumatic Cylinder Backstepping Position Controller Design with Real-Time Closed-Loop Stiffness and Damping Tuning. *IEEE Transactions on Control Systems Technology*, 24(2):541–552.

Abry, F., Xavier, B., Sylvie, S., and Eric, B. (2013b). Non-linear position control of a pneumatic actuator with closed-loop stiffness and damping tuning. *2013 European Control Conference (ECC)*, pages 1089–1094.

Alamilla D, M., Moreau, R., and Redarce, T. (2019). A new method to render virtual walls for haptic systems: Tracking wall. Application to needle insertion simulation. In *ICVARS'19 Proceedings of the 2019 3rd International Conference on Virtual and Augmented Reality Simulations*, pages 33–38.

Alès Roux, P.-J., Herzig, N., Lelevé, A., Moreau, R., and Bauer, C. (2016). 3D Haptic Rendering of Tissues for Epidural Needle Insertion using an Electro-Pneumatic 7 Degrees of Freedom Device. In IEEE, editor, *2016 IEEE IROS*, Daejeon, South Korea. IEEE.

Asadian, A., Patel, R. V., and Kermani, M. R. (2011). A distributed model for needle-tissue friction in percutaneous interventions. *Proceedings - IEEE International Conference on Robotics and Automation*, pages 1896–1901.

Asadian, A., Patel, R. V., and Kermani, M. R. (2014). Dynamics of translational friction in needle-tissue interaction during needle insertion. *Annals of Biomedical Engineering*, 42(1):73–85.

Balint, P. V., Kane, D., Hunter, J., McInnes, I. B., Field, M., and Sturrock, R. D. (2002). Ultrasound guided versus conventional joint and soft tissue fluid aspiration in rheumatology practice: A pilot study. *Journal of Rheumatology*, 29(10):2209–2213.

Barbé, L., Bayle, B., De Mathelin, M., and Gangi, A. (2006). Needle insertions modelling: Identifiability and limitations. *IFAC Proceedings Volumes (IFAC-PapersOnline)*, 6(PART 1):129–134.

Barnouin, C., Zara, F., and Jaillet, F. (2018). Real-time Ultrasound Rendering for Ultrasound-Guided Puncture Training. In *Journées Françaises d'Informatique Graphique (JFIG 2018)*, Poitiers, France.

Barnouin, C., Zara, F., and Jaillet, F. (2020). A real-time ultrasound rendering with model-based tissue deformation for needle insertion To cite this version. In *15th International Conference on Computer Graphics Theoryand Applications, GRAPP 2020.*, Valleta, Matal.

Basdogan, C. and Srinivasan, M. a. (2002). Haptic Rendering in Virtual Environments. In *Handbook of virtual environments: Design, implementation, and applications*, number 1, pages 117–134.

Bobrow, J. E. and McDonell, B. W. (1998). Modeling, identification, and control of a pneumatically actuated, force controllable robot. *IEEE Transactions on Robotics and Automation*, 14(5):732–742.

Brett, P. N., Parker, T. J., Harrison, a. J., Thomas, T. a., and Carr, a. (1997). Simulation of resistance forces acting on surgical needles. *Proceedings of the Institution of Mechanical Engineers. Part H, Journal of engineering in medicine*, 211(4):335–347.

Brown, R. H., Schneider, S. C., and Mulligan, M. G. (1992). Analysis of Algorithms for Velocity Estimation from Discrete Position Versus Time Data. *IEEE Transactions on Industrial Electronics*, 39(1):11–19.

Chawda, V., Celik, O., and O'Malley, M. K. (2011). Application of Levant's differentiator for velocity estimation and increased Z-width in haptic interfaces. *2011 IEEE World Haptics Conference*, pages 403–408.

Coles, T. and John, N. W. (2010). The effectiveness of commercial haptic devices for use in virtual needle insertion training simulations. *3rd International Conference on Advances in Computer-Human Interactions, ACHI 2010*, pages 148–153.

Coles, T. R., Meglan, D., Member, S., and John, N. W. (2011). The Role of Haptics in Medical Training.pdf. 4(1):51–66.

Colgate, J., Grafing, P., Stanley, M., and Schenkel, G. (1993). Implementation of stiff virtual walls in force-reflecting interfaces. In *Proceedings of IEEE Virtual Reality Annual International Symposium*, pages 202–208.

Constantinescu, D., Salcudean, S. E., and Croft, E. A. (2005). Haptic rendering of rigid contacts using impulsive and penalty forces. In *IEEE Transactions on Robotics*, volume 21, pages 309–323.

Conti, F., Barbagli, F., Balaniuk, R., Halg, M., Lu, C., Morris, D., Sentis, L., Warren, J., Khatib, O., and Salisbury, K. (2003). The CHAI libraries. In *Proceedings of Eurohaptics 2003*, pages 496–500.

Corrêa, C. G., Nunes, F. L., Ranzini, E., Nakamura, R., and Tori, R. (2019). Haptic interaction for needle insertion training in medical applications: The state-of-the-art. *Medical Engineering and Physics*, 63:6–25.

Courtecuisse, H., Jung, H., Allard, J., Duriez, C., Lee, Y., and Cotin, S. (2010). GPU-based Real-Time Soft Tissue Deformation with Cutting and Haptic Feedback. In *Special Issue on Biomechanical Modelling of Soft Tissue Motion*, volume 103. Elsevier.

Culbertson, H., Schorr, S. B., and Okamura, A. M. (2018). Haptics: The Present and Future of Artificial Touch Sensation. *Annual Review of Control, Robotics, and Autonomous Systems*, 1(1):385–409.

Douglas, R. J. (2014). Aspiration and Injection of the Knee Joint: Approach Portal. *Knee Surgery & Related Research*, 26(1):1–6.

Fessell, D. P., Jacobson, J. A., Craig, J., Habra, G., Prasad, A., Radliff, A., and Van Holsbeeck, M. T. (2000). Using sonography to reveal and aspirate joint effusions. *American Journal of Roentgenology*, 174(5):1353–1362.

Feygin, D., Keehner, M., and Tendick, R. (2002). Haptic Guidance: Experimental Evaluation of a Haptic Training Method for a Perceptual Motor Skill. *Proceedings 10th Symposium on Haptic Interfaces for Virtual Environment and Teleoperator Systems. HAPTICS 2002*, (March):40–47.

Forest, C., Comas, O., Vaysière, C., Soler, L., and Marescaux, J. (2007). Ultrasound and needle insertion simulators built on real patient-based data. *Studies in health technology and informatics*, 125:136–139.

Goksel, O., Sapchuk, K., and Salcudean, S. E. (2011). Haptic simulator for prostate brachytherapy with simulated needle and probe interaction. *IEEE Transactions on Haptics*, 4(3):188–198.

Gonenc, B. and Gurocak, H. (2012a). Haptic interface with hybrid actuator for virtual needle insertion and tissue cutting. In *Haptics Symposium 2012, HAPTICS 2012 - Proceedings*, pages 451–455.

Gonenc, B. and Gurocak, H. (2012b). Virtual needle insertion with haptic feedback using a hybrid actuator with DC servomotor and MR-brake with Hall-effect sensor. *Mechatronics*, 22(8):1161–1176.

Gordon, A., Barnett, A. C., Kim, I., and Moore, J. Z. (2015). Needle insertion force model for haptic simulation. *ASME 2015 International Manufacturing Science and Engineering Conference, MSEC 2015*, 2:18–20.

Granry, J.-C. and Moll, M.-C. (2012). État de l'art (national et international) en matière de pratiques de simulation dans le domaine de la santé. Technical report, Haute Autorité de la Santé (HAS).

Grottke, O., Ntouba, A., Ullrich, S., Liao, W., Fried, E., Prescher, A., Deserno, T. M., Kuhlen, T., and Rossaint, R. (2009). Virtual reality-based simulator for training in regional anaesthesia. *British Journal of Anaesthesia*, 103(4):594–600.

Heng, P. A., Wong, T. T., Yang, R., Chui, Y. P., Xie, Y. M., Leung, K. S., and Leung, P. C. (2006). Intelligent inferencing and haptic simulation for Chinese acupuncture learning and training. *IEEE Transactions on Information Technology in Biomedicine*, 10(1):28–41.

Herzig, N. (2016). *De la Conception à la Commande d ' une Nouvelle Interface Haptique 4 Axes Hybride Pneumatique Électrique pour la Simulation d ' Accouchement : le BirthSIM*. PhD thesis, INSA de Lyon.

Herzig, N., Moreau, R., Leleve, A., and Pham, M. T. (2016). Stiffness control of pneumatic actuators to simulate human tissues behavior on medical haptic simulators. *IEEE/ASME International Conference on Advanced Intelligent Mechatronics, AIM*, (July):1591–1597.

Herzig, N., Moreau, R., Redarce, T., Abry, F., and Brun, X. (2015). Non linear position and closed loop stiffness control for a pneumatic actuated haptic interface: The BirthSIM. *IEEE International Conference on Intelligent Robots and Systems*, 2015-Decem:1612–1618.

Kataoka, H., Washio, T., Chinzei, K., Mizuhara, K., Simone, C., and Okamura, A. M. (2002). Measurement of the Tip and Friction Force Acting on a Needle during Penetration. In *Lecture Notes and Computer Science*, pages 216–223.

Kikuuwe, R., Takesue, N., and Fujimoto, H. (2007). Passive virtual fixtures based on simulated position-dependent anisotropic plasticity. In *Proceedings - IEEE International Conference on Robotics and Automation*, pages 3263–3268.

Kuchenbecker, K. J., Fiene, J., and Niemeyer, G. (2006). Improving contact realism through event-based haptic feedback. In *IEEE Transactions on Visualization and Computer Graphics*, volume 12, pages 219–229.

Kurita, Y., Ohtsuka, H., Nagata, K., and Tsuji, T. (2014). Haptic rendering of a needle insertion by enhancing the real force response of a base object. In *Haptics Symposium 2014, HAPTICS 2014*, pages 357–360.

Le, M.-Q. (2011). *Development of Bilateral Control for Pneumatic Actuated Teleoperation System*. PhD thesis, INSA de Lyon.

Li, Z., Jin, L., Lang, J., and Petriu, E. (2014). Haptic Dissection of Deformable Objects using Extended Finite Element Method by. *IEEE 2014 IEEE International Symposium on Haptic, Audio and Visual Environments and Games (HAVE)*.

Magee, D. (2005). A computer based simulator for ultrasound guided needle insertion procedures. *IEE International Conference on Visual Information Engineering (VIE 2005)*, pages 301–308.

Magee, D., Zhu, Y., Ratnalingam, R., Gardner, P., and Kessel, D. (2007). An augmented reality simulator for ultrasound guided needle placement training. *Medical and Biological Engineering and Computing*, 45(10):957–967.

Magill, J. C., Byl, M. F., Hinds, M. F., Agassounon, W., Pratt, S. D., and Hess, P. E. (2010). A novel actuator for simulation of epidural anesthesia and other needle insertion procedures. *Simulation in Healthcare: The Journal of the Society for Simulation in Healthcare*, 5(3):179–84.

Pedersen, T. H., Meuli, J., Plazikowski, E. J., Buttenberg, M., Kleine-Brueggeney, M., Seidl, C., Theiler, L., and Greif, R. (2017). Loss of resistance: A randomised controlled trial assessing four low-fidelity epidural puncture simulators. *European Journal of Anaesthesiology*, 34(9):602–608.

Peetrons, P. and Court-Payen, M. (2009). Ultrasound-Guided Musculoskeletal Interventional Procedures. pages 385–398. Springer Berlin ISBN: 978-3-540-49929-9.

Podder, T. K., Sherman, J., Messing, E. M., Rubens, D. J., Fuller, D., Strang, J. G., Brasacchio, R. A., and Yu, Y. (2006). Needle insertion force estimation model using procedure-specific and patient-specific criteria. *Annual International Conference of the IEEE Engineering in Medicine and Biology - Proceedings*, pages 555–558.

Raitor, M., Walker, J. M., Okamura, A. M., and Culbertson, H. (2017). WRAP: Wearable, restricted-aperture pneumatics for haptic guidance. *Proceedings - IEEE International Conference on Robotics and Automation*, pages 427–432.

Ryden, F. and Chizeck, H. J. (2013). A proxy method for real-time 3-DOF haptic rendering of streaming point cloud data. In *IEEE Transactions on Haptics*, volume 6, pages 257–267.

Salisbury, K., Brock, D., Massie, T., and Swarup, N. (1995). Haptic rendering: Programming touch interaction with virtual objects. In *Proceedings of the 1995 Symposium on Interactive 3D Graphics*, pages 123–130.

Salisbury, K., Conti, F., and Barbagli, F. (2004). Haptic rendering: Introductory concepts. *IEEE Computer Graphics and Applications*, 24(2):24–32.

Sclaverano, S., Chevreau, G., Vadcard, L., Mozer, P., and Troccaz, J. (2009). BiopSym: A simulator for enhanced learning of ultrasound-guided prostate biopsy. *Studies in Health Technology and Informatics*, 142(1):301–306.

Simone, C. and Okamura, A. M. (2002). Modeling of Needle Insertion Forces for Robot-Assisted Percutaneous Therapy. In *Proceedings of the 2002 IEEE International Conference on Robotics & Automation*, number May, pages 2085–2091.

Sofka, C. M., Collins, A. J., and Adler, R. S. (2001). Use of Ultrasonographic Guidance in Interventional Musculoskeletal. *Journal of Ultrasound in Medicine*, pages 21–26.

Stramigioli, S. (1996). Creating Artificial Damping By Means of Damping Injection. *Proceedings of the ASME Dynamic Systems and Control Division*, DSC.58:601–606.

Thomasset, D., Scavarda, S., Sesmat, S., and Belgharbi, M. (1999). Analytical model of the flow stage of a pneumatic servo-distributor for simulation and nonlinear control. *Proceedings of the Sixth Scandinavian International Conference on Fluid Power. Tampere, Finland, May 26-28 1999*, 3:848–860.

V. Lawry, G., J. Kreder, H., Hawker, G., and Jerome, D. (2010). *Fam's Musculoskeletal Examination and Joint Injection Techniques*. Elsevier Health Sciences.

Vidal, F., Jhon, N., and Healey, A. (2008). Simulation of ultrasound guide needle puncture using patient specific data with 3D textures and volume haptics. In *Computer Animation And Virtual Worlds*, volume 19, pages 111–127.

Yang, T., Yin, H., Zhao, X., Han, J., and Xu, W. (2014). Interaction modeling and simulation of a flexible needle insertion into soft tissues. *Proceedings for the Joint Conference of ISR 2014 - 45th International Symposium on Robotics and Robotik 2014 - 8th German Conference on Robotics, ISR/ROBOTIK 2014*, pages 611–616.

Y.C. Fung (1993). *Biomechanics. Mechanical Properties of Living Tissues*. Springer Science ISBN:978-1-4757-2257-4, New York, 2 nd edition.

Zhang, X., Sun, W., and Song, A. (2014). Layered rhombus-chain-connected model for real-time haptic rendering. *Artificial Intelligence Review*, 41(1):49–65.

Zhu, Y., Magee, D., Ratnalingam, R., and Kessel, D. (2007). A training system for ultrasound-guided needle insertion procedures. *Medical image computing and computer-assisted intervention: MICCAI - International Conference on Medical Image Computing and Computer-Assisted Intervention*, 10:566–574.

Zilles, C. and Salisbury, J. (1995). A constraint-based god-object method for haptic display. In *Proceedings IROS 1995*, volume 3, pages 146–151.

FOLIO ADMINISTRATIF

THESE DE L'UNIVERSITE DE LYON OPEREE AU SEIN DE L'INSA LYON

NOM : ALAMILLA DANIEL DATE de SOUTENANCE : 12/03/2020

Prénoms : Ma. De los Angeles

TITRE : Development of a haptic simulator for practicing the intraarticular needle injection under echography.

NATURE : Doctorat Numéro d'ordre : 2020LYSEI017

Ecole doctorale : Electronique, Electrotechnique, Automatique (EEA)

Spécialité : Automatique

RESUME :

La ponction articulaire est une technique courante utilisée par les rhumatologues pour soulager la douleur. L'utilisation de repères anatomiques aide à guider l'aiguille à l'intérieur de l'articulation. Cependant, sans l'aide de l'imagerie, les praticiens ont du mal à placer correctement l'aiguille et la plupart du temps il est nécessaire de réaliser une deuxième insertion articulaire.
L'injection intra-articulaire de l'aiguille sous échographie est une solution pour faciliter la procédure. Il s'agit cependant d'un processus difficile car le praticien doit développer une coordination motrice-visuelle pour insérer l'aiguille et la guider en utilisant comme référence une image 2D générée par la sonde ultrasonore.
Pour maîtriser cette technique, les pratiquants peuvent s'exercer sur des cadavres, des mannequins et des simulateurs. Les simulateurs offrent certains avantages par rapport aux cadavres et aux mannequins, mais la plupart d'entre eux ne permettent pas de modifier l'environnement de travail (morphologie et / ou pathologie du patient,…) ou de choisir le point d'insertion, ce qui limite le réalisme de la formation.
Sous l'impulsion de SAMSEI, le projet SPARTE vise à développer un simulateur d'injection intra-articulaire entièrement fonctionnel. Ce projet est soutenu par 4 laboratoires et un établissement de santé. Dans ce travail de doctorat, les principales contributions sont: une nouvelle méthode à faible coût de calcul appelée «mur de suivi» couplée à des dispositifs virtuels pour le contrôle de la position et de l'orientation de l'aiguille, afin de restituer les forces lors de l'insertion de l'aiguille; l'étude et la validation de trois lois de commande différentes appliquées à un actionneur pneumatique pour restituer les forces lors de l'utilisation d'une sonde à ultrasons; et enfin la conception d'un simulateur fonctionnel complet où les utilisateurs peuvent expérimenter l'insertion de l'aiguille avec un guidage échographique.

MOTS-CLÉS : Haptique, Simulateur médicaux, Robotique Médicale, Contrôle de raideur

Laboratoire (s) de recherche : Laboratoire Ampère UMR CNCR 5005

Directeur de thèse : Tanneguy REDARCE
Co-directeur de thèse : Richard MOREAU

Président de jury :

Composition du jury : POISSON Gerard (Rapporteur), BARTHOD Christine (Rapportrice), VIEYRES Pierre, ZARA Florence, PROMAYON Emmanuel, REDARCE Tanneguy, MOREAU Richard.